Asymmetric division in single cell nematode embryos outside the Caenorhabditis genus

Dureen Samandar Eweis

PSL UNIVERSITÉ PARIS

institut Curie

THÈSE DE DOCTORAT

DE L'UNIVERSITÉ PSL

Préparée à l'Institut Curie

Asymmetric division in single cell nematode embryos outside the *Caenorhabditis* genus

Division asymétrique dans les embryons unicellulaires de nématodes hors du genre *Caenorhabditis*

Dureen SAMANDAR EWEIS

Date de soutenance prévu le 24 Septembre 2021

Ecole doctorale n° 515
Complexité du vivant

Spécialité
Biologie cellulaire et développement

Composition du jury:

Phong TRAN Directeur de recherches, Institut Curie	*Président*
Anne PACQUELET Chargée de recherches, IGDR	*Rapporteuse*
Einhard SCHIERENBERG Professeur, Université de Cologne	*Rapporteur*
Ana XAVIER DE CARVALHO Directrice de recherches, i3S/IBMC	*Examinatrice*
Lionel PINTARD Directeur de recherches, IJM	*Examinateur*
Julie PLASTINO Directrice de recherches, Institut Curie	*Directrice de thèse*

Acknowledgments

Choosing to do a PhD in Paris, a new city that I really did not know, has been so far one of the best decisions I have made. Since I moved to Paris and joined Institut Curie, I have had the support of many friends and colleagues. I hope I am able to express my gratitude to each person here.

Importantly, before starting, my project could be carried out thanks to the funding I received from the European Union's Horizon 2020 research and innovation programme under the Marie Skłodowska-Curie grant agreement No 666003 as well as funding for my fourth year from Fondation pour la Recherche Médicale (FRM).

To start, I would like to thank my jury members for having accepted to evaluate my work and discuss it with me, especially the reporters of my manuscript, Anne Pacquelet and Einhard Schierenberg. I would also like to thank my TAC members, François Robin, Jean-Léon Maître and Michel Gho. François, for personally teaching me a protocol I desperately wanted to work and Jean-Léon for the great discussions and ideas! The support from you both has truly come into my project. I also thank Marie Delattre for the discussions and advice, and for helping with experiments herself.

I want to thank Buzz Baum and Francesca Farina. Francesca for insisting on helping me find a good PhD position, your support meant a great deal to me. Buzz, thank you for welcoming me in your lab, even though it was short, it was inspiring and mind opening to work with you and your team, you are a wonderful person and I look forward to keep having catch-up talks with you.

I would also like to thank the Training Unit of Institut Curie, for making our transfer to Paris so easy. Thank you to Graça, Melanie, Anemone and Ana-Rita for taking care of us throughout. Thank you for organizing a program that allowed us to have friends that became family in Paris.

A big thank you goes to all of ADIC, especially the team of 2017-2019. I loved working with all of you, it has been a great addition to my memories and my experience at Curie and Paris. Thank you to Marco Lucchino, for showing me that you can be very good at so many things!

Thank you to my team: Cécile for being so caring of us and making sure we were always doing well. Karine, for your smile and laugh, spreading much positivity and the motivation to do better. And of course I want to thank Julie, my mentor. Thank you for having been so supportive, patient and optimistic throughout. Your constant curiosity and excitement about science has been very special to me and I know you will keep inspiring young scientists who will train with you. I truly admire the way you connect thoughts and ideas, even when completely unrelated to science, always so honest and humble. I will miss very much popping into your office for just a quick question and then ending up talking for an hour about whatever it was on our mind that day. Thank you for making me feel so included in the team from the very beginning, for making it so easy to talk to you about anything and for making the whole experience unforgettable. Having you three women as the leaders of the team has

been very inspiring, you were able to show us how different expertise can be brought together in a team and more so you did it by showing us how supportive you are of each other and of us. Not many people can say they were part of a team led by three women and I feel lucky to do so! Thank you also to my team members, Sirine and Johan. Although we did not get much time together, you have both sent such positive vibes.

To all of my colleagues in the department of PCC/UMR168 thank you for making the work and social environment really so unique! The random talks in the halls, for our lunches together, the legendary bar trials, the seminar trials, the *pots* and spontaneous parties. Thank you all for your scientific discussions and support as a whole. There are so many specific people to thank: John, Alicia, Kortyna, Lorena, Aude, Fahima, Maud, Anne-Marie, Joanna, Lucie, Oleg and many more for sure. Thank you all.

To my office mates, Thanh, Theb, Koyomi and Achille, thank you for the endless talks and discussions, for the interest in each other's projects and for sharing the obsession of food! Thank you for making the office a place I looked forward to be in every day.

I want to also thank my friends from the same PhD program. Raquel for being my 'let's make a change' partner, for our talks about culture, people and books and our trips together. Ozge, for being my scientific partner and I like to think almost a collaborator. Anna, thank you for always bringing such a joyful and lively vibe wherever we are. Thank you to Julia, for being one of the first faces I met in Paris, for being a sincere friend and keeping our friendship so special. Deep, thank you for your constant support and for motivating me to keep going no matter what. Claudia, always optimistic and strong, thank you for reminding me to be so myself. Thank you to Xavi, for our unforgettable talks, tours of Paris, and sharing the love of cooking and trying new food. Thank you also to Ram and Maciej for being very good friends throughout this journey.

To my older team members and my friends, Maj, Antoine, Camille and Hanane. Thank you for being you, for being born!! What great luck I had to have you 'normal guys' in the same team. I met you as my colleagues and today you are my very dear friends. Thank you for the talks, for the morning coffees, for the shoulder to cry on and for always finding a solution together. For our gossip sessions and for our dinners. Thank you for being the sweetest people I have met. Majdo, habeebti, thank you for taking care of me like your little sister; you made Paris feel like home very quickly.

Paris really has become home for me and of course I want to thank the family I made in Paris, Silvia, Sandra, Tommaso and Danny. It's hard to think that just 4 years ago I met you for the first time as first-day PhD students. Thank you for wanting to be together 24/7, for having our rooms as different parts of a big house. For being the people to complain to whenever it was needed and when things weren't easy. For also having the most fun times in Paris and everywhere else we have travelled to together. Silvia y Sandra, gracias por ser como mis hermanas en Paris, gracias para todos los momentos que hemos vivido juntas. No quiero pensar com sería no vivir con vosotras en la misma ciudad pero sé que vamos a tenernos para siempre y nunca olvidaré cuanto me habeis hecho mi vida feliz en Paris. Tommaso, thank you for being my go-to-person, for telling me what I needed to hear and for always wanting to

dance (at least before Covid19 hit). Danny, thank you for being so you, so honest and kind; I have loved traveling with you and cannot wait to do it again. I want to thank my other travel partner, Sammy! Our trip is one of my favourite highlights during these last four years and I couldn't have imagined a better travel partner. Thank you also for making pani-puri nights so cool and for teaching me so much more about the Indian cuisine.

To my friends in Palestine, thank you to Anas, for being the most genuine person I have met, for your kindness and for encouraging me to keep going further. And of course Bisan, the famous Biso, for making the world such an adventurous place, for reminding me to never get stuck in my comfort zone and to be curious about new hobbies and activities.

I want to thank my family. My khalo Waleed and Daud and my khalto Juana. Thank you for constantly wanting to know me better and for wanting to support me in any way possible. Khalto habeebti, you know you are my role model, thank you for inspiring me ever since I was a kid. To Razan, for making me believe you can get what you want when you want it bad enough. To Ammo George and aunti Norma, for giving me a home for four years and taking care of me like your daughter.

I want to thank Achille, for being the best part of my day, for making me feel so calm and for inspiring me to be more curious and ask challenging questions. Thank you for making this last year particularly special, habeebi.

My deepest gratitude goes to my parents, brother and sister. Mama, baba, thank you for everything. For the constant support and understanding, for always being there and encouraging me not to give up and to keep trying. Thank you for teaching me to be optimistic and grateful and to always try to put things in perspective. Thank you for always being interested in what I do and for always putting my education as well as Nader's and Irene's as priority. Nader, habeebi, thank you for being so honest and always being by my side and Irene for being an amazing inspiration and support and for being able to make me laugh wholeheartedly.

Finally, I want to dedicate this thesis in memory of my late grandparents, Sido Butros Eweis and Teita Hind Abdullah. They were both passionate about education and knowledge. Sido's kindness and love for learning and mastering different languages by himself has been an important inspiration for me. My very modern Teita taught me the love of maps, books, music, being strong-hearted and kind to all. I wish we had more time with you both.

Table of Contents

Preface

The fundamental process of asymmetric cell division (ACD) leads to daughter cells of distinct fates, and often, distinct size. ACD and its regulation have been well-studied in the hermaphroditic *Caenorhabditis elegans* embryo, especially concerning how symmetry of the actomyosin cortical cytoskeleton is broken by a sperm-derived signal leading to polarity establishment in the one-cell embryo. Importantly, asymmetric division of the one-cell embryo is conserved in all nematodes yet the cellular features as seen in DIC imaging are surprisingly highly variable. Investigating asymmetric division in non-*C. elegans* nematode embryos is key for a more complete understanding of the mechanisms behind this crucial process. For my PhD, I chose to examine ACD of single-cell embryos of *Diploscapter pachys* and *Pristionchus pacificus*. For the parthenogenetic nematode *D. pachys*, how polarity is triggered is a mystery since this species lacks sperm, the origin of the symmetry breaking cue in *C. elegans*. Despite also being hermaphroditic, *P. pacificus* displays exaggerated cortical shape changes as compared to *C. elegans* that I wanted to understand.

This thesis is divided into four chapters. In the first chapter, I introduce the importance of ACD and consequences of its misregulation, as well as the main model systems that have been used to understand the mechanisms of ACD. In the second chapter, I detail what is known about ACD in the well-studied *C. elegans* embryo. The third and fourth chapters summarize the results I obtained during my PhD, concerning *D. pachys* and *P. pacificus*, respectively. The third chapter begins with an introduction about *D. pachys*, and then follows the results I obtained for this embryo encompassing the major part of my PhD and a manuscript submitted for peer review. In the fourth chapter, I introduce *P. pacificus* and I describe the experiments I carried out in an attempt to obtain a transgenic worm line. A general conclusion closes the thesis with an appended annex section, consisting of the submitted manuscript on *D. pachys* and a published review article that I wrote during my PhD on the roles of actin in the morphogenesis of the *C. elegans* one-cell embryo.

Chapter 1: Mechanisms that orchestrate asymmetric cell division in different model systems

1.1. Introduction: Importance and implications of asymmetric cell division

The fundamental process of asymmetric cell division (ACD) entails the division of one cell giving rise to two cells with a distinct fate, and in most cases, of different size (elaborated on in section 1.4). The generation of this cell-type diversity is crucial in many biological contexts. In development, ACD is used to form different cell populations, which become different parts of the organism. The first cell division of the *Caenorhabditis elegans* embryo is such an event where the daughter cells have different fates and where only one daughter cell gives rise to germ cell descendants (Sulston et al., 1983). ACD of stem and progenitor cells leads to one self-renewing daughter cell to renew the stem cell population while the other cell differentiates. The first division of the mouse neocortical progenitor cells is also asymmetric, generating one stem cell-like progenitor cell and a differentiated cell. The progenitor cell is then able to divide again, either symmetrically or asymmetrically, making more progenitor cells or more differentiated cells as needed, a strategy to increase the number of neural cells produced from one starting progenitor cell (Costa et al., 2008; Pilz et al., 2018; Wang et al., 2009). During mouse oogenesis, oocytes divide asymmetrically in order to produce a large mature oocyte and a considerably smaller polar body containing unwanted DNA (Longo and Chen, 1985; Maro and Verlhac, 2002; Verlhac et al., 2000). Finally, erythroblasts undergo ACD with the aim of excluding the nucleus and producing an enucleated red blood cell (Keerthivasan et al., 2011; Koury et al., 1989; Simpson and Kling, 1967).

The ability to produce both self-renewing and differentiating daughter cells is a central feature of stem cell biology. In addition to the mouse neocortical progenitor cell mentioned above, other examples of stem/progenitor cells that go through ACD include mouse muscle cells (Shinin et al., 2006), mouse skin cells (Lechler and Fuchs, 2005), human and mouse intestinal cells (Quyn et al., 2010), mouse mammary gland tissues (Cicalese et al., 2009), and mouse haematopoietic precursor cells (Wu et al., 2007). In these cases ACD is a strategy for ensuring a balance between differentiated and self-renewing cells (Loyer and Januschke, 2020; Morrison and Kimble, 2006). In order to control the number of cells needed in case of injury and regrowth for example, stem cells can also divide symmetrically. Therefore, it is important that stem cells have the ability to switch between symmetric and asymmetric cell division. A defect in this balance or in the process of ACD can lead to complications in tissue homeostasis and repair.

Recent studies have emphasized that ACD is also important in oncogenic progression (Morrison and Kimble, 2006). Cancers can be heterogeneous and they can use self-renewal mechanisms for proliferation (Jaworska et al., 2020; Matsui, 2016). Studies in mouse model

systems have shown that stem cells are at the root of colon and brain tumours (Barker et al., 2009; Kwon et al., 2008). An over-proliferation of cells and even tumorigenesis have been identified as outcomes of dysfunctional ACD-related genes in the *Drosophila melanogaster* (Caussinus and Gonzalez, 2005). Defects in the process of ACD as well as the generation of a stem cell pool that loses control over growth and proliferation are important subjects under investigation. To understand or predict how these misregulations can arise, thorough studies of the mechanisms governing the process of ACD are crucial. The ability to observe cellular dynamics during the process of ACD in a cell and manipulate the genome to test the different players of the process are important qualities of a well-established model system. In the following section, I describe two such systems that have been used for decades in order to understand ACD.

1.2. Model systems used to study ACD

Among the well-studied model systems used to understand ACD are the *C. elegans* single cell embryo and the *D. melanogaster* neuroblast lineage. Pioneering research on both systems has lead to exciting discoveries that reveal the complex mechanisms regulating the process of ACD. Notably, the mechanisms controlling ACD are well conserved in both species.

The *C. elegans* single cell embryo is the result of oocyte fertilization upon passing through the spermatheca of the hermaphrodite worm where both male and hermaphrodite sperm are stored (Figure 1.1.A). The neuroblasts of the *D. melanogaster* are stem cell-like progenitors resulting from a delamination of the neuroepithelium. Neuroblasts go through ACD to bring about glial and neural cells of the embryo and larva (Prehoda, 2009). Due to some differences in the ACD process of embryonic and larval neuroblasts, only the embryonic *D. melanogaster* neuroblast is discussed here (Figure 1.1.B).

During the first division of the *C. elegans* embryo and the *D. melanogaster* neuroblast, one stem cell-like cell that sustains the ability to self-renew is produced, P1 in *C. elegans* and a daughter neuroblast (NB) in *D. melanogaster.* The other daughter cell inherits fate-determinants allowing it to produce differentiated descendants: in *C. elegans,* the AB or anterior cell and in *D. melanogaster*, the ganglion mother cell (GMC) (Figure 1.1).

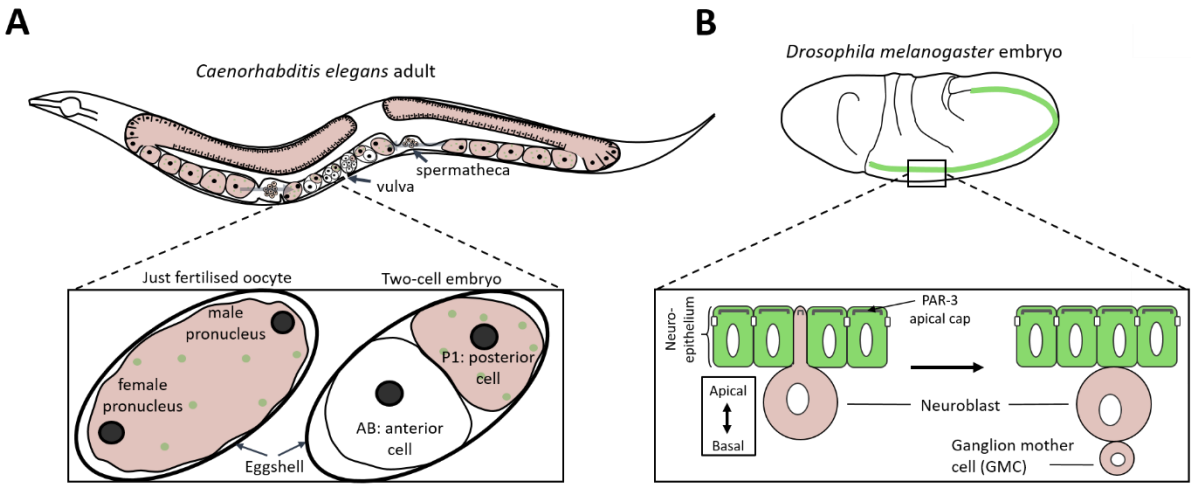

Figure 1.1. Anatomy of classic animal model systems used to study ACD. A. *C. elegans* hermaphrodite adult; zoom in on single cell and two-cell embryo (drawing inspired from *The Updike Lab*). **B**. Embryo of the *D. melanogaster;* zoom in on neuroblast cells (*adapted from Prehoda, 2009).*

As was mentioned, many different cell types undergo ACD. In the following sections, I will highlight the main features that accompany ACD and given that the *C. elegans* embryo and the *D. melanogaster* neuroblast are well-established model systems for ACD, I will carry out a brief description of as well as a comparison between the two species. I will also expand each section to briefly describe conserved mechanisms in other cell types. An elaboration on the mechanisms of ACD in the *C. elegans* embryo is in Chapter 2.

1.3. Mechanisms of cell polarity

1.3.1. Polarity establishment: initiation of cellular polarity

Two different mechanisms of polarization give rise to ACD. One mechanism relies on the asymmetric partitioning of cellular components leading to cell polarity and finally daughter cells of different cellular fate. Such a mechanism of polarity establishment and ACD is referred to as intrinsic (Figure 1.2) (Januschke and Gonzalez, 2010; Loyer and Januschke, 2020). Another mechanism, referred to as extrinsic, is the asymmetric exposure of the mother cell to external cues or the asymmetric positioning of the daughter cells relative to external cues (Figure 1.2) (Broadus and Doe, 1997; Siegrist and Doe, 2006). In the latter type, initially, daughter cells may be symmetric in cellular fate components and upon exposure to different signals from their environment, each cell acquires a different fate. In this context, the division is asymmetric as a result of the ultimate fate of the daughter cells even though the division of the mother cell was symmetric.

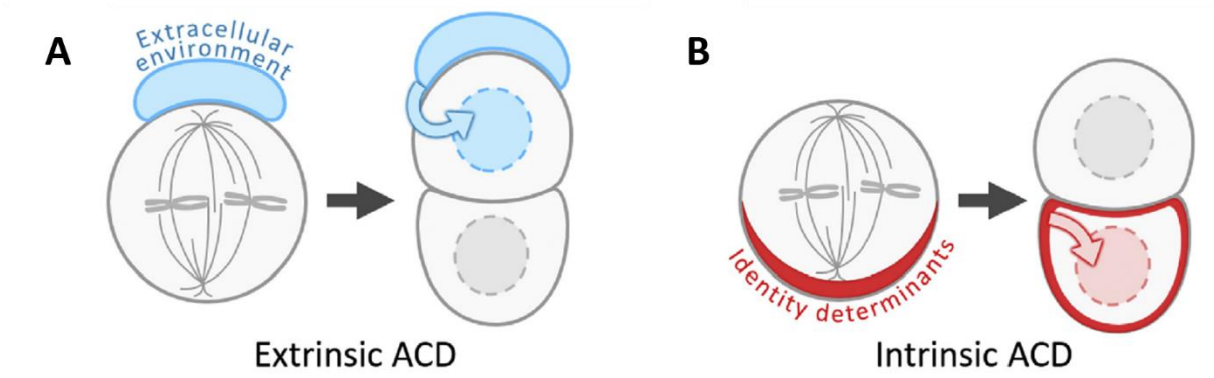

Figure 1.2. A. Extrinsic vs B. intrinsic signalling for polarity establishment (*adapted from Loyer and Januschke, 2020).*

In intrinsic ACD, the organization of cellular asymmetry leads to cell polarity wherein two different poles of the cell are biochemically and structurally distinct (Li, 2013; Loyer and Januschke, 2020). Cell polarity can dictate the orientation and position of the mitotic spindle due to the interaction of the cytoskeleton with the polarized cortical components that consequently specifies the final position of the cleavage site (Loyer and Januschke, 2020), although the manner in which events are coordinated in order to achieve ACD can vary in different cell-types. In ACD of the *C. elegans* embryo and the *D. melanogaster* neuroblast, cell polarity, spindle orientation and positioning, and cell division are synchronized in a clear hierarchal manner (Figure 1.1). In budding yeast, however, polarity of the cell is established in concomitant with site of division and prior to spindle positioning. In mouse oocytes the asymmetric positioning of the spindle leads to cell polarity and specification of the division site (Li, 2013).

Finally, in some cell types, both asymmetric exposure to extrinsic cues and intrinsic partitioning of fate regulators can regulate the asymmetric division process of one cell. Fertilization of the *C. elegans* oocyte by sperm initiates asymmetry and signalling from the neural epithelium orients the division of *D. melanogaster* neuroblast, an extrinsic cue in both cells induces an intrinsic cell polarity.

1.3.2. Polarity proteins

Upon receiving the extrinsic polarity signal, the *C. elegans* embryo and the *D. melanogaster* neuroblast both undergo intrinsic separation of cellular components, more specifically partitioning proteins (PAR) that lead to cell polarity and eventually two daughter cells, each of a distinct fate. In order for the *C. elegans* embryo and the *D. melanogaster* neuroblast to establish cell polarity, an asymmetric localization of the PAR proteins is required (Figure 1.3). The first study that lead to the discovery of these proteins was carried out in 1988 using the *C. elegans* single cell model (Kemphues et al., 1988) wherein *par* mutant embryos

gave rise to symmetric daughter cells and abnormal second cleavage patterns. The mechanisms of PAR protein localization in *C. elegans* are thoroughly reviewed in (Pacquelet, 2017; Rose and Gonczy, 2014).

A polarity cue from sperm components (discussed more thoroughly in Chapter 2) after fertilization of the *C. elegans* oocyte leads to symmetry breaking which involves a contraction of the cortex that drives a posterior-to-anterior flow. This cortical flow localizes anterior PARs (aPARs) to the anterior cortex including the oligomeric scaffold PAR-3, the adaptor PAR-6, the atypical kinase PKC-3 and the small GTPase CDC-42. In turn, the aPARs exclude the RING domain protein PAR-2 from the anterior cortex thus localizing it at the posterior pole along with the other posterior PAR proteins (pPARs): the kinase PAR-1, the tumor suppressor LGL-1 and a GTPase-activating protein (GAP) for CDC-42, called CHIN-1 (Goehring et al., 2011; Munro et al., 2004). A negative feedback loop created by mutually inhibitory interactions between pPARs and aPARs enhances the established polar asymmetry (details in section 2.2 and 2.3) (Goehring, 2014; Gonczy, 2008). At the anterior cortex, CDC-42 plays a role in polarity via direct binding to PAR-6 thus enhancing PAR-6 accumulation at the anterior pole (Aceto et al., 2006). PKC-3 inhibits the anterior localization of pPARs via direct phosphorylation. PKC-3 is also an essential partner of PAR-3 and PAR-6 and PKC-3/PAR-3/PAR-6 clusters form at the anterior pole for maintaining PAR polarity. At the posterior cortex, PAR-2 recruits PAR-1 which inhibits PAR-3 localization at the posterior cortex. Astral microtubules emanating from the sperm centrosome also have a role in polarity by protecting PAR-2 at the posterior cortex from inhibitory effects of PKC-3 (more on PAR protein regulation in section 2.2 and 2.3) (Motegi et al., 2011).

The neuroepithelium of the *D. melanogaster* embryo exhibits a polarity due to increased PAR-3 (Bazooka or Baz in *D. melanogaster*) localization at the apical cap (Figure 1.3.B) (Prehoda, 2009). This polarity is inherited by the *D. melanogaster* neuroblasts delaminating from the epithelial layer and the PAR-3 apical cap is further enhanced by a series of phosphorylation of the aPARs driven by the mitotic kinase Aurora-A during late interphase all through the end of cell mitosis (Wirtz-Peitz et al., 2008). Apical PAR-3 engages with Cdc-42 in order to recruit and activate PAR-6 and atypical kinase aPKC. The apical aPKC/PAR-3/PAR-6 network ensures an exclusion of GMC fate determinants from the apical pole and the activation of aPKC leads to the displacement of the scaffold protein Miranda (Mira) from the apical cortex to the basal cortex (Figure 1.3.B) (Atwood and Prehoda, 2009). The basal localization of Mira is not entirely dependent on aPKC activation as the actomyosin network also has a central role for the proper localization of both Mira at the basal cortex and the aPKC/PAR-3/PAR-6 at the apical cortex (Prehoda, 2009).

PAR proteins are conserved across many organisms and Cdc-42 also plays a central role for achieving cell polarity in most eukaryotic cells (Etienne-Manneville, 2004). PAR-3, for example, is found in mammals as PARD3 and PAR-3 like (PARD3B) that localize apically or at junctions, respectively, in different cell types, reviewed in (Thompson, 2021). Moreover, the regulation of ACD via the aPKC/PAR-3/PAR-6 network is found not only in the *D. melanogaster* and *C. elegans* but also in the mouse and chicken (Ohno, 2001; Suzuki and Ohno, 2006).

The cell polarity attained by the asymmetric placement of the PAR proteins at their respective poles is important in dictating the subsequent steps for achieving ACD in the *C. elegans* embryo and *D. melanogaster* neuroblast (Figure 1.3).

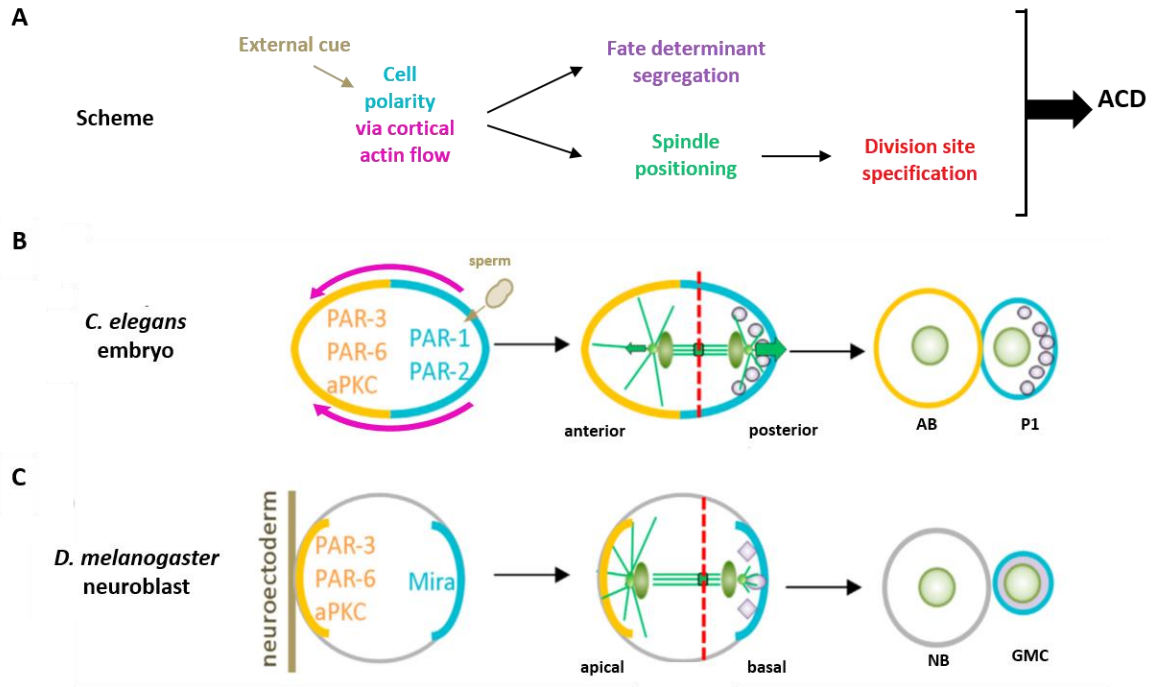

Figure 1.3. ACD in two well-established model systems. A. Scheme for sequence of events leading to ACD. ACD in the **B.** *C. elegans* embryo and **C.** *D. melanogaster* neuroblast *(adapted from Rong Li, 2013).*

1.4. Daughter cells: differentiation of cellular fate and size

1.4.1. Cell fate determinants of the differentiated cell

As I previously introduced, a smaller posterior P1 cell from the first division of the *C. elegans* embryo is produced which gives rise to the germline of the worm and some somatic lineages while the anterior AB cell only generates somatic cells. The segregation of polarity proteins during ACD assigns germ plasm fate determinants such as PIE-1, POS-1, MEX-1 and MEX-3 to the posterior cell. These proteins play a role in controlling mRNA translation of the P blastomeres (P-cell lineage) and a loss of function of any one of them leads to embryonic lethality (Wang and Seydoux, 2013). The MES-1 protein is assigned to the posterior cell in order to regulate the cell-cell signalling in later embryonic stages. Without MES-1, the fate of the fourth P-cell is lost and germ cells are not produced, thus bringing about a sterile worm (Berkowitz and Strome, 2000; Strome et al., 1995). While RNA-rich granules (P granules) were previously thought to be necessary for proper germ cell production, the concentration of P granules does not necessarily correlate with the generation of germline cells (Gallo et al., 2010).

Similarly, in the *D. melanogaster* neuroblast, the evolutionarily conserved cell fate determinant Numb is asymmetrically distributed during mitosis to the daughter cell destined for differentiation (GMC) as a result of Mira localization at the basal cortex. Numb is a

repressor of the Notch signalling pathway and plays an important role for neural differentiation and regulation of embryonic development. *D. melanogaster* embryos carrying a *numb* mutantion undergo a significant reduction in number of neurons (Rhyu et al., 1994; Uemura et al., 1989). Correct gene expression in differentiated daughter cells of the *D. melanogaster* neuroblast require another fate determinant called Prospero, a transcription factor, which colocalizes strongly with Numb (Hirata et al., 1995; Knoblich et al., 1995). Both Numb and Prospero are localized asymmetrically as a result of proper cell polarity.

The asymmetric segregation of fate determinants, especially in regards to mRNA, has been demonstrated in other systems such as budding yeast, ascidian eggs, mouse embryos, Xenopus embryos, *D. melanogaster* oocytes and chick embryos (Johnston, 1995; Wang et al., 2018; Yamada et al., 2005). In the *D. melanogaster* oocyte, for example, *oskar* mRNA localizes to the cell posterior via transport along polarized microtubules. The asymmetric segregation of *oskar* mRNA leads to recruitment and anchoring of germ plasm components to the posterior cortex that determine cell fate (Tanaka et al., 2021). In budding yeast cells, Ash1 mRNA, cell fate determinant, is organized into particles and anchored at the cortex of the cell distal tip via transport along actin filaments, thus giving rise to an asymmetric distribution of proteins that determine cell fate (Takizawa et al., 1997).

1.4.2. Positioning of the mitotic spindle

Daughter cell size of the *D. melanogaster* neuroblast and the *C. elegans* embryo is determined by the position of the cleavage furrow, which in turn is controlled by the position of the mitotic spindle (Glotzer, 2004). A mitotic spindle placed in the center of the cell gives rise to two daughter cells of the same size. Upon displacement of the spindle closer to one pole, one larger and one smaller daughter cell are produced. Extreme asymmetry due to a large displacement of the spindle is sometimes necessary like in the case of polar body exclusion and enucleation although generally, cell size asymmetry in mitotic division of somatic cells is mild (Neumuller and Knoblich, 2009). In the *C. elegans* embryo and the *D. melanogaster* neuroblast, the spindle is initially placed at a central location of the cell. During anaphase, there is net movement of the spindle towards one pole where an asymmetric cleavage plane is set, thus, generating a smaller daughter cell (P1 in *C. elegans* and GMC in *D. melanogaster*).

The asymmetric displacement of the spindle in the *C. elegans* embryo is carried out by pulling forces primarily generated by the microtubule motor protein dynein. Dynein is recruited to the cell cortex by a ternary complex composed of two G-protein coupled receptors called GPR-1 and GPR-2, a large coiled-coil protein LIN-5, and heterotrimeric G protein alpha subunits Gα. An enrichment of GPR proteins is observed at the posterior cortex in a PAR-2- and PAR-3-dependent manner (Park and Rose, 2008). The posterior-directed spindle movement is a result of increased dynein motor activity on the microtubules at the posterior cortex (details in section 2.5), possibly due to asymmetric localization of GPR proteins (Rodriguez-Garcia et al., 2018). While in *C. elegans* the increased localization of GPR

proteins at the posterior cortex is opposite the PAR-3 anterior localization, in *D. melanogaster* neuroblasts, both PAR-3 and the GPR-1/2 homologue Pins localize at the apical cortex. The apical positioning of PAR-3 leads to recruitment of an adaptor protein called Inscuteable (Insc) that interacts with Pins and recruits it to the cortex (Morin and Bellaiche, 2011). Two different pathways via Pins exist in order to orient and position the spindle prior to pulling forces via Dynein/Dynactin interaction. Comparable to *C. elegans*, division of the neuroblast produces daughter cells of different size as a result of spindle asymmetry established during anaphase (Kaltschmidt et al., 2000; Morin and Bellaiche, 2011). However, unlike the asymmetric displacement of the spindle during anaphase in the *C. elegans* embryo due to posterior pulling forces, the neuroblast spindle asymmetry is dependent on the apical spindle arm itself. At the onset of anaphase, the spindle !:become shorter at the basal side thus effectively shifting the cleavage plane toward the basal cortex and leading to a GMC significantly smaller than the sibling neuroblast (Figures 1.B and 3.C) (Kaltschmidt et al., 2000).

Important to note is that while spindle displacement is evident in the *C. elegans* embryo for an asymmetric cleavage, in *C. elegans* Q. neuroblasts, a different mechanism exists. Spindle elongation, similar to that in *D. melanogaster* neuroblast, is also observed in *C. elegans* QR.a cell (daughter cell of first QR neuroblast ACD), however, one study showed that myosin polarization at the anterior pole is the main drive for an asymmetric cleavage. Increased stiffness and constriction the anterior pole due to myosin results in a cleavage closer to the anterior pole and two asymmetric daughter cells (Ou et al., 2010). A spindle-independent mechanism for determining the cleavage furrow site has also been revealed in the *D. melanogaster* neuroblast (Cabernard et al., 2010). In neuroblasts that lack the mitotic spindle, the basal localization of furrow proteins Pavarotti, Anillin and Myosin via cortical proteins can displace the furrow towards the basal side bringing about an asymmetric cleavage. This study highlights the existence of a cleavage furrow displacement mechanism that maybe be part of redundant pathways in the *D. melanogaster* neuroblast but dominant in other species for example.

The ternary complex is also conserved in vertebrates and exists as NuMA-LGN-Gαi where NuMa is the microtubule binding protein, LGN, the linker protein and Gαi1/2/3, the membrane-binding proteins. In most cells, the positioning and/or orientation of the spindle is driven by the motor dynein and the ternary complex. Astral microtubules are pulled on either via dynein sliding on microtubules and/or the use of the energy from coupling microtubule depolymerization with anchorage at the cortex, reviewed in (Kiyomitsu, 2019). Dynein-independent mechanisms of spindle positioning have also been reported wherein myosin (Myo10) directly binds to microtubules and has a role in orienting the centrosome and spindle in mammalian cells (Kwon et al., 2015).

1.4.3. Physical asymmetry of daughter cells

An intriguing question following the previous section is, why does the cell go through such intricate mechanisms for spindle displacement when fate determinants have already

been partitioned in the *C. elegans* embryo and *D. melanogaster* neuroblast. Is the physical asymmetry of the daughter cells vital for continued and successful development?

Previously, achieving similar size daughter cells from the *C. elegans* single cell embryo was attempted by manipulation of the PAR proteins (Kemphues et al., 1988) or the spindle positioning protein machinery at the cortex (Colombo et al., 2003; Gotta and Ahringer, 2001; Gotta et al., 2003). However, since the first approach alters with intrinsic cellular components and the second approach leads to severe division defects, the significance of asymmetry solely based on the size of the daughter cells could not be determined. A study published just this year was the first to describe the significance of establishing a physical asymmetry of the *C. elegans* daughter cells (Jankele et al., 2021). By using two different sophisticated systems that targeted spindle positioning during metaphase, they were able to generate similar size daughter cells and they discovered that indeed the size of the daughter cells matters. The embryonic development of *C. elegans* is compromised significantly upon equalizing of daughter cell size. The more equal in size the daughter cells were manipulated to be lead to a higher percentage of embryonic lethality (Jankele et al., 2021). Lethality due to equalized daughter cell size could be due to improper localization of components needed for later cell divisions or disrupted cell-cell interactions of later embryonic stages.

Generation of equal sized daughter cells of the *D. melanogaster* neuroblast has been carried out by either disrupting the asymmetric segregation of basal determinants (Kitajima et al., 2010) or by disrupting the spindle orientation but with no effect on apical/basal cortical polarity (Cabernard and Doe, 2009) or altering Myosin flow for cleavage mispositioning (Roubinet et al., 2017). The neuroblast in the first two studies gave rise to equally sized cells of neuroblast identity, thus losing the ability to produce differentiated cells from the first division.

1.5. Conclusion

The comparison between different models presented this chapter emphasizes the importance of ACD and the conserved and different regulatory mechanisms of the process. As was highlighted, the *D. melanogaster* and *C. elegans* single cell embryo are classic model organisms that have been in use since the 1980s. Research on these animals continues to bring interesting and new insights about the process of ACD. In chapter 2, the *C. elegans* single cell ACD model will be presented in further details as concerns ACD regulation studies that have been made possible due to the availability of extensive tools for observing and manipulating this species.

Chapter 2: The *Caenorhabditis elegans* embryo: a model organism for understanding symmetry breaking and asymmetric cell division

2.1. Chapter preface

As briefly introduced in chapter 1, the *C. elegans* single cell embryo has been studied extensively in order to understand symmetry breaking, polarity establishment, spindle positioning, and the cell shape changes that accompany ACD. A scheme below summarizes the main events of the ACD process in the one-cell *C. elegans* embryo that I will describe in this chapter. Briefly, in the just-fertilized zygote (Figure 2.1.A), cortical ruffles are evident all around the circumference of the embryo due to the highly dynamic and contractile cortical actomyosin layer. Symmetry is broken when the sperm contents approach the future posterior pole locally downregulating contractility there and initiating the retraction of the actomyosin cortex to the future anterior pole (Figure 2.1.B). This flow of actomyosin density towards the anterior pole leads to an invagination at the boundary between high and low actomyosin activity similar to ruffles but much deeper, called the pseudocleavage furrow (Figure 2.1.C). Anterior-directed cortical flow is concomitant with the segregation of the aPARs to the anterior of the embryo, while pPARs are recruited to the posterior cortex (Figure 2.1.B-D). During cortical polarity establishment, the maternal and paternal pronuclei meet at the posterior pole (Figure 2.1.D), and migrate to the cell center in a microtubule-dependent manner (Figure 2.1.E) (microtubules will be discussed but not shown in scheme below). During anaphase, the mitotic spindle is subsequently off-centered as a result of an imbalance of microtubule pulling forces from the anterior versus the posterior cortex (Figure 2.1.F), resulting in unequally-sized daughter cells (Figure 2.1.G).

In this chapter, I will summarize and discuss the studies that have revealed how ACD of the single-cell *C. elegans* embryo is brought about.

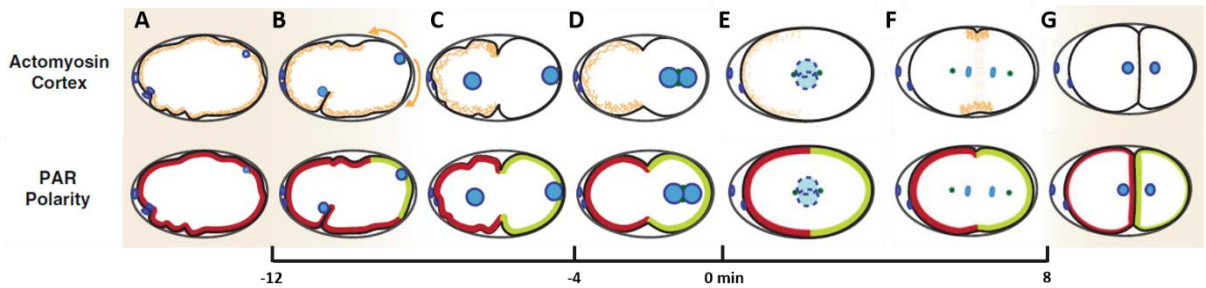

Figure 2.1. Scheme of main events of ACD in the *C. elegans* embryo. aPARs: PAR-3/PAR-6/PKC-3 represented in red colour in PAR polarity panel and pPARs: PAR-1 and PAR-2 represented in green. Microtubules not shown here (*adapted from Begasse and Hyman, 2011*).

2.2. Maturation and fertilization of the oocyte

At the distal end of the gonad arms of the *C. elegans* worm are proliferating germline stem cells (Huelgas-Morales and Greenstein, 2018) (Figure 2.2.A). As the worm develops, cells move closer to the spermatheca, which is situated at the proximal end of the gonad arm, enter meiosis I and consequently differentiate into oocytes (Figure 2.2.A). The oocyte in closest proximity to the spermatheca is called the -1 oocyte. It is arrested at meiotic prophase I and only resumes maturation when it receives a sperm-secreted signal called major sperm protein (MSP) (Figure 2.2.B) (Huelgas-Morales and Greenstein, 2018). The nucleus of the -1 oocyte is moved to the distal pole of the cell, and the nuclear envelope breaks down as it enters meiotic M phase (Figure 2.2.B) (McCarter et al., 1999). Nuclear envelope breakdown allows access of the chromosomes (highly condensed bivalents at this stage) to microtubules, thus bringing about the assembly of the acentriolar meiotic spindle (McNally, 2013). A morphological transformation accompanies meiotic maturation of the oocyte via cortical rearrangement, and the shape of the oocyte changes from cylindrical to ovoid (Figure 2.2.B) (McCarter et al., 1999).

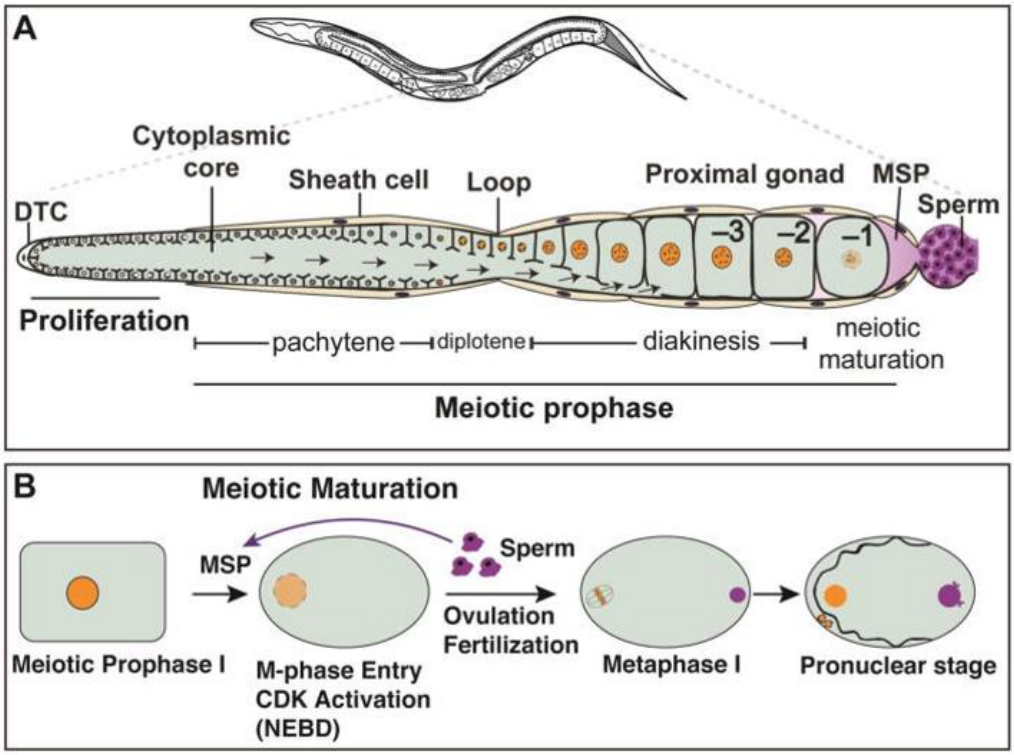

Figure 2.2. Oocyte meiotic maturation in *C. elegans*. A. The *C. elegans* hermaphrodite gonad is composed of two U-shaped arms (one shown here). Meiotic maturation is spatially restricted to the most proximal (−1) oocyte. **B.** The -1 oocyte undergoes meiotic maturation in response to MSP from sperm (purple) (*from Huelgas-Morales and Greenstein, 2018)*.

The maturation of the oocyte and ovulation, involving the passage of the oocyte from the gonad into the spermatheca, occurs approximately every 23 minutes in *C. elegans* hermaphrodite worm (McCarter et al., 1999). The MSP signal released by the sperm becomes

distributed in the entire gonad arm in a gradient manner with the highest concentration near the spermatheca (Huelgas-Morales and Greenstein, 2018). Importantly, the sheath cells of the worm gonad act as the main MSP sensor and only allow maturation of the oocyte in the presence of sperm. Therefore, in unmated, feminized worms, due to the absence of sperm and MSP, the sheath cells inhibit maturation of oocyte arresting them in diakinesis (Govindan et al., 2006; Hall et al., 1999; Huelgas-Morales and Greenstein, 2018).

The arrested oocyte is initially unpolarized due to the uniform localization of PAR-2 at the cortex of the oocyte, and the absence of cortical PAR-6 (Figure 2.3) (Reich et al., 2019). Prior to the fertilization of the oocyte, two kinases, aurora-A kinase (AIR-1) and polo-like kinase (PLK-1) maintain this unpolarized state (Reich et al., 2019). In *plk-1* and *air-1* oocytes, higher levels of anterior PAR-6 is observed associating at the cell membrane as compared to wild-type oocytes, indicating premature membrane association (Figure 2.3.B). Even more striking is that while in wild-type oocytes, PAR-2 is lost uniformly from the membrane during ovulation, in *air-1* and *plk-1* oocytes, PAR-2 remains membrane-bound at the oocyte pole closer to the spermatheca (Figure 2.3.C). AIR-1 and PLK-1 thus prevent early loading and/or polarization of PAR proteins at the membrane, enforcing the dependence on the mature sperm centrosome cue (Reich et al., 2019).

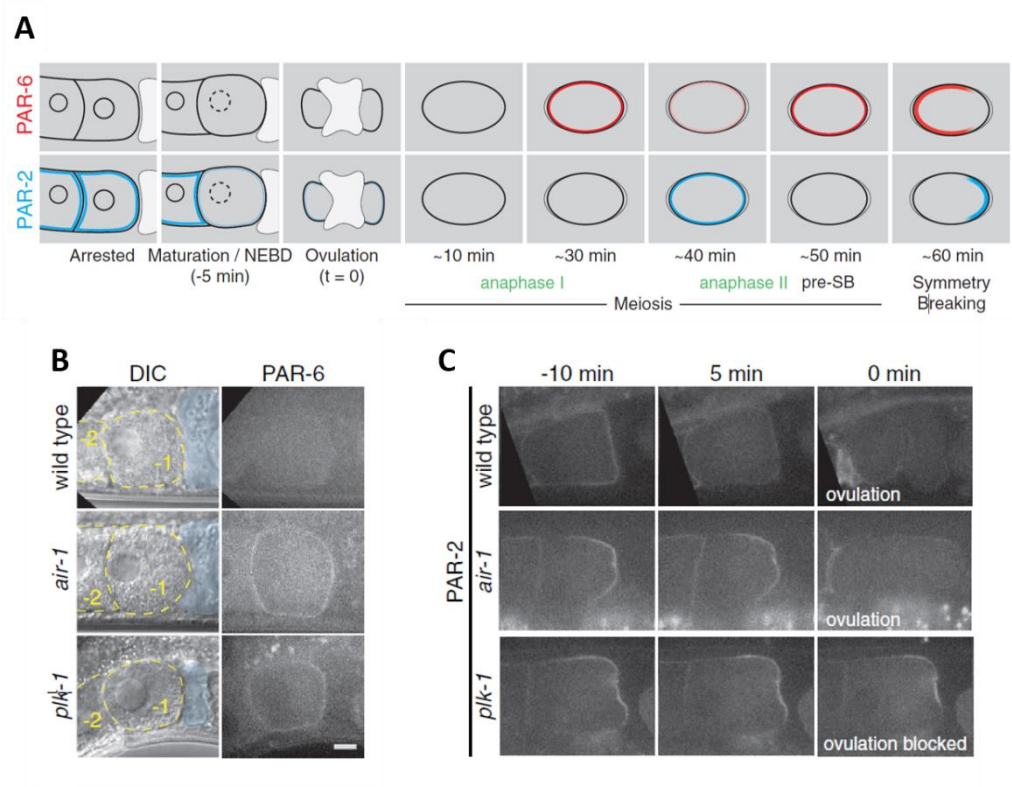

Figure 2.3. AIR-1 and PLK-1 Suppress Premature PAR Network Activation and Responsiveness to Polarizing Cues. A. Scheme of PAR-2 and PAR-6 in wild-type oocytes and embryos. **B.** Premature PAR-6 membrane association in *air-1; plk-1* oocytes. Dashed yellow lines mark -1 oocytes. Spermatheca are in blue. **C.** PAR-2 asymmetry in *air-1; plk-1* -1 oocytes *(adapted from Reich et al., 2019).*

Upon fertilization of the oocyte inside the spermatheca, the zygote begins to form an extracellular matrix known as the eggshell, which provides the zygote with physical protection

(Olson et al., 2012). Fertilization also triggers cytoplasmic streaming in the embryo, as evidenced by the movements of yolk granules, which are transported by kinesin-1 around the entire embryo (McNally et al., 2010). During this time, the cortex of the embryo remains isotropic, and the female pronucleus is undergoing meiotic divisions at what will become the anterior pole of the embryo. It is important that the sperm contents, including genetic material, be retained at the site of sperm entry at the posterior pole despite cytoplasmic streaming so as not to interfere with the completion of meiosis. This posterior limitation of the sperm DNA is due to cortical actin, which keeps the sperm DNA from getting captured by the meiotic spindle, by an as-yet-unidentified mechanism (Panzica et al., 2017). In embryos where actin polymerization is reduced, either by interfering with the actin assembly proteins or by applying inhibitory drugs, the sperm DNA is distributed throughout the embryo because of cytoplasmic flows.

2.3. Breaking symmetry: initiation of cell polarity

2.3.1. Site of polarity cue

As was mentioned already, the newly fertilized *C. elegans* zygote is unpolarized or 'axially naïve' and the first visual sign of asymmetry is the loss of cortical contractility (smoothening) over the future posterior pole, while the anterior cortex remains active (ruffling). In 1996, an important study put forth how establishment of the anteroposterior (AP) axis of the embryo is determined by sperm entry (Goldstein and Hird, 1996). Sperm contents are generally found at the pole opposite that of the female pronucleus, and that is where the posterior pole forms (Figure 2.4.A). However, Goldstein and Hird observed that in some mutants, the sperm was adjacent to the female pronucleus, but the sperm location still coincided with the future posterior pole (Figure 2.4.B).

The study concludes that upon fertilization, the sperm or sperm-derived pronucleus/centrosome complex (SPCC) causes a cytoplasmic arrangement in the embryo that generates the AP asymmetry. In some other cases, sperm entry was described to occur at lateral sides of the embryo and due to cytoplasmic rearrangement initiated by the sperm, the sperm is repositioned to the closest pole (Figure 2.4.C).

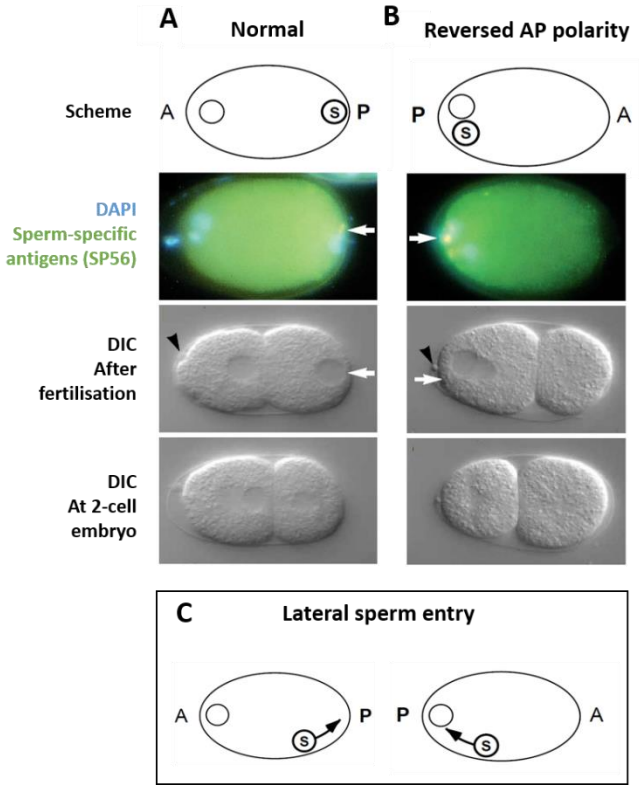

Figure 2.4. The AP axis is specified by the sperm; **A.** normal and **B.** reversed. Scheme in top panel shows embryo AP-axis specification determined by sperm entry. Arrowhead in images marks polar body at the future anterior end. Arrow marks male pronucleus. Lowest panel: 2-cell stages; the smaller cell (P1) forms on the side in which the sperm entered. **C**. The sperm enters in other locations (lateral entries): sperm moves to closest pole due to cytoplasmic flows *(adapted from Goldstein and Hird, 1996).*

A recent study confirmed and built on the 1996 result, using live imaging to reveal that fertilization always occurs at the pole opposite of the female pronucleus (Figure 2.5) (Kimura and Kimura, 2020). Infrequently, prior to symmetry breaking, a flow of the cytoplasm driven by kinesin-1 or UNC116 in *C. elegans* occurs and shifts sperm components away from the cortex (McNally et al., 2012; McNally et al., 2010). As mentioned above, actin filaments at the cortex have a role in limiting this movement (Panzica et al., 2017). However, in some zygotes, the sperm components are shifted by the meiotic cytoplasm flow to the opposite pole where the female pronucleus is located. The polarity cue is initiated at that pole upon centrosome maturation, leading to symmetry breaking and actomyosin contractility away from the centrosome, thus determining the posterior pole (Figure 2.5).

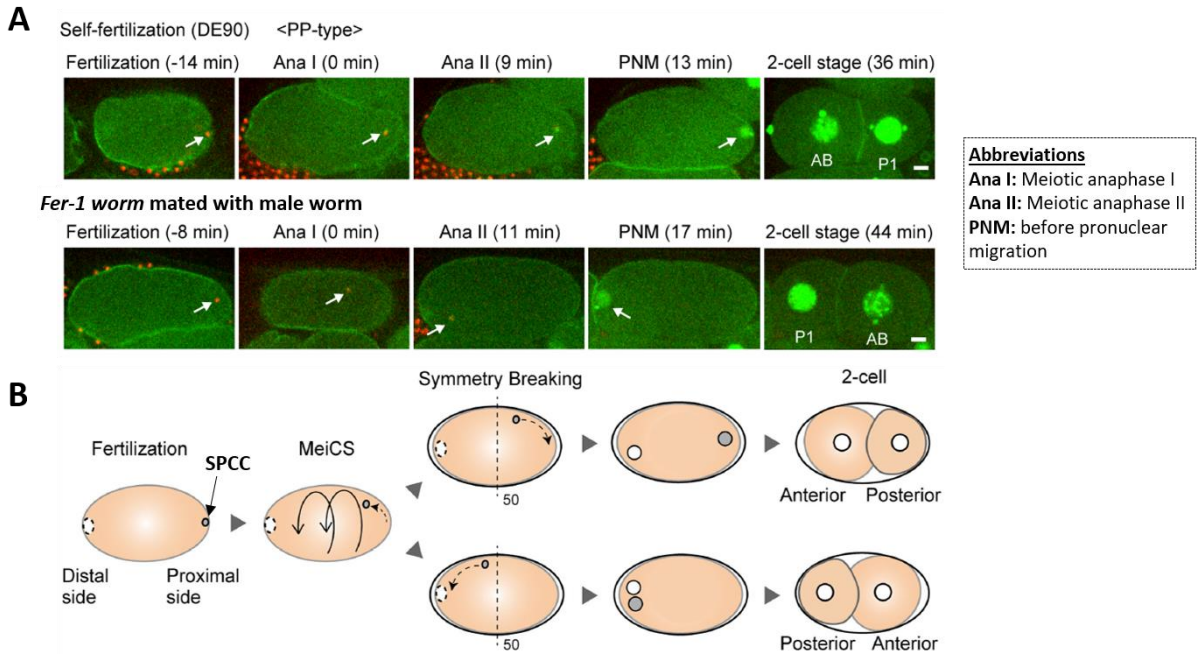

Figure 2.5. SPCC stochastically moves within the zygote before cell polarization. A. Time series images of *C. elegans* zygotes (DE90 strain) expressing mCherry::histone, GFP::PH, GFP::histone and TBG-1::GFP at different stages. White arrows indicate position of SPCC. Representative examples of reversed anteroposterior axis specification shown in bottom panel. The timing of meiotic anaphase I is set to 0 min. Scale bars 5 µm. **B.** Summary of the SPCC dynamics during cell polarization *(adapted from Kimura and Kimura, 2020).*

Importantly, this study sheds light on the misleading use of the term 'sperm entry' to describe the site of polarity cue. In fact, the site of polarization is the final SPCC position upon centrosome maturation. A significant delay exists between fertilization and symmetry breaking as a result of extensive regulation of signalling specific to a mature centrosome and also due to the presence of meiotic streaming, the site of entry does not always correspond to the site of polarization (Cowan and Hyman, 2004; Goldstein and Hird, 1996; Schierenberg, 1996). Furthermore delaying or blocking maturation of the centrosome leads to delays or failures in polarity establishment even though sperm entry was normal in these cases (Cowan and Hyman, 2004; Cowan and Hyman, 2006; Hamill et al., 2002; O'Connell et al., 2000).

2.3.2. Molecular nature of the polarity cue

Although for a long time fertilization was known to trigger symmetry breaking of the zygote, what remained to be identified was the mechanism and molecular nature of the polarity cue delivered during fertilization. It had been shown that anucleate sperm can induce posterior cortical polarity, indicating that the polarizing cue is not the sperm nucleus (Sadler and Shakes, 2000). The sperm-derived centrosome came on stage for its role in symmetry breaking when ablation experiments of the centrosome and silencing of genes of centrosome-related proteins resulted in a delay or even absence of anterior-directed contractility and the lack of polarization of PAR-2 proteins at the posterior pole (Cowan and Hyman, 2004; Hamill et al., 2002; Munro et al., 2004; O'Connell et al., 2000; Siegrist and Doe, 2007). Importantly,

ablation of the centrosome after polarity is induced does not block polarity establishment or maintenance indicating that the centrosome is required only for initiating polarity (Cowan and Hyman, 2004).

Building on the role for the sperm centrosome in symmetry breaking, in 2006 several studies presented the molecular links between fertilization and local weakening of the actomyosin network. While these studies pointed out that weakening of the actin network requires CYK-4, a RhoGAP, highly enriched on sperm associated membranes that modulates RHO-1 local activity thus clearing posterior RHO-1 & ECT-2 (RhoGEF) proteins (Jenkins et al., 2006; Motegi et al., 2006; Schonegg and Hyman, 2006), later studies contradicted the findings. A study showed that in CYK-4 mutated embryos, the anterior-posterior polarity is not affected and asymmetric daughter cells similar to wild-type embryos are produced shedding doubt on the role of CYK-4 in symmetry breaking (Zhuravlev et al., 2017).

The role for the centrosomal mitotic kinase Aurora A (AIR-1) in local inhibition of actomyosin contractility was revealed only in 2019 (Figure 2.6) (Kapoor and Kotak, 2019; Klinkert et al., 2019; Zhao et al., 2019). The phosphorylated, active form of AIR-1 is released from the centrosomes into the cytoplasm which then drives the inhibition of cortical actomyosin contractility in the vicinity of the centrosomes at the posterior of the embryo (Figure 2.6). It was observed that embryos with a GFP-tagged version of AIR-1 were not completely wild-type, but they carried out most AIR-1-dependent processes normally, including centrosome maturation. The AIR-1 GFP-tagged embryos however failed to correctly clear actomyosin from the future posterior pole during symmetry breaking. This effect was suggested to be due to a defect in diffusion of the GFP-labelled protein (Zhao et al., 2019). Experiments in which the position of the centrosome was manipulated supported this hypothesis wherein moving the centrosome closer to the cortex improved the actomyosin clearing defect while moving it further away from the cortex exacerbated the actomyosin clearing defect (Zhao et al., 2019). The studies demonstrated that the role of AIR-1 in symmetry breaking was a result of its effect on ECT-2, altering its localization and perhaps its GEF activity by an unknown mechanism, and thus decreasing RHO-1 activity and the activity of its downstream effector myosin.

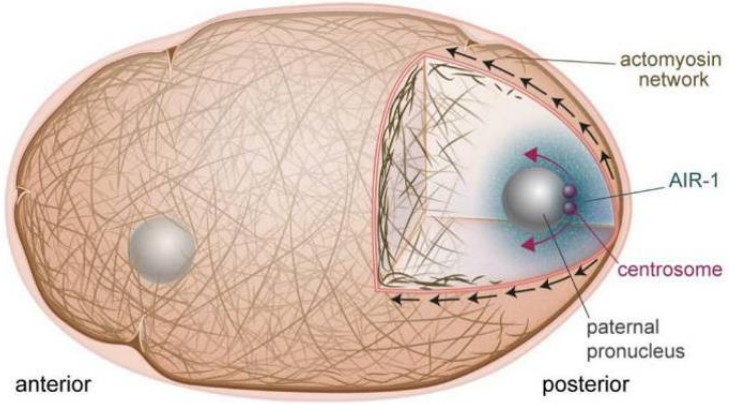

Figure 2.6. Symmetry breaking in the one-cell embryo. AIR-1 (blue cloud) diffuses from the centrosome (red spheres) and downregulates actomyosin at the adjacent cortex. This causes a local weakening, and produces cortical flows (black arrows) directed away from this point, which also serve to separate the centrosomes (red arrows) *(from Samandar Eweis and Plastino, 2020).*

In addition to its centrosomal role in initiating cortical flow, studies have also showed that non-centrosomal AIR-1 globally downregulates cortical actomyosin during polarity establishment. Embryos that lack AIR-1 show increased contractility of the cortex, and become bipolar with reduced non-muscle-myosin II (NMY-2) and increased PAR-2 at both poles (Figure 2.7.A and B). Weak cortical flows are also directed toward the embryo center from both poles in AIR-1 deficient embryos, while in control embryos, strong flows run from posterior to anterior poles (Figure 2.7.C) (Kapoor and Kotak, 2019; Klinkert et al., 2019; Reich et al., 2019; Zhao et al., 2019). Similar bipolarization of the embryo was also shown to occur in wild-type embryos when fertilized with acentrosomal sperm (Klinkert et al., 2019) meaning that centrosomal AIR-1 plays a key instructive role in preventing bipolarity and assuring asymmetry. The question then remains as to why PAR-2 domains occur at both poles. One study proposes that this could be due to curvature (Klinkert et al., 2019). They tested the hypothesis by placing *air-1* depleted embryos in triangular chambers and observed that PAR-2 domains emerged in regions with the highest curvature. The accumulation of PAR-2 at curved regions could be biochemically driven by lipid affinities or due to geometrical considerations, where the curved surface of the poles restricts diffusion out of the immediate vicinity (Figure 2.7.C) (Klinkert et al., 2019). These studies all together suggest that a basal activity of non-centrosomal AIR-1 exists for global downregulation of actomyosin and prevention of spontaneous PAR-2 bipolarization events of the embryo.

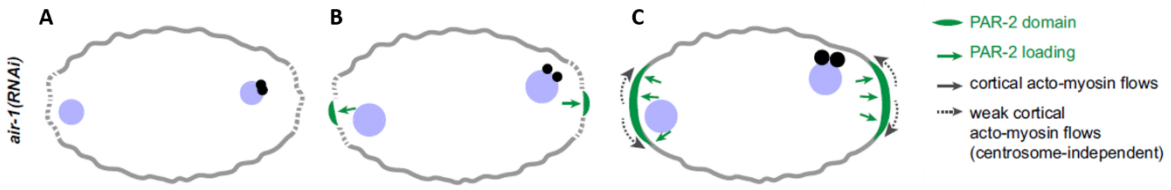

Figure 2.7. Working model of AIR-1 function during symmetry breaking in the bipolar phenotype in *air-1* RNAi embryos. A-C Upon *air-1*(RNAi), symmetry is broken spontaneously at the two poles of the zygote. **C.** Curvature-dependent PAR-2 membrane attachment increases the dissociation of NMY-2. Feedback loop created inducing weak cortical flows toward the center from either side, which drives the recruitment of more PAR-2 and the segregation of anterior and pPAR proteins (*adapted from Klinkert et al., 2019*).

Another important study published in 2020 highlighted the role of mitochondrial-hydrogen-peroxide signalling in symmetry breaking (De Henau et al., 2020). An enrichment of paternal mitochondria associated with the paternal pronucleus, as well as presence of maternal mitochondria (Figure 2.8.A), occurs in the area for symmetry breaking of the embryo and this is correlated with a local increase in cortical H_2O_2 (Figure 2.8.B and C). Moreover, this study shows via optogenetic manipulation that the release of H_2O_2 from the mitochondria is sufficient to induce symmetry breaking, however it is not sufficient to induce full polarity establishment as seen in unmanipulated embryos (De Henau et al., 2020). The signalling for symmetry breaking from the mitochondrial H_2O_2 could thus provide a partial explanation to the existence of centrosome-independent polarity cues.

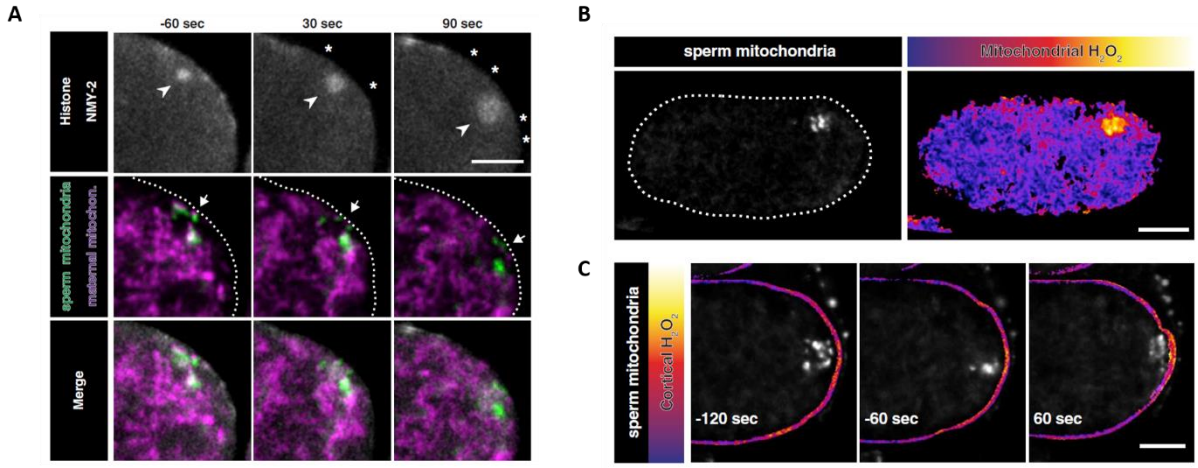

Figure 2.8. Sperm Mitochondria High in H_2O_2 Together with Maternal Mitochondria Promote Symmetry Breaking. A. Time-lapse images of a zygote with markers for NMY-2, histone, maternal, and sperm mitochondria (arrowhead/ paternal pronucleus; arrow: sperm mitochondria). **B**. Representative image of a zygote with markers for sperm mitochondria and outer mitochondrial H_2O_2 levels. **C.** Time-lapse images of a zygote with markers for sperm mitochondria and cortical H_2O_2 levels (A, C: t(0) = contact between paternal pronucleus and cortex). Scale bar 10 µm for B, 5 µm for A and C (*Adapted from De Henau et al., 2020).*

As seen in the preceding sections, the *C. elegans* single-cell embryo is an excellent system for revealing redundant and cryptic pathways in the important process of symmetry breaking. While we now know much more about the players and mechanisms giving rise to cell polarization, further studies on the dynamics and exact composition of the actin cytoskeleton and PAR proteins will be useful to decipher how this cell spatial organization is brought about.

2.3.3. Cortical flow and PAR proteins in cell polarity

As was briefly introduced in section 1.3.2 and the preface of this chapter, anterior-directed actomyosin contractility creates cortical flow important for setting the polarity axis of the embryo for both the actin cytoskeleton and PAR proteins (Figure 2.9). The flow of actomyosin density towards the anterior pole also leads to a traveling pseudocleavage furrow which then fades over the course of polarity establishment (Figure 2.9.A) (Munro et al., 2004; Reymann et al., 2016).

In addition to the two-way street of PAR and cortical actin co-regulation, a recent novel study indicates a role for cytoplasmic flows in polarity establishment. A focused-light-induced cytoplasmic streaming (FLUCS) system induces controllable cytoplasmic flows in the embryo via temperature changes, and these cytoplasmic flows are shown to drive cortical flows mirrored by PAR protein domain relocation (Mittasch et al., 2018). Upon moving the PAR-2 domain to the anterior pole by flow, the embryo divided with an inverted size asymmetry (smaller anterior cell).

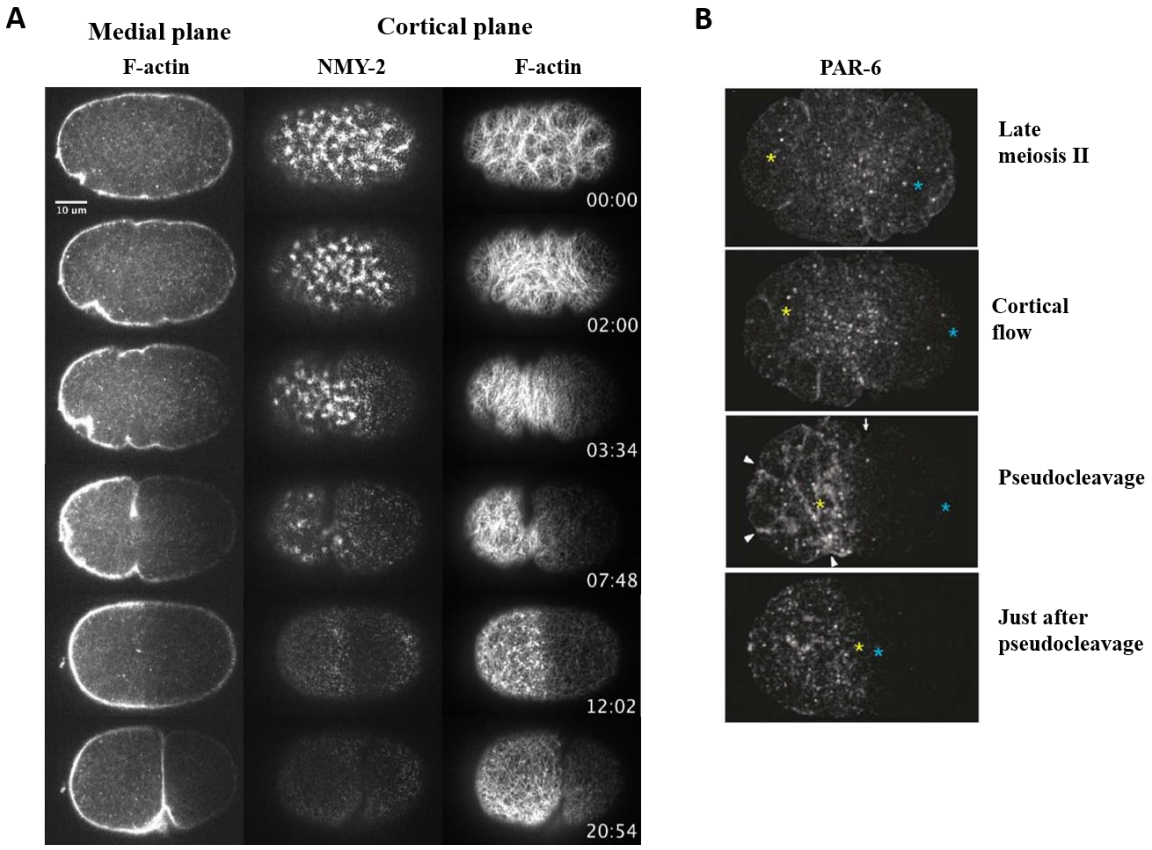

Figure 2.9. Actomyosin and PAR-6 distribution during ACD of the single cell *C. elegans* embryo. A. Actomyosin gel dynamics in the *C. elegans* zygote. Cortical and medial planes of an embryo expressing both Lifeact::mKate2 and endogenous NMY-2::GFP. Time indicated on bottom right (min:s). (*Adapted from Reymann et al., 2016*). **B.** Cortical transport of PAR-6::GFP establishes an anterior PAR-6::GFP cap, shown in embryo from late meiosis II to just after pseudocleavage (*adapted from Munro et al., 2004).*

While actin flows contribute to PAR localization, actomyosin tension can also affect the biochemistry of PAR proteins. A recent study shows that actomyosin tension causes conformational changes in PAR-3 thus allowing for PAR-3 oligomerization (Wang et al., 2017). PAR-3 clusters are lost in embryos lacking cortical tension molecules like NMY-2, however, they can be rescued by artificial increases in cortical tension applied via osmotic shock for example. The oligomerization of PAR-3 is important because it induces clustering of PKC-3, and the clustering of both proteins is important for their proper transport to the anterior pole (Wang et al., 2017). Clustering can reduce diffusion and increase association with cortical actomyosin layer, both of which could favor advective transport by flows (Rodriguez et al., 2017). Indeed longer residence time of PAR-3 oligomers at the cortex has been linked to more efficient transport (Dickinson et al., 2017).

Importantly, a positive feedback loop exists in which the PAR proteins also regulate the actomyosin cortical flow: depletion of either PAR-3 or Cdc-42 lead to a severe reduction in cortical flow and a limited expansion of the ECT-2 devoid region at the site of polarity cue (Motegi and Sugimoto, 2006; Munro et al., 2004). Another example of this is the effect of PAR proteins on cortical myosin dynamics. Measuring the kinetics of NMY-2 association and

dissociation to the cortex reveals that NMY-2 association with the cortex is identical for the posterior and anterior domains, but that the dissociation of NMY-2 is twice as high in the posterior domain as compared to the anterior region (Gross et al., 2019). This is strictly dependent on PAR-6: an increase in PAR-6 leads to a decrease in the dissociation of NMY-2 at the cortex. Such mechanochemical feedback is another element that could contribute to ensure the robustness of embryo polarity.

All together, studies have illustrated that actomyosin contractility and resulting flows are robustly controlled by multiple over-lapping mechanisms in the *C. elegans* embryo. The result of this polarization phase in the embryo is the formation of two cortical domains that have different actomyosin activity and different PAR protein occupancy that are maintained for the rest of the division process (more details in section 2.4).

2.3.4. Role of microtubules in cell polarity

While cortical actin flows contribute to the polarization process by augmenting the robustness of the PAR polarity response, they are not essential for polarization. Experiments using embryos that lack cortical flow still undergo symmetry breaking as a result of PAR-2-dependent polarization in conjunction with centrosomal microtubules (Motegi et al., 2011) (Zonies et al., 2010). Thus, polarization of the cell in the absence of long-range actin dynamics is possible due to the self-organizing properties of the PAR network. Based on the non-essential role for cortical flow in polarization and the role of microtubules in protecting PAR-2 from exclusion at the posterior cortex, the hypothesis is that any localized cue favouring the cortical binding of one class of PARs could be sufficient to induce a cascade of self-organizing interactions within the PAR network (Motegi et al., 2011).

The rearrangement of PAR proteins upon symmetry breaking in the *C. elegans* embryo includes a recruitment of PAR-2 to the cortex nearest the centrosome. In the absence of cortical flows, the loading of PAR-2 at the cortex is microtubule-dependent and has been shown to correlate spatially and temporally with centrosome/cortex contact (Figure 2.10.) (Motegi et al., 2011; Siegrist and Doe, 2007). In turn, PAR-2 recruits PAR-1 at the posterior pole leading to exclusion of PKC-3/PAR-3/PAR-6 complex, thus enhancing polarity. In wild-type embryos, once the cortical flow ceases after polarity establishment, an essential role played by PAR-2 is to prevent aPARs from returning to the posterior cortex during polarity maintenance (Cuenca et al., 2003; Munro et al., 2004).

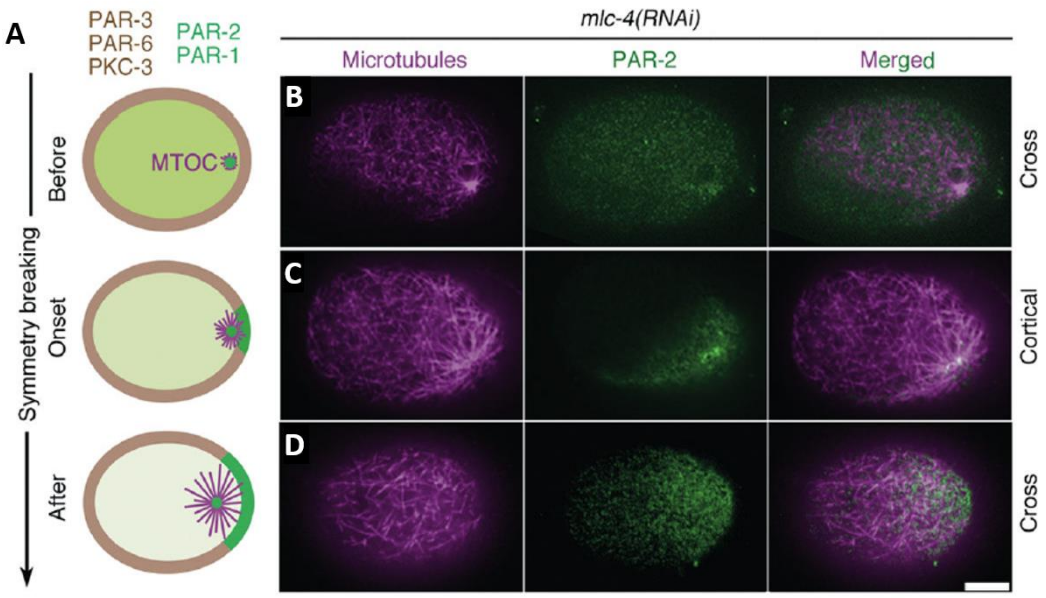

Figure 2.10. PAR-2 dynamics at symmetry breaking. A. Embryo schematics showing the distribution of PAR-1 and PAR-2 (green), aPARs (brown), and MTOC/microtubules (magenta). **B-D**. Confocal images of fixed *mlc-4(RNAi)* zygotes stained for tubulin (magenta) and PAR-2 (green). Scale bar, 10 µm (*adapted from Motegi et al., 2011*).

Although studies have shown that loading of PAR-2 via microtubules is important for establishing polarity, the role of microtubules remain controversial. In embryos treated with microtubule depolymerizing drugs and in tubulin-depleted embryos, normal development of cortical polarity is observed (Cowan and Hyman, 2004; Sonneville and Gonczy, 2004; Strome and Wood, 1983). However, in another study the normal polarization of *tubulin* (RNAi) embryos is explained by the appearance of a small aster wherein symmetry breaking occurs with a delay. Moreover, in zygotes treated with RNAi against *spd-5*, an important protein for centrosome maturation thus leading to a weak nucleation of microtubules, a lack of PAR-2 posterior cortical polarity is observed meaning even with the presence of some microtubules, the lack of centrosome maturation has an effect on polarity (Tsai and Ahringer, 2007). While the role of microtubules in polarity establishment remains to be investigated further, it seems that formation of PAR-2 posterior cortical polarity and posterior cortical smoothening requires a functional centrosome and is not correlated with the presence or amount of microtubules (Cowan and Hyman, 2004; Hamill et al., 2002; O'Connell et al., 2000).

2.4. Poles of the cell: maintenance of the established cell polarity

Polarity establishment of embryo is followed by polarity maintenance of the cell wherein the mutual inhibition between aPARs and pPARs is critical, recently reviewed in (Lang and Munro, 2017). FRAP experiments have shown that during maintenance phase, anteriorly located PAR-6 and posteriorly located PAR-2 can still diffuse across their domain boundary (Goehring et al., 2011; Gross et al., 2019). These studies emphasized on the importance of

polarity maintenance mechanisms needed in order to prevent the spreading of the PAR proteins. A major role played by the PKC-3 is its direct exclusion of pPARs. By phosphorylating PAR-1, PAR-2 and LGL-1, PKC-3 prevents the proteins from associating to the anterior cortex (Hao et al., 2006; Motegi et al., 2011). PAR-3/PAR-6 also have a role in restricting CHIN-1 clusters to the posterior pole which has a role in restricting the spatial extent of anterior CDC-42 as well as anterior restriction of NMY-2.

In turn, PAR-2 excludes aPAR proteins partly by recruiting PAR-1 that phosphorylates PAR-3 and ensures its exclusion from the posterior pole (Figure 2.11) (Motegi et al., 2011). PAR-2, PAR-3 and PAR-6 regulate myosin at the cortex as evidenced by embryos depleted of either of these proteins, which show a spread of NMY-2 towards the posterior cortex during polarity maintenance although the mechanism by which this occurs has not been revealed yet (Small and Dawes, 2017). CDC-42 is localized anteriorly in a PAR-6 dependent-manner and as part of a positive feedback loop it has the role of restricting PAR-6 at the anterior cortex (Figure 2.11) (Gotta and Ahringer, 2001; Motegi and Sugimoto, 2006; Schonegg and Hyman, 2006). The anterior localization of CDC-42 maintains augmented actomyosin at the anterior cortex giving rise to a more dynamic and contractile anterior pole (Motegi and Sugimoto, 2006).

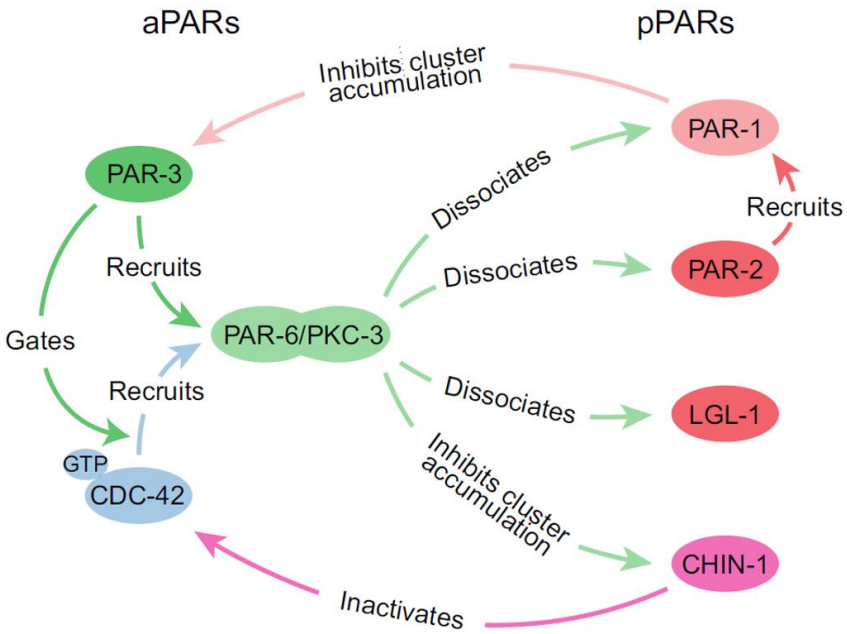

Figure 2.11. Core molecular interactions that underlie the dynamic stabilization of PAR asymmetries. A functional view of the PAR network emphasizing the consequences of protein-protein interactions. For clarity, some interactions documented in other contexts (e.g. inhibition of aPKC by LGL or by PAR-3) have been omitted here *(adapted from Lang and Munro, 2017).*

As was mentioned earlier, during the polarity establishment phase of the embryo, the dissociation rate of NMY-2 was found to be twice as high at the posterior cortex as compared to the anterior cortex. This was also found to be the case during the polarity maintenance phase of *C. elegans* embryos (Gross et al., 2019). Moreover, the anterior dissociation rate of NMY-2 was similar to what was found for NMY-2 dissociation rates during cortical flow

(Nishikawa et al., 2017), indicating that reaction kinetics of NMY-2 do not vary between polarity establishment and maintenance phase in the embryo.

The complexity of the reciprocally supportive and antagonistic interactions between the PAR protein network and the contribution of the actomyosin cortex reinforce PAR localization at embryo poles to ensure cell polarity is maintained until final events of cell division. The AP-axis polarity is required for spindle positioning which brings about cleavage and cell division which is discussed in the next section.

2.5. Last dance of the first cell division: displacing the spindle and cleavage furrow

2.5.1. Spindle displacement

The mitotic spindle forms from the paternal centrosome pair, and in order for proper spindle formation to take place, the centrosomes must first be separated. Cortical dynein at the actomyosin cortex, and also bound to microtubules emanating from the centrosomes, is shown to be the main player in this process (De Simone et al., 2016). Cortical dynein is swept with the cortical flow towards the anterior pole and pulls with it the centrosomes. In experiments where either NMY-2 or RHO-1 is depleted leading to impaired cortical flow, centrosome separation was delayed. Since AIR-1 on the centrosome is what is responsible for breaking the symmetry of the embryo and triggering cortical flow, centrosomes are perfectly positioned to harness flow for separation (Figure 2.6).

As was briefly described in section 1.4, the spindle of the *C. elegans* single cell embryo is first positioned at a center location of the cell, and during anaphase, it is shifted closer to the posterior pole due to a net force from the posterior pole (Gonczy, 2008). An absence of pulling forces results from a loss of any one of the ternary complex proteins leading to an equal cell division even though AP polarity is not affected in the embryo (Colombo et al., 2003; Gotta et al., 2003; Nguyen-Ngoc et al., 2007; Srinivasan et al., 2003).

The motor dynein is a minus-end-directed motor and thus the cortex-anchored dynein motors can generate a pulling force by attempting to move towards the minus end of the astral microtubules that are found near the centrosomes of the mitotic spindle (Figure 2.12) (Gonczy, 2008; Kotak, 2019). Anchorage of the dynein motor at the cortex prohibits its movement so the motor instead pulls the astral microtubules towards the cortex. When dynein heavy chain or dynein-associated proteins are interfered with, a remarkable reduction of pulling forces is observed (Couwenbergs et al., 2007; Nguyen-Ngoc et al., 2007).

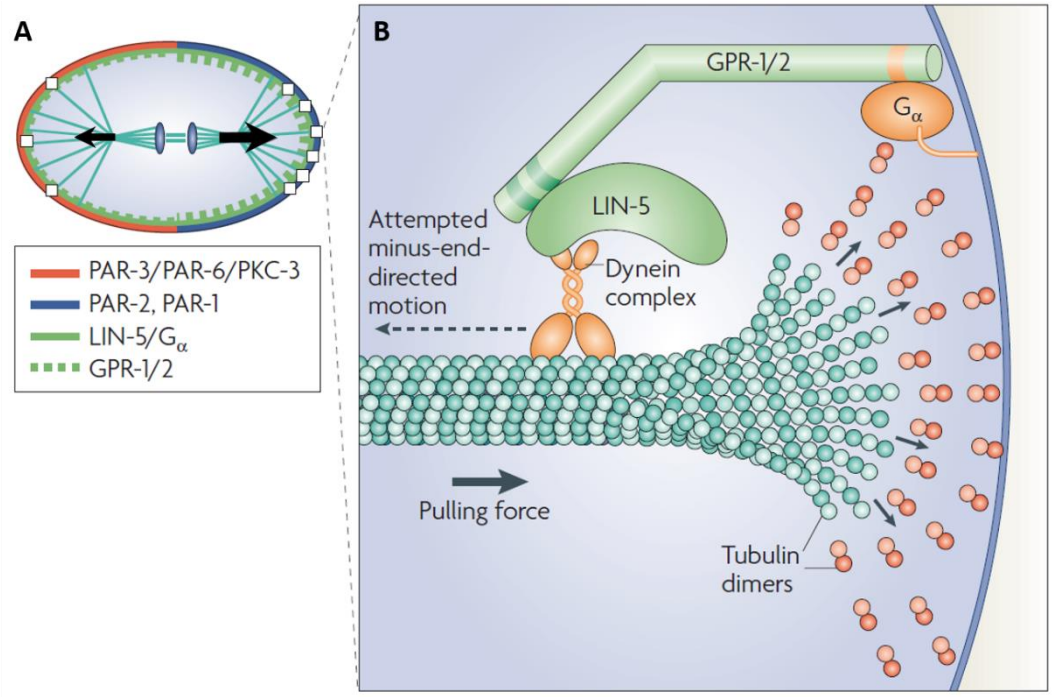

Figure 2.12. Cortical force generation during spindle positioning in *C. elegans.* A. One-cell *C. elegans* embryo. Arrows indicate extent of pulling forces on spindle. **B.** Magnified view of dynein with ternary complex at cortex. (*adapted from Gonczy, 2008*).

Dynein activity however is not the whole story for spindle positioning. Microtubule depolymerization also plays a role as evidenced by the fact that pulling forces on the spindle are reduced in a β-*tubulin* mutant that is known to be resistant to depolymerization induced by cold or depolymerizing drugs. Likewise, stabilizing microtubules with taxol abolishes pulling forces (Nguyen-Ngoc et al., 2007). These studies indicate the role of microtubule depolymerization and dynamics in the positioning of the spindle.

Since dynein is recruited at the cortex by the ternary complex, studies have suggested that the effective displacement of the mitotic spindle towards the posterior pole is due to the asymmetric enrichment of the ternary complex components at the posterior cortex (Colombo et al., 2003; Gotta et al., 2003; Park and Rose, 2008; Schmidt et al., 2017; Srinivasan et al., 2003). Indeed, depletion of any one of the ternary components causes a reduction in cortical dynein (Nguyen-Ngoc et al., 2007). However, the cortical recruitment and anchoring of dynein by the ternary complex does not provide an explanation as to why there is a larger net pulling force exerted on the posterior side, as cortical dynein distribution does not appear to be asymmetric (Gönczy et al., 1999; Nguyen-Ngoc et al., 2007). A recent study shows that there is an increased effective binding rate of dynein motors at the posterior cortex, possibly due to the higher number of dynein cortical anchors (GPR-1/2) there (Rodriguez-Garcia et al., 2018). Although this does not result in more dynein at the posterior cortex, it means that binding events are more productive and thus lead to higher pulling forces at the posterior.

In keeping with importance of binding of dynein at the cortex, in experiments where Gα and GPR1/2 are replaced with an artificial anchor that is localized via a light-activated

system, sufficient pulling forces for spindle positioning are induced (Fielmich et al., 2018). Direct localization of just the dynein motor with the artificial anchor failed to produce pulling forces. However, upon artificial anchoring of LIN-5 in Gα and GPR1/2 depleted zygotes, pulling forces are induced. This indicates a dynein motor activating function of LIN-5 in addition to its anchoring function.

In conclusion, spindle positioning in the *C. elegans* embryo is driven primarily by pulling forces as a result of dynein motor dynamics at the cell cortex and the asymmetric positioning of the spindle is brought about by an asymmetry of the motor dynamics at the embryo poles rather than the asymmetric quantity of the motor.

2.5.2. Cytokinetic ring formation and furrow ingression

The final step for ACD of the *C. elegans* embryo involves the formation of the cytokinetic ring that is comprised of actin filaments, myosin and accessory proteins. The cytokinetic ring brings about cytokinesis, which includes furrow formation and division of the single cell embryo. The initiation of cytokinesis requires the presence of the mitotic spindle: the central spindle and astral microtubules, reviewed in (D'Avino et al., 2005; von Dassow et al., 2009). In the *C. elegans* embryo, the furrow is formed around the spindle mid-zone after it has been displaced from the cell center towards the posterior pole. Experiments in which the PAR proteins have been made symmetric (Kemphues et al., 1988) or the force-generating cortical complexes are manipulated (Jankele et al., 2021) give rise to centrally-located mitotic spindles, and cleavage furrow formation at the center of the cell to produce two equally-sized daughter cells. These experiments seem to indicate that the cleavage furrow follows the spindle mid-zone. However when the spindle is asymmetrically cut by a laser, two furrows form, one midway between the spindle asters and another close to the spindle mid-zone, although the two merge before the end of cytokinesis (Bringmann and Hyman, 2005). Also, in embryos lacking ZYG-9 (an important protein for rapid microtubule growth), a spatial separation of the central spindle-dependent and aster-dependent furrow, leads to two separate furrows at either pole of the cell (Tse et al., 2011). These results suggest that both the spindle mid-zone and the aster position inform the position of the cleavage furrow via independent pathways.

Moreover, the positioning of the furrow can evolve over the course of cytokinesis. This has been observed in mutant embryos with excessive anterior contractility, where the furrow initially forms in the cell anterior region, but later shifts posteriorly along with an anterior shift of the nucleus to avoid DNA segregation defects (Pacquelet et al., 2019). The shifts are produced as a result of blebs on the anterior side of the furrow that presumably release tension to allow for repositioning of the nascent cleavage furrow and for creating cytoplasmic flows that help displace the nucleus (Pacquelet et al., 2019).

A main role of astral microtubule dynamics in positioning the spindle is brought about by inhibiting myosin accumulation at the embryo pole via direct recruitment of anillin (ANI), a cytoskeletal organizing protein (Tse et al., 2011). In ANI-1 depleted embryos, myosin fails to

coalesce and is distributed throughout the entire embryo in contrast to wild-type embryos where larger NMY-2 foci become evident at the equatorial region of the cell and the anterior pole. The role of anillin, therefore, is to spatially organize coalesced myosin for cleavage furrow formation during anaphase. Following anaphase, however, a conserved activator of AIR-1 called TPXL-1 localizes to astral microtubules, activates AIR-1, leading to the polar clearing of ring proteins including anillin, thus terminating its role at the pole for myosin regulation (Mangal et al., 2018).

Furrow assembly and ingression have been shown to require myosin and its activators RHO-1 GTP and RHO GEF ECT-2 (Guo and Kemphues, 1996; Jantsch-Plunger et al., 2000; Morita et al., 2005). Actin filament alignment is also important for the formation of the cytokinetic ring, and converging cortical flow at the cell equator has been shown sufficient for alignment (Figure 2.13) (Reymann et al., 2016) although the role of myosin in actin alignment is also crucial (Leite et al., 2020). Localized actin polymerization also participates in the formation of the cytokinetic ring, but not in the formation of the pseudocleavage furrow, meaning that flows can create a furrow on their own, even if other redundant mechanisms exist. In keeping with this, experiments where the myosin machinery is perturbed in order to mildly reduce the cortical flow still allow actin filaments to align to create a furrow. Importantly, drastic reductions of the cortical flow abolish furrow formation (Reymann et al., 2016).

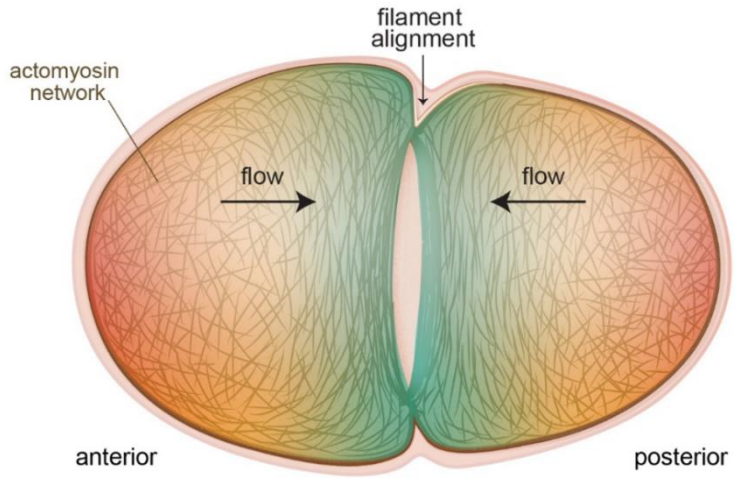

Figure 2.13. Cortical flows align filaments to form the contractile ring for cytokinesis of the one-cell *C. elegans* embryo. Flow of actomyosin cortex at the poles toward the equator (black arrows). Flows progressively transform the unorganized actin filament network at the poles (red shading) into aligned structure of the cytokinetic ring (blue shading) (*from Samandar Eweis and Plastino, 2020*).

After formation and positioning of the furrow comes ingression. Since the cytokinetic ring is an actomyosin ring, it was originally assumed that furrow ingression was driven by contraction. However, some studies show evidence that ingression of the furrow is not driven by myosin motor activity, but rather it is the myosin's actin cross-linking activity coupled with depolymerization (Lord et al., 2005; Ma et al., 2012; Mendes Pinto et al., 2012). Recently, the

analysis of different myosin motor mutants and/or their ability to cross-link actin filaments confirmed that NMY-2 motor activity was required throughout the formation and constriction of the actomyosin ring in the *C. elegans* embryo (Osorio et al., 2019). The densification and alignment of actin during cytokinetic ring assembly were shown to be regulated by activity of the NMY-2, rather than the ability of the motor to cross-link actin filaments although cross-linking of actin filaments is still important for the furrow. Cross-linking activity is known to play a role in modulating contractility, and in the *C. elegans* cytokinetic ring, there exists an optimal amount of cross-linking: too much or too little cross-linking activity is damaging for contraction (Descovich et al., 2018).

As I have shown in the previous sections of this chapter, we now know much about the process of ACD and its regulation in the *C. elegans* embryo. In the past few decades, comparative studies have also been carried out to understand ACD in other nematode species. In the next section, I discuss some of the studies that have brought into light non-*C. elegans* nematode embryos.

2.6. Zooming out: ACD in other nematode embryos

As described in the previous sections of this chapter, ACD and its regulation have been well studied in the *C. elegans* embryo. More specifically, we now have a good understanding of how symmetry of the actomyosin cortical cytoskeleton is broken by a sperm centrosome-derived AIR-1 signal leading to polarity establishment in the embryo. Comparative developmental analysis, both morphologically and genetically, have been carried out on different nematode species. What is interesting is that while asymmetric division of the single-cell embryo leading to daughter cells of distinct date and size is highly conserved in

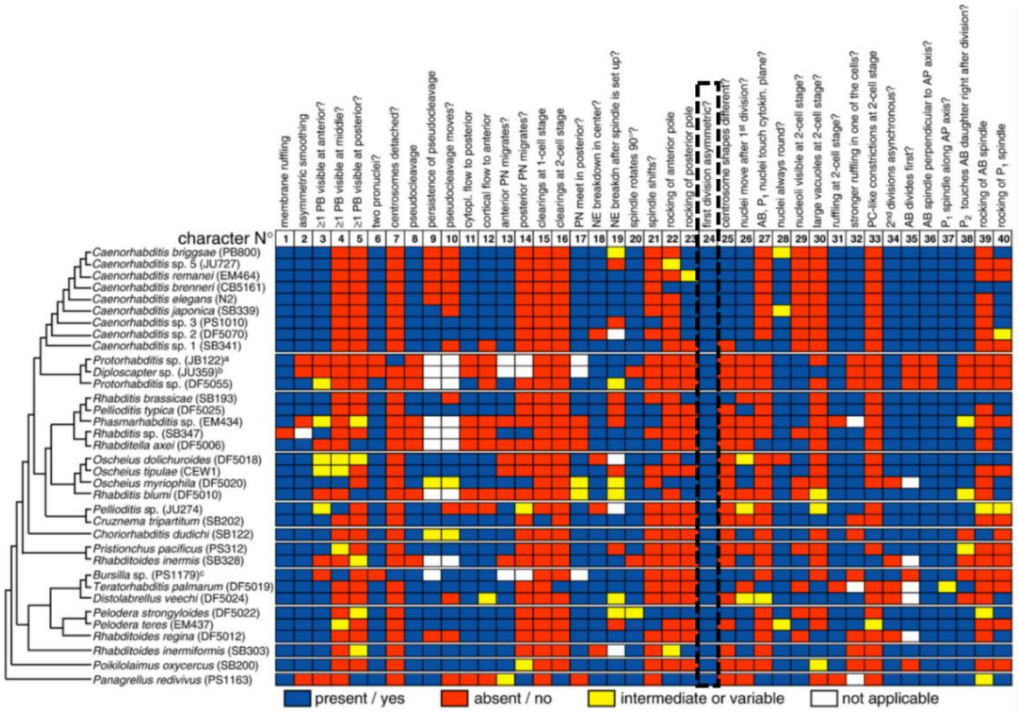

nematodes, the cellular dynamics leading up to division can be very variable (Figure 2.14) (Brauchle et al., 2009).

Figure 2.14. Phenotypic differences in early embryogenesis between 34 rhabditid species. Character states are color-coded as specified in the key. PB=polar body, PN=pronucleus, PC=pseudocleavage, NE=nuclear envelope. Black dotted line around feature 24 highlights conservation of first division being asymmetric in all species (*adapted from Brauchle et al., 2009).*

As also highlighted in previous sections, the mechanisms behind the cellular features leading up to asymmetric division of the single cell embryo are well understood in *C. elegans*. In the study of Brauchle et al., features of the first cell division of 34 different rhabditids are compared primarily to the known ones of *C. elegans* as well as to other features observed in the rest of the worm species of the study (Brauchle et al., 2009). Some cellular features such as membrane ruffling and asymmetric smoothing as well as the presence of 2 pronuclei and the alignment of the P1 spindle along the AP axis are found to be well conserved in most species (character numbers 1,2,6 and 37, respectively, in figure 2.14). Other features such as the presence and dynamics of a pseudocleavage, nuclear envelope breakdown after setting up of the spindle and visibility of polar bodies at either cell pole are more variable (Figure 2.14). Even within the same group of worms (*Caenorhabditis* for example), embryos demonstrate differences in cellular morphology and events during ACD.

In another study, DIC movies of the process of ACD in 42 different nematode species were filmed in order to shed light on the variety of the dynamics of the mitotic spindle (Figure 2.15) (Valfort et al., 2018). In figure 2.15, still images from movies of four nematode species filmed as part of the study are shown (*Pristionchus pacificus* will be elaborated on in Chapter 4). While in *C. elegans* the contour of the posterior becomes smooth at pronuclear meeting and anterior is more dynamic, in *P. pacificus* and *Choriorhabditis cristata* these features are different and dynamics are exaggerated. Posterior smoothening in *P. pacificus* extends more towards the anterior zone and a substantially small and dynamic constriction is formed at the opposite pole that remains during nuclear centering/spindle positioning and only starts to disappear during cleavage. For *C. cristata*, anterior ruffling seems to extend more than the other species and with exaggerated dynamics as compared to *C. elegans*. Upon nuclear centering in *C. cristata*, the cell becomes more spherical and the spindle is shifted along the AP axis and undergoes rotation just before cleavage. In *Diploscapter sp*. pronuclear meeting does not occur since it only contains one nucleus. Movies of this species begin already at nuclear centering and the contour of the cell seems quite smooth throughout until division with minor movements of the spindle (Figure 2.15, last panel).

The variation in cellular features continues onto later stages of embryology in nematode species (Dolinski et al., 2001; Schulze and Schierenberg, 2011; Skiba and Schierenberg, 1992). In *C. elegans* and some other species, cells at the 4-cell stage inside the eggshell are aligned in a diamond-like shape (oblique) (Figure 2.16: Group I, H). Other species demonstrate a linear arrangement (tandem) (Figure 2.16: Group I, E, J, M-P) or T-shape (partial tandem) (Figure 2.16: Group II, C, F, G). An interesting finding in 2011 was that cleavage patterns seem to be dictated in early embryos due to the presence of one or more polarity

organizing center(s) (Schulze and Schierenberg, 2011). In *C. elegans*, sperm components dictate polarity while other species seem to be guided by a mid-body component and other

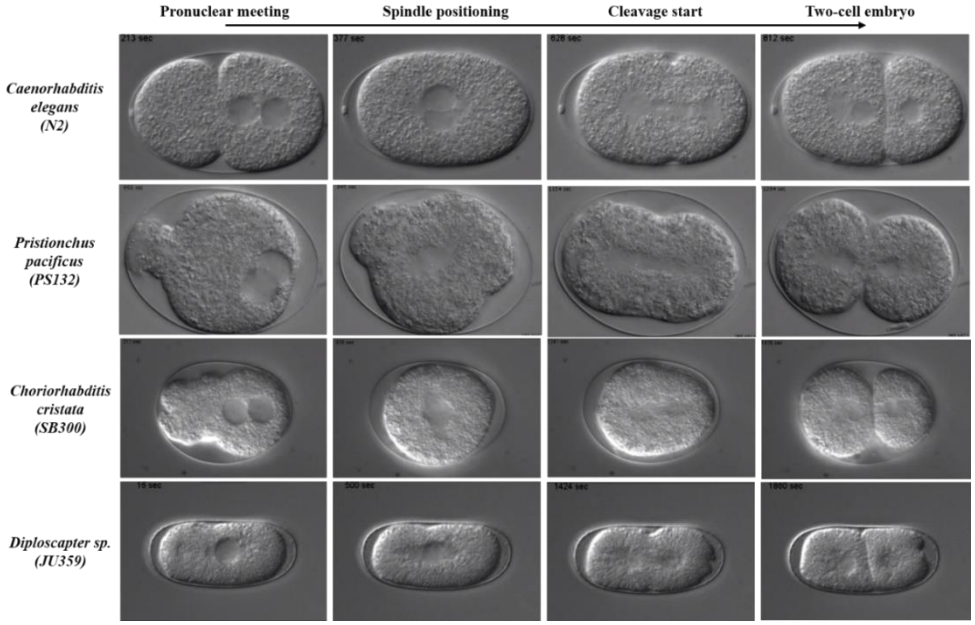

species establish polarity independent of the sperm or lack sperm altogether (Goldstein et al., 1998; Schulze and Schierenberg, 2011) (more on the latter species in the next section).

Figure 2.15. DIC still images of movies of different single cell nematode embryos shown until division. Images taken from films of ACD of 4 different nematode embryos found on http://www.ens-lyon.fr/LBMC/NematodeCell/videos. Timeline shows a still image at the corresponding events: pronuclear meeting, spindle positioing, cleavage start (invagination of membrane) and 2-cell embryo. High variation of cellular morphology seen mainly in early stages of pronuclear meeting and spindle positioning. *Diploscapter* sp. is a parthenogenetic species and has only one nucleus, so no pronuclear meeting occurs (*from Valfort et al., 2018).*

Group I

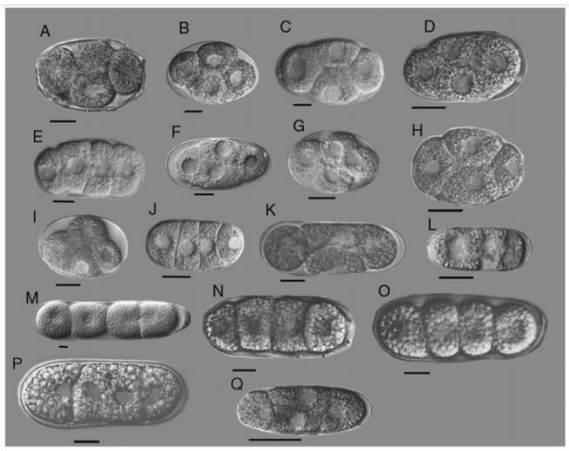

Group I
A–J: Rhabditina: **A.** *Teratorhabditis*. **B.** *Bunonema*. **C.** *Cruznema*. **D.** *Mesorhabditis*. **E.** *Diploscapter*. **F.** *Rhabditella*. **G.** *Rhabditis*. **H.***Caenorhabditis*. **I.** Unnamed (PS1010). **J.** *Protorhabditis*. **K.** Aphelenchidae (*Aphelenchus*). **L.** Aphelenchoididae (*Aphelenchoides*). **M–P**. Tylenchina: **M.** Belonolaimidae (*Belonolaimus*). **N.** Heteroderidae (*Meloidogyne*). **O–P.** Pratylenchidae (*Pratylenchus* and *Nacobbus*). **Q.** Teratocephalidae (*Teratocephalus*).

Group II

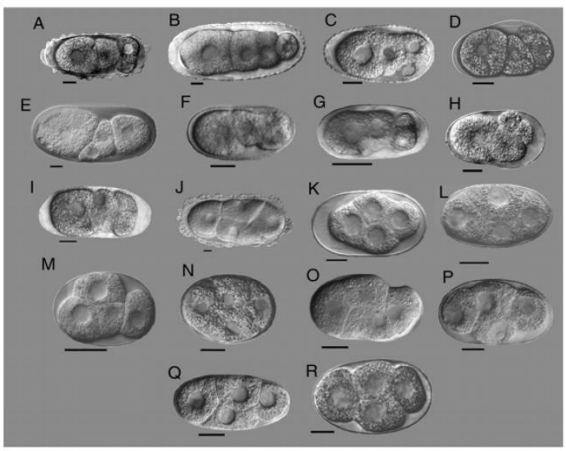

Group II
A-I. Cephalobidae**: A.***Chiloplacus*. **B.***Zeldia*. **C.***Cephalobus*. **D.***Acrobeloides*. **E**.*Acrobeles*. **F.***Eucephalobus*. **G.***Pseudoacrobeles*. **H.***Nothacrobeles*. **I.***Cervidellus*. **J–L.**Diplogastrina. **J.***Diplenteron*. **K**. *Aduncospiculum*. **L.** *Pristionchus*. **M.** *Goodeyus.* **N-Q.**Panagrolaimidae**: N.***Halicephalobus*. **O.***Panagrellus*. **P.***Panagrobelus*. **Q.** *Panagrolaimus*. **R**. Brevibuccidae (*Plectonchus*)

Figure 2.16. DIC images of different nematode embryos at four-cell stage highlighting variety in early embryogenesis. Representative nematodes of different suborders categorized into group I and group II. Scale bars 20 µm. *(Adapted from Dolinski et al., 2000)*.

All these observations suggest that crucial steps of early embryogenesis can be achieved via diverse means. This was therefore the drive of my PhD: to understand the process of ACD in non-*C. elegans* nematodes and reveal the different ways ACD could be achieved, with the long-term goal of shedding light on the variety of mechanisms behind the fundamental process of ACD in general.

For my PhD studies, I chose to investigate the single cell embryo of two species: *Pristionchus pacificus* and *Diploscapter pachys*. This choice was motivated by the fact that both species were entirely sequenced and easily cultivatable in the lab, and some genetic manipulations were known to be possible. Furthermore, visual inspection of DIC movies indicated that these species displayed drastically altered dynamics at different stages of embryogenesis as compared to *C. elegans*, thus suggesting mechanistic variability. *P. pacificus*, although not as closely related to *C. elegans* as *D. pachys* (Figure 2.17), is a hermaphroditic worm, meaning the oocyte undergoes fertilization like *C. elegans*, but the embryo undergoes shape changes, including a persistent anterior bulge, which are never observed in *C. elegans* (Figure 2.15).

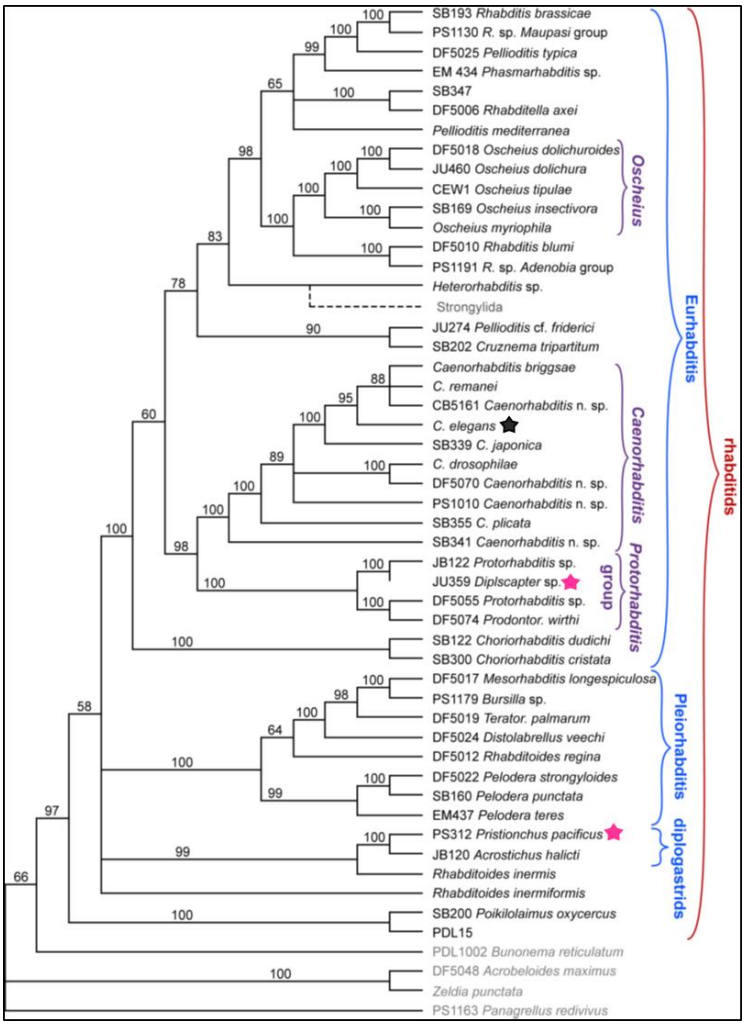

Figure 2.17. Phylogenetic tree of rhabditids worms. Black star highlights position of *C. elegans*. Magenta stars highlight *P. pacificus* and *D. pachys*. (*Adapted from Kiontke and Fitch, 2005*).

My aim with this species was to characterize the actin cytoskeleton of the embryo via live labeling in order to understand the origin of these shape changes, using gene bombardment to introduce cytoskeleton labels, shown to be successful by (Namai and Sugimoto, 2018). For the parthenogenetic nematode *D. pachys*, my focus was to understand how polarity was triggered in this species since it lacks sperm. In the next two chapters, I detail what is currently known about the embryo of these two species, and then describe the approaches I attempted and the results I obtained during my PhD. In the case of *D. pachys*, I draw conclusions as to the mechanism of symmetry breaking for ACD in the absence of a sperm-derived cue.

Chapter 3: *Diploscapter pachys:* A parthenogenetic close relative of *C. elegans* as a new model for understanding symmetry breaking and asymmetric cell division

3.1. Introduction: *D. pachys*, other parthenogenetic species and alternative polarity cues

3.1.1. The *D. pachys* nematode and genome

D. pachys is an asexual nematode and also evolutionarily a close relative of the sexually reproducing *C. elegans*. It is a novel model organism with a fully sequenced genome completed only 4 years ago (*D. pachys* strain PF1309) (Fradin et al., 2017). The *D. pachys* adult worm is about 0.5 mm in length (half the size of the *C. elegans* adult). Although half the size of *C. elegans*, *D. pachys* worms produce embryos that are 75% the size of *C. elegans* embryos with an identical aspect ratio (width/length) of 0.6 (Figure 3.1). Moreover, both embryos divide to produce P1 and AB daughter cells with an AB/P1 ratio of 1.3. *C. elegans* embryos develop inside the uterus until the 32-cell stage embryo before being laid while most *D. pachys* embryos are laid prior to the first cell division. The lifecycle of the *D. pachys* worm from single cell to egg-laying adult is around 8 days, 2.5 times longer than that of *C. elegans.*

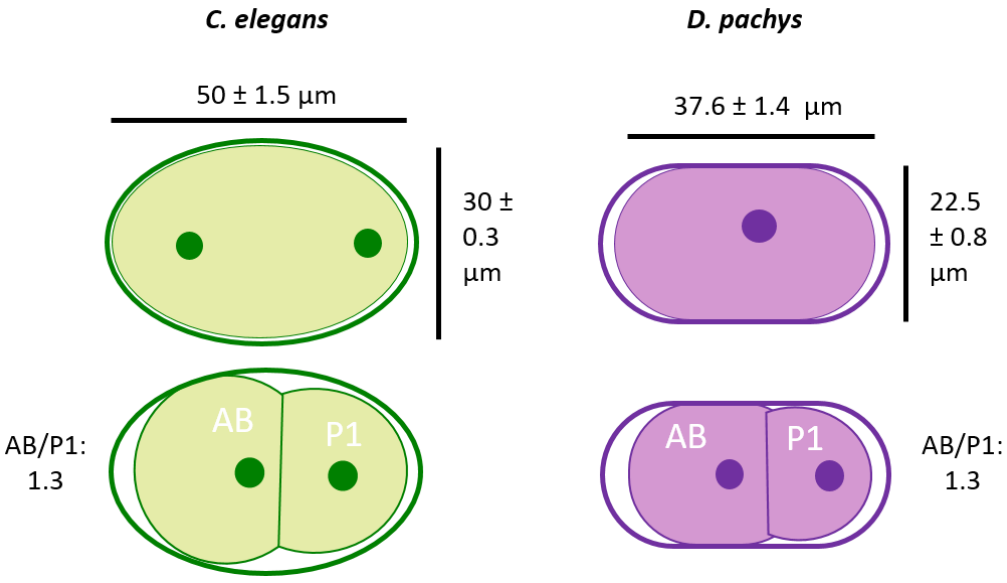

Figure 3.1. Average dimensions of single cell embryos and AB/P1 ratio of 2-cell embryo in *C. elegans* and *D. pachys*. The width of the single cell embryo of *D. pachys* is around 23 µm (N=43), smaller than the *C. elegans* embryo (~30 µm; N=7), but the length is also proportionally shorter, yielding the same aspect ratio (scheme shown not to scale). For AB/P1 the length along the AP axis of AB is 30% larger than P1 (N=43).

As a result of the fusion of six ancestral chromosome domains, *D. pachys* worms carry only one pair of chromosomes (Fradin et al., 2017). As an asexual species, *D. pachys* oocytes appear to skip meiosis I and undergo a single meiosis II-type nuclear division. Upon meiosis II, the dividing oocyte extrudes separated sister chromatids into one polar body leaving a heterozygous diploid oocyte which then becomes an embryo without fertilization (Figure 3.2) (Fradin et al., 2017).

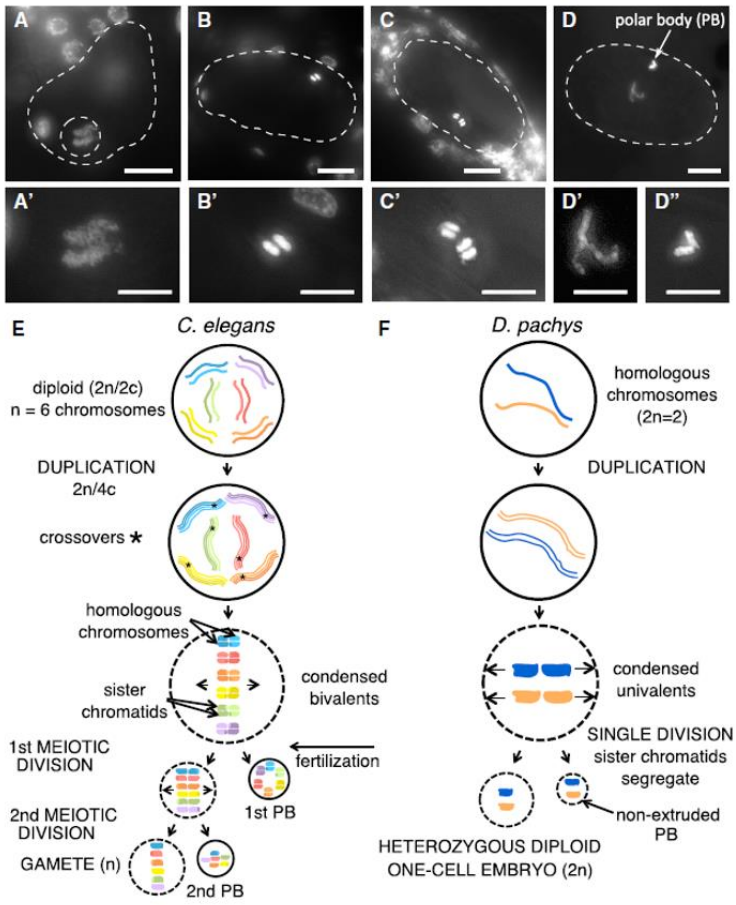

Figure 3.2. *D. pachys* oocyte maturation and comparison of oogenesis between *C. elegans* and *D. pachys*. A-D. Stages of maturation of DAPI-stained *D. pachys* oocytes. Scale bar 5 µm. **E-F.** Schematic of oogenesis in *C. elegans* and *D. pachys.* (*Adapted from Fradin et al., 2017*).

3.1.2. Embryos of other *Diploscapter* and parthenogenetic nematodes

Diploscapter worms belong to the *Protorhabditis* group within which both sexual and asexual species exist (Figure 3.3). The presence of asexually reproducing species in the group is based on the observation that some species have only one nucleus and no sperm in the female gonad (Fradin et al., 2017; Lahl et al., 2006). *Diploscapter coronatus*, a sister species of *D. pachys* has also been used in evolutionary studies and also for understanding parthenogenesis. The genome of *D. coronatus* has been analyzed recently, also showing that the worm contains only one pair of chromosomes (Hiraki et al., 2017). The study brings insight about the basis of genetics in parthenogenetic reproduction by uncovering orthologs of *C.*

elegans genes but also the lacking of genes involved in sex determination and meiosis. The genes found to be lacking for meiosis in *D. corontaus* are similar to the list of genes found to be lacking for meiosis I in *D. pachys*, adding evidence to the model of meiosis I skipping in the species (Figure 3.2) (Fradin et al., 2017). *D. coronatus* has also been used to shed light on steps of early embryogenesis that I will describe in the rest of this section.

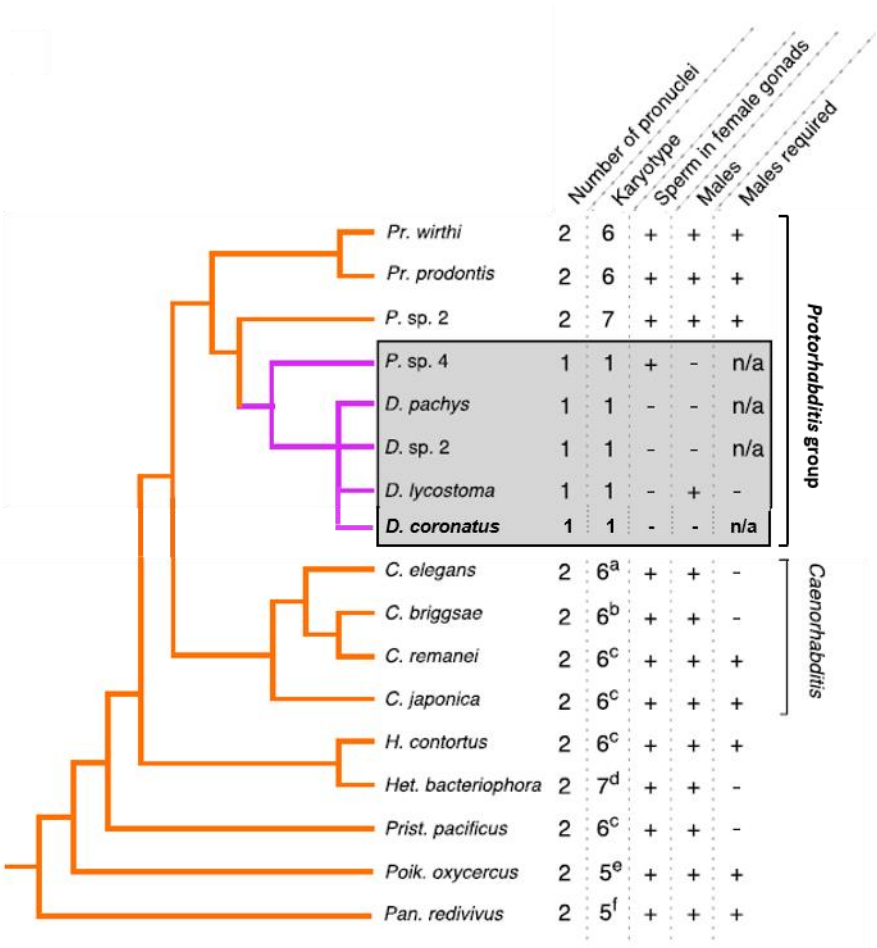

Figure 3.3. Phylogenetic relationships and reproductive modes of the *Protorhabditis* group and related nematodes. A. Molecular phylogeny and key aspects of reproductive biology for sexually reproducing lineages (orange) and asexually reproducing lineages (purple, gray box) of the *Protorhabditis* group. Grey box: *P.* sp.4: *Prodontorhabditis* sp. 4 (JB122), *D. pachys* : *Diploscapter pachys* (PF1309), *D.* sp 2 : *Diploscapter* sp. 2 (JU359), *D. lycostoma* and *Diploscpater lycostoma* (PS2017) and *D. coronatus* (PDL0010): *Diploscapter coronatus*. (*Adapted from Fradin et al., 2017*).

Interestingly, species in the *Protorhabditis* group such as *Protorhabditis* sp.4 have been found to have sperm, but only a single nucleus and no males. It was then found that the sperm provided no genetic material but may be present in order to activate the oocyte to embryo in a process of pseudogamy, which has been already shown in other nematodes (Figure 3.3) (Grosmaire et al., 2019; Launay et al., 2020). Genetic contribution is also lacking from the few males of the *Diploscpater lycostoma* worms where no mating between the male and female occurs, no sperm is found in the female and only single-nuclei embryos exist before the first embryo division. It is hypothesized that pseudogamy is an intermediate step in the transition from sexual to asexual species (Launay et al., 2020).

As mentioned in earlier sections, the *C. elegans* oocyte completes meiosis upon fertilization. Meiotic divisions of the *C. elegans* oocyte usually occur at the pole opposite that of fertilization and polarity initiation, giving two separate polar body (PB) extrusions at the anterior pole as a result of meiosis I and meiosis II (Figure 3.4.A). In a study where the number of PBs as well as their position in the embryo is looked at for different parthenogenetic worms including *D. coronatus*, no correlation is found between the peripheral PB position and future posterior cell (Figure 3.4.B) (Lahl et al., 2006). Whether the polarity of these parthenogenetic embryos arises inside the uterus was investigated by observing in utero embryo development. While in *C. elegans* the posterior cell of the embryo is almost always toward the vulva due to sperm-derived polarity cue upon the oocyte entering the spermatheca (Figure 3.4), in the parthenogenetic embryo *Acrobeloides nanus*, it is the anterior cell that is towards the vulva 98% of the time, indicating that AP-axis determination is imposed in the uterus. In *D. coronatus* embryos, the posterior cell is towards the vulva in 50% of embryos, so seemingly independent of an external signal and occurring by chance (Figure 3.4.B) (Lahl et al., 2006).

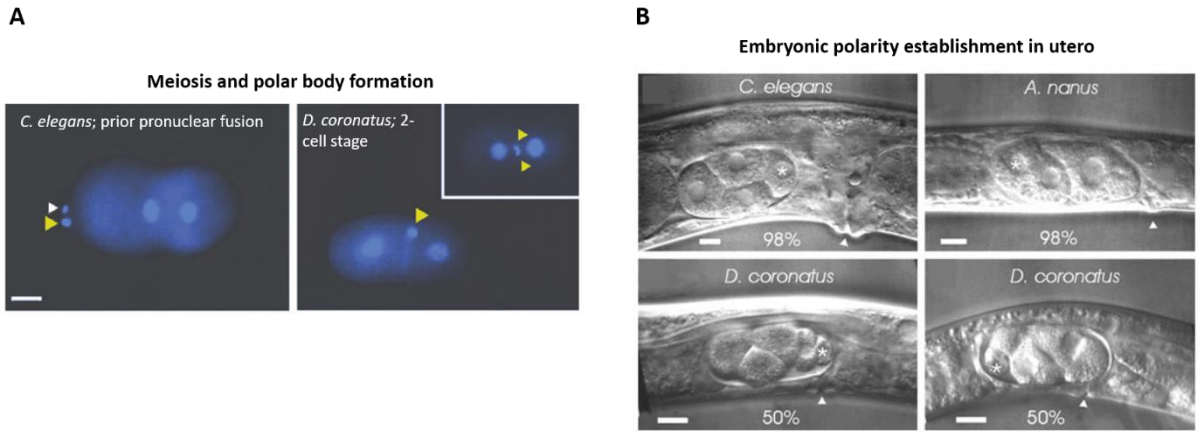

Figure 3.4. A. Meiosis and formation of polar bodies in different nematode embryos. Epifluorescence visualizing DAPI-stained nuclei. Arrowheads (yellow), first PB or its descendants; arrowheads (white), second PB; bar, 10 µm**. B. Embryonic polarity establishment inside the uterus of different nematodes.** Arrowheads, position of the vulva; asterisk defines posterior pole; %, proportion of embryos behaving as shown; Scale bar 10 µm; (*Adapted from Lahl et al., 2006*).

As I have previously described, the asymmetric localization of PAR protein at cell poles is important in setting and maintaining cell polarity in *C. elegans* embryos as well as in other asymmetrically dividing cells. PAR polarity in *C. elegans* is also a central feature for the correct positioning of the spindle machinery to give rise to an asymmetric cell division. However antibody staining for PAR-1, a well conserved PAR in ACD, shows that PAR-1 is symmetric in two parthenogenetic single-cell embryos: *Diploscapter* sp. (JU359) and *Protorhabditis* sp. (JB122) (Figure 3.5) (Brauchle et al., 2009). Moreover, in a genomic comparative study, orthologs for *C. elegans* PAR-2 were not found in *D. coronatus* (Kraus et al., 2017). These results are important for understanding mechanisms of polarity in parthenogenetic zygotes, however it does not contradict that polarity is indeed established in the single cell embryo.

The embryos of these parthenogenetic worms produce a smaller posterior cell vs. a larger anterior daughter cell, each of which divides asynchronously to give rise to differently-fated progeny, features that define an established asymmetry of the zygote (Figure 3.6.F-I) (Brauchle et al., 2009; Delattre and Goehring, 2021; Kraus et al., 2017; Schulze and Schierenberg, 2011). The results obtained for the PAR proteins in these embryos indicates that indeed there are alternative pathways for establishing and maintaining polarity in some nematode embryos that remain to be uncovered. Moreover, in *Protorhabditis* sp., PAR-1 is observed to be asymmetric in the 2-cell and 4-cell stage similar to what is seen in *C. elegans* indicating that perhaps different mechanisms define polarity in the one cell embryo as compared to later embryos in *Protorhabditis* sp. (Brauchle et al., 2009) (Figure 3.5).

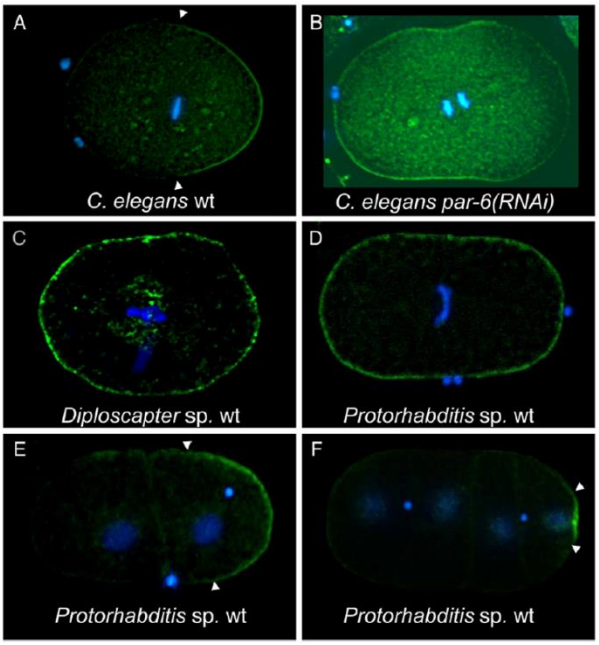

Figure 3.5. PAR-1 localization in species of the *Protorhabditis* group. Fluorescent staining of embryos with PAR-1 antibodies (green) and DAPI (blue). **A.** Posterior PAR-1 localization in wild-type *C. elegans* one-cell stage embryos. **B-D.** PAR-1 all around the cortex in a one-celled embryo of *C. elegans par-6* (RNAi), *Diploscapter* sp. (JU359) and *Protorhabditis* sp. (JB122). **E.** Asymmetric PAR-1 in two-cell *Protorhabditis* embryo **F.** four-cell *Protorhabditis* sp. (JB122) embryo. (*From Brauchle et al., 2009*)

In addition to the lack of *par-2 C. elegans* orthologs in *D. coronatus*, the genomic comparative study of *D. coronatus* with other nematodes revealed that in *D. coronatus* there is also an absence of *gpr-1* and *gpr-2*, important proteins in spindle positioning in *C. elegans* (Kraus et al., 2017). By looking at DIC images of *D. coronatus* (Figure 3.6), differences as compared to *C. elegans* are revealed wherein firstly a constriction occurs at the anterior of the cell and is maintained up until the start of cleavage (Figure 3.6.B). Moreover, while no shift of the posterior aster occurs, an eccentric position of the single nucleus is maintained, thus leading to an asymmetric division (Kraus et al., 2017). The subsequent division of the bigger daughter cell of *D. coronatus* is along the AP-axis, unlike *C. elegans*, potentially explained by the lack of *gpr-1* and *gpr-2* genes in *D. coronatus.*

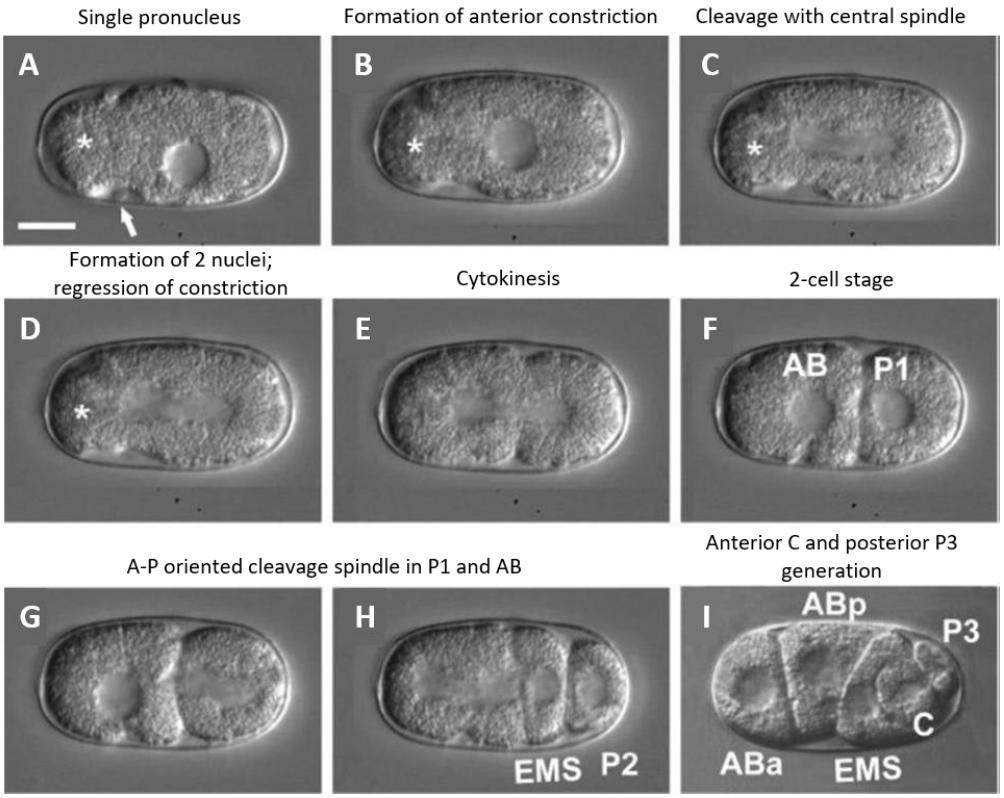

Figure 3.6. Early embryogenesis of *D. coronatus*. DIC images starting from **A.** single pronucleus embryo until **I.** embryo with diving P2 cell. Arrow, single polar body; asterisk, separated anterior cytoplasm. Scale bar 10 µm. Orientation, anterior: left. (*Adapted from Kraus et al., 2017*).

3.1.3. Sperm-independent cues for symmetry breaking

Alternative mechanisms of symmetry breaking independent from the sperm centrosome in nematode embryos have been nicely described in a recent review (Delattre and Goehring, 2021) (Figure 3.7) and some concepts were discussed in Chapter 2. The conclusion is that the existence of parthenogenetic nematodes indicates that the sperm centrosome is not absolutely required. Indeed even in some species possessing sperm, symmetry breaking does not appear to depend on sperm as the posterior pole and cytoplasmic flows do not correlate with sperm position (Goldstein et al., 1998). In addition, even in cases where symmetry breaking normally does depend on the sperm centrosome, like in *C. elegans*, the cue from the sperm can be eliminated either by disturbing the actin cytoskeleton, depolymerizing microtubules or directly ablating the centrosome, and yet the embryos maintain their capability of establishing polarity (Goehring et al., 2011; Klinkert et al., 2019). In mutant and RNAi experiments where zygotes are arrested in meiosis in the absence of sperm asters, the posterior cell is determined by the meiotic spindle (Wallenfang and Seydoux, 2000). A study also showed that in *C. elegans* zygotes that have been arrested in meiosis due to mutation of the anaphase-promoting-complex, anillin present at the meiotic spindle induces asymmetric localization of PAR-2 and posterior fate determinant, PIE-1, at the pole of the meiotic spindle (Tse et al., 2011). All together these data are consistent with the idea

that symmetry breaking in parthenogenetic species could be the result of the eradication of regulatory mechanisms that force polarity to depend on the sperm cue. In the absence of regulation, cryptic polarizing mechanisms could act to prepare the cell for ACD. In such a context, the main candidates as the source of a polarizing cue are the oocyte pronucleus or the meiotic spindle.

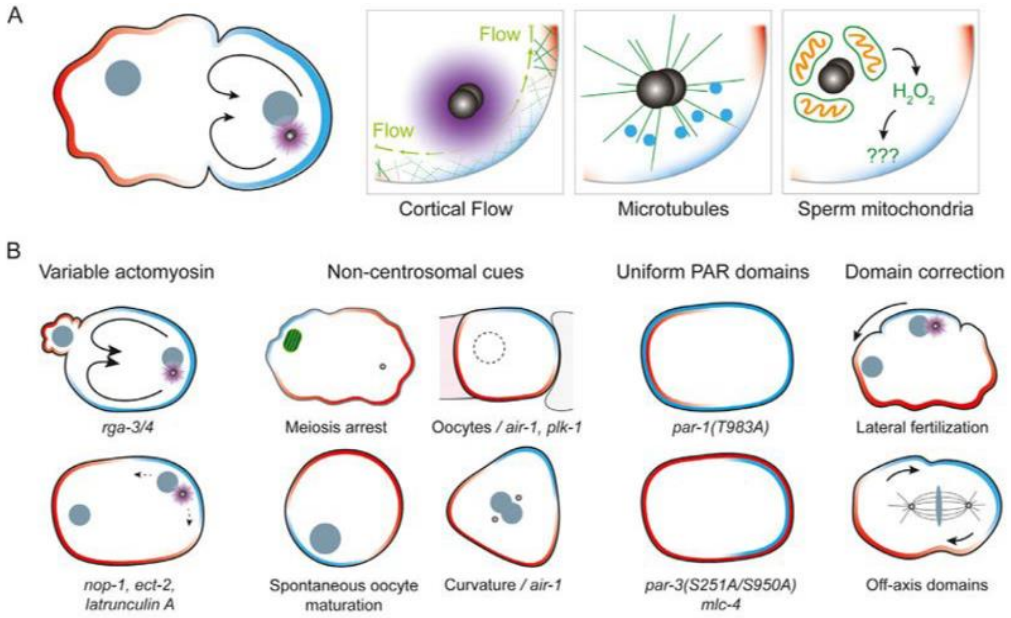

Figure 3.7. Variations in symmetry breaking. **A.** Symmetry breaking in the wild-type *C. elegans* zygote is triggered by semi-redundant cues **B.** Perturbed *C. elegans* embryos are capable of polarization under diverse regimes. (*Adapted from Delattre and Goehring, 2021*).

3.1.4. Project Goal

Considering that most of the knowledge we have on the process of asymmetric cell division in nematode embryos has emerged from studies on the *C. elegans* embryo, looking at embryos of non-*C. elegans* species could provide a new perspective on the mechanisms that drive the process of ACD, and shed light on how well they are conserved. Moreover, while studies indicate all nematode species undergo a first asymmetric cell division, how the sequence of events leading up to ACD are coordinated in non-*C. elegans* embryos is still unknown.

I aimed to answer three main questions during my PhD using the *D. pachys* embryo. First, what is the polarity cue for symmetry breaking in the *D. pachys* embryo? Also, when is asymmetry established? Given the significant actin asymmetry that is observed in *C. elegans* and the role of astral microtubules in coordinating ACD, does the cytoskeleton of the *D. pachys* embryo play a role in symmetry breaking and polarity establishment similar to that seen in the *C. elegans* embryo?

The lack of genetic manipulation tools for live labelling of the cytoskeleton and polarity proteins in *D. pachys* worms (more details in sections 3.3) limits the approaches that can be used to answer these questions. However, just as discoveries were made for *C. elegans* using

DIC microscopy and fixed staining before the development of genetic tools, an important first step for understanding the *D. pachys* embryo is a thorough characterization of the early embryo and the identification of how similar or different it is from the already well-established and well-studied *C. elegans* model system.

In the following section, I will present a thorough description of my main results, obtained with the *D. pachys* embryo, that both complement and augment the studies I have described in this section about different non-*C. elegans* embryos. In the subsequent section, I will describe the approaches that did not work in my hands with *D. pachys*. These two sections are an extended version of a manuscript titled "Asymmetry is defined during meiosis in the oocyte of the parthenogenetic nematode Diploscapter pachys" which has been submitted for publication, and is also attached in the annex section at the end of this thesis. In the last part of this chapter, after my conclusions, I summarize the materials and methods I used for studying the *D. pachys* single cell embryo.

3.2. Results and Discussion

3.2.1. Description of early development of *D. pachys* embryo

Upon dissecting gravid *D. pachys* females, most embryos were at the one-cell stage, meaning that they were laid before their first mitotic division as was also observed in other parthenogenetic species (Lahl et al., 2006). Moreover, 80% were post-meiotic (or zygotes) as evidenced by a clearly delimited round shape of the nucleus (n = 34/43), while others were just before or undergoing meiotic division (oocytes or pre-meiotic embryos). For most oocytes and zygotes that were filmed, it took around 50 minutes to proceed to cleavage, and in general four recognizable stages were characterized, namely membrane ruffling, membrane smoothening, cleavage start and scission (Figure 3.8). Ruffling was the longest stage, lasting between 20 and 45 minutes depending on the oocyte/zygote. Around five minutes before nuclear envelope breakdown (NEBD), membrane ruffling abated and there was a smoothening of the embryo contour. The lack of ruffling seen in DIC films of a sister species *Diploscapter* sp. (JU359) (Figure 2.15) (Valfort et al., 2018) is most probably due to start of imaging at the smoothening stage. Moreover, unlike observations in *D. coronatus* (Figure 3.6) (Kraus et al., 2017), no maintained anterior constriction was observed in *D. pachys.* Rather, the ruffling followed by smoothening was observed for the entire *D. pachys* oocyte/zygote contour (Figure 3.8). The beginning of cleavage in *D. pachys* embryos was recognized by membrane invagination and the time it took for cleavage completion was around five minutes (Figure 3.8). The impression from observation of DIC movies of *D. pachys* oocytes/zygotes was that they displayed more membrane activity overall as compared to *C. elegans*. However, the asymmetric smoothening of one pole was lacking in *D. pachys*, there was no identifiable pseudocleavage furrow and cytoplasmic flows were chaotic (details in the following).

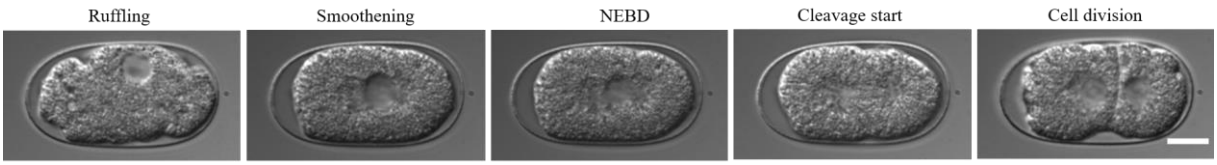

Figure 3.8. DIC still images of ACD in *D. pachys* embryos. Duration of events normalized to time of cleavage start; average time for each event written below images. Scale bar 10 µm.

D. pachys embryos were also observed to hatch between slide and coverslip, displaying recognizable stages as compared to *C. elegans*, but taking around 38 hours from the time of cleavage initiation of the first cell division, as opposed to nine hours for *C. elegans*. At the 2-cell stage of *D. pachys* embryos, one blastomere was slightly smaller than the other, and the smaller cell went on to divide before the other in an asymmetric manner, revealing that the embryo was indeed polarized, as was also reported previously for the closely related worm *D. coronatus* (section 3.1) (Lahl et al., 2006). By analogy with *C. elegans* and other nematodes,

this cell was thus considered the posterior cell P1. In *D. pachys*, as in other members of the *Diploscapter* genus (Figure 3.6), the mitotic spindle in both AB and P1 oriented along the longitudinal axis of the embryo (Figure 3.9) (Goldstein, 2001; Lahl et al., 2009).

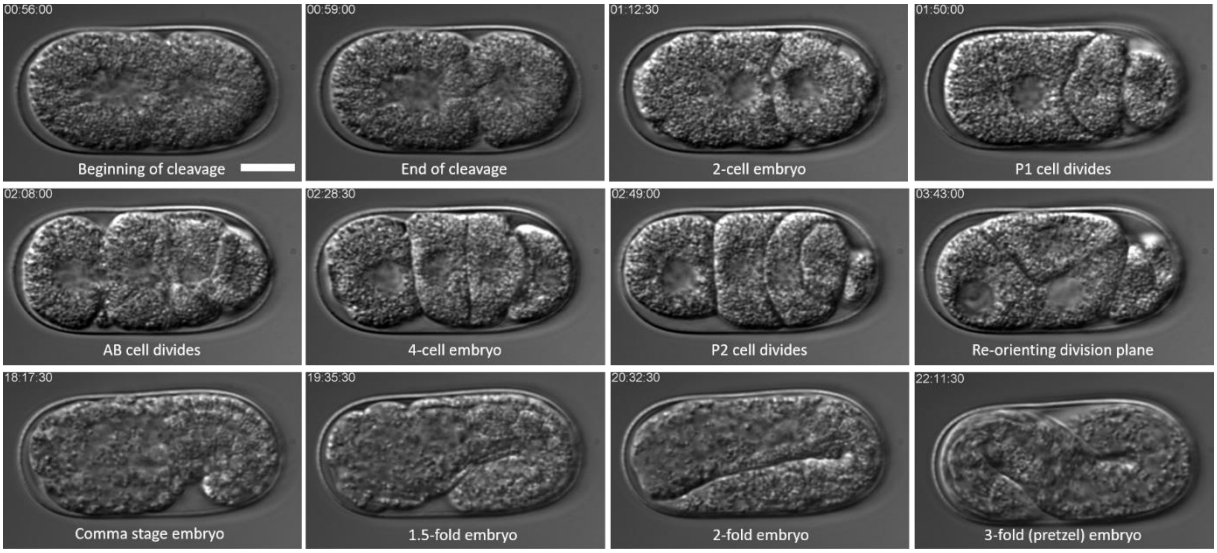

Figure 3.9. DIC still images from full embryogenesis movie of *D. pachys* worm starting cleavage to 3-fold embryo. Timestamp at upper left corner of each image. Most recognizable events of embryogenesis are shown; hatching image not shown here. Scale bar 10 µm.

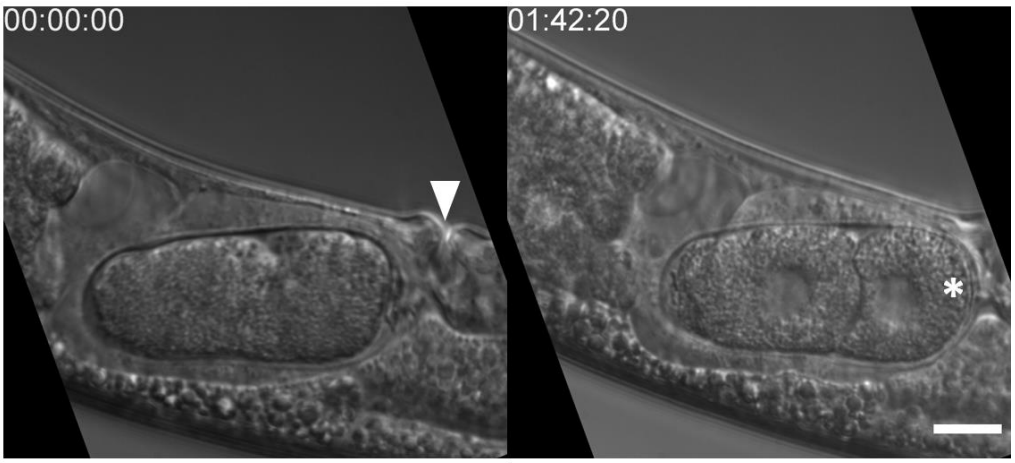

Figure 3.10. In utero imaging of *D. pachys* embryos. Left image shows beginning of movie and right image shows embryo after division. Arrowhead points to vulva and asterisk marks posterior cell. Scale bar 10 µm.

In order to evaluate whether an in-utero polarity signal exists in *D. pachys* worms, using an anesthetic, I observed and evaluated cell positioning from one-cell to two-cell embryos. My results confirmed what was previously reported for *D. coronatus*: there was no correlation between oocyte orientation in the uterus and the location of the posterior cell: 50% of embryos had their posterior pole adjacent to the vulva and 50% had their anterior pole towards the vulva (N = 11) (Figure 3.10) and also (Lahl et al., 2006).

3.2.2. Evidence for symmetry breaking in the one-cell embryo of *D. pachys*

Although the position of the maternal nucleus was variable at the beginning of filming, it was often positioned in the future posterior half of the embryo. Without exception by the end of smoothening, the nucleus had traveled to the part of the embryo that would become the posterior pole, and positioned at 46 ± 3% (N = 43) of the total length of the embryo by the onset of metaphase (Figure 3.11). Indeed outlier embryos in both the anterior and posterior directions showed the most dramatic movements toward the 46% mark just before and during the smoothening period, and ended up dividing asymmetrically like the others (Figure 3.11). This result showed a strict correlation between the position of the post-meiotic nucleus and the position of the posterior pole.

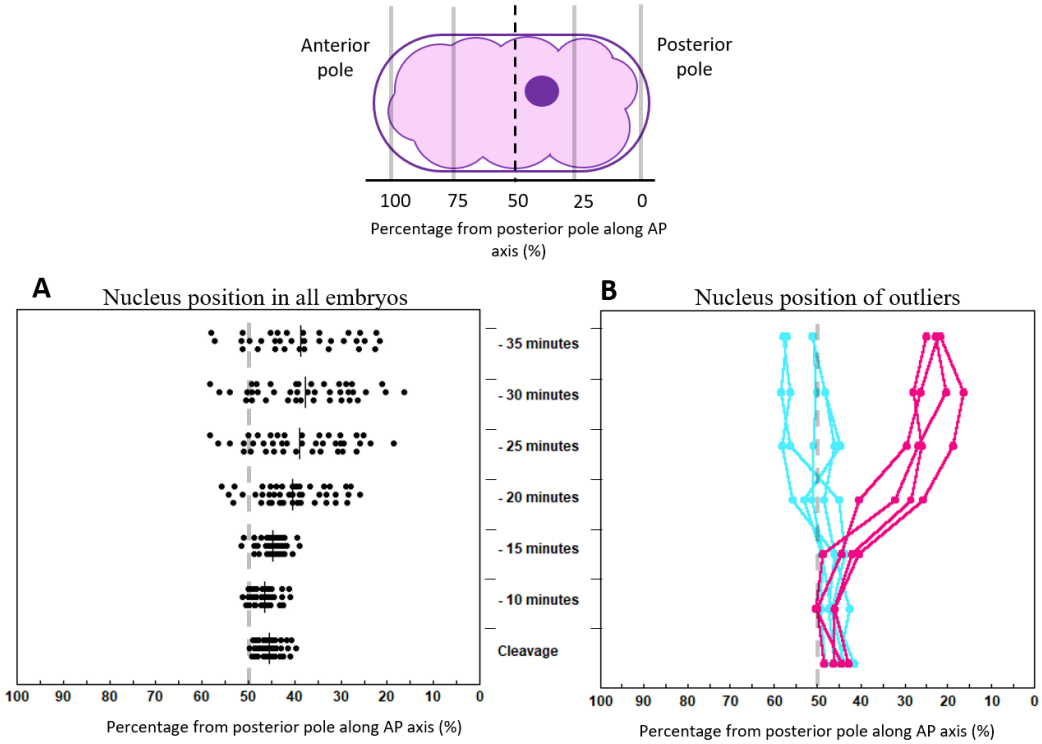

Figure 3.11. Nuclear positioning during the first cell division of *D. pachys* embryos. Top scheme showing how position of nucleus (dark purple sphere) is measured as a percentage of the AP-axis from the posterior pole (0% on x-axis). **A.** Scatter plot of nuclear position quantification over time, normalized to cleavage. **B.** Outlier embryos in which nucleus is positioned ≥ 50 % (cyan lines) or ≤ 30% from posterior pole (magenta lines). All embryos end with cleavage 46 % from posterior pole (N=43).

The question was then if this were causal: did the proximity of the nucleus to one pole define that pole as posterior? To test this, I perturbed the initial position of the female pronucleus by centrifuging live embryos that were adhered to microscope slides in order to shift the nucleus to one side of the embryo and see if indeed that pole became the posterior. Centrifugation of cells has previously been done in fibroblasts in order to shift the nucleus

(Zhu et al., 2017) and in *C. elegans* embryos to shift yolk granules (Bossinger and Schierenberg, 1992; Schlicht and Schierenberg, 1991).

After centrifuging *D. pachys* embryos, I only considered and studied embryos that were positioned with their long AP axis parallel to the centrifugation force (scheme shown at the top in Figure 3.11). Due to the duration of the centrifugation treatment, most (90%) of the embryos were post-meiotic. Just after centrifugation, in the majority of cases, the post-meiotic nuclei were found at the pole opposite to the centrifugal force (24/27 embryos) (Figure 3.12). This was unanticipated, but it indicated that most nuclei were less dense than other contents of the embryo. I then observed subsequent embryo development to evaluate which end of the embryo became the posterior pole. In 13/24 embryos, the nucleus remained at its post-centrifugation pole, and that became the posterior cell as evaluated by both size and by P1 cell division (dividing before AB) (Figure 3.12.A). In the remaining 11 embryos, however, the nucleus moved to the opposite pole, and that then became the posterior cell (Figure 3.12.B). Taking the main population of post-meiotic embryos, the data suggested that polarity of the embryo was set upstream of post-meiotic nuclear positioning since the initial location of the nucleus after centrifugation did not correlate with the future posterior pole of the embryo. This early pole definition also explained the behavior of anteriorly-positioned outliers, which migrated directionally toward the future posterior pole (Figure 3.11.B).

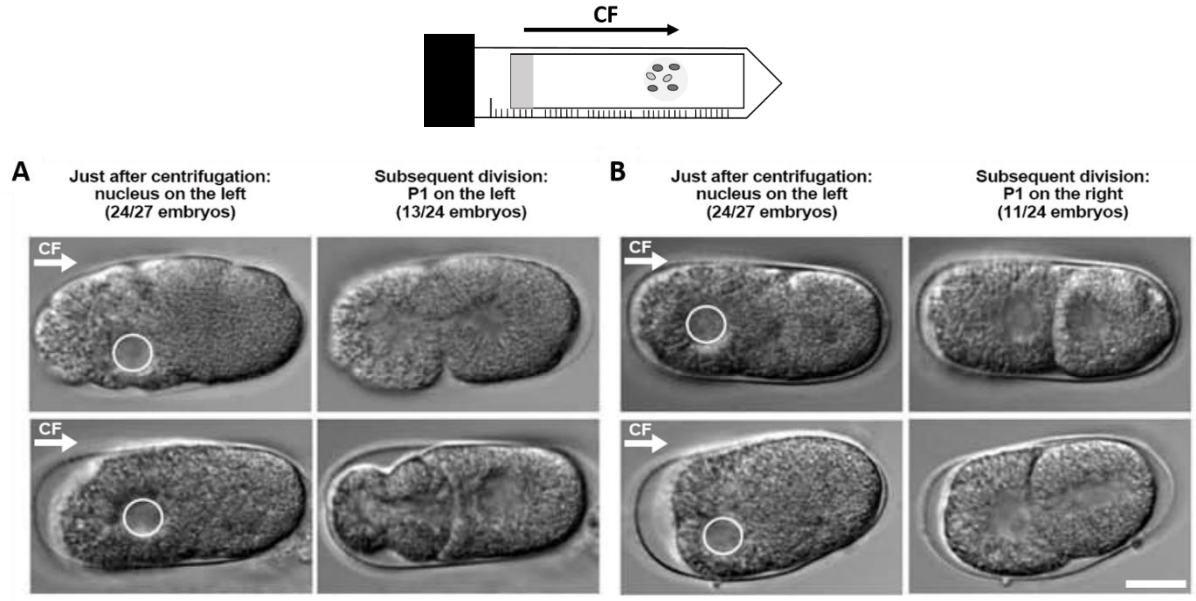

Figure 3.12. Nucleus in 50% of centrifuged embryos returns to preferred pole. A and B. Images on the left show single cell with nucleus to the left just after centrifugation treatment, after their division, images are shown on the right. **A.** Posterior cell at same pole as starting nuclear position as shown by smaller cell (top panel) and cell dividing first (lower panel). **B**. Posterior cell is at opposite pole of starting nuclear position. Scheme on top of figure: slide with dissected embryos (ovals) inside falcon tube to be centrifuged. Only aligned embryos (darker ovals) are regarded.

All together with the results from the previous section, my results indicated that symmetry was broken in the *D. pachys* embryo, and embryo poles were dissimilar before the first mitotic division despite the lack of a sperm or uterine cue.

3.2.3. Cortical ruffling and actin cytoskeleton are not polarized in post-meiotic embryos

This early polarity establishment in *D. pachys* echoed what was known for the *C. elegans* embryo where polarity is established well before nuclear positioning for division. As was discussed in section 2.2, polarization of the *C. elegans* embryo is represented by dissimilar cortical dynamics at the two embryo poles. This is visible by live DIC microscopy as enhanced ruffling at the anterior pole vs. smooth posterior during pronuclear meeting and centering, as well as by live or fixed actin cytoskeleton labelling, which shows enrichment of actin and myosin at the anterior pole (Munro et al., 2004; Reymann et al., 2016; Strome, 1986). I therefore looked for some indication of whether the *D. pachys* embryo also had polarized cortical activity by assessing DIC movies. With the help of a software engineer, Varun Kapoor, at the PictBDD platform at Institut Curie, I created masks via machine learning to automatically detect embryo contours over time (Figure 3.13).

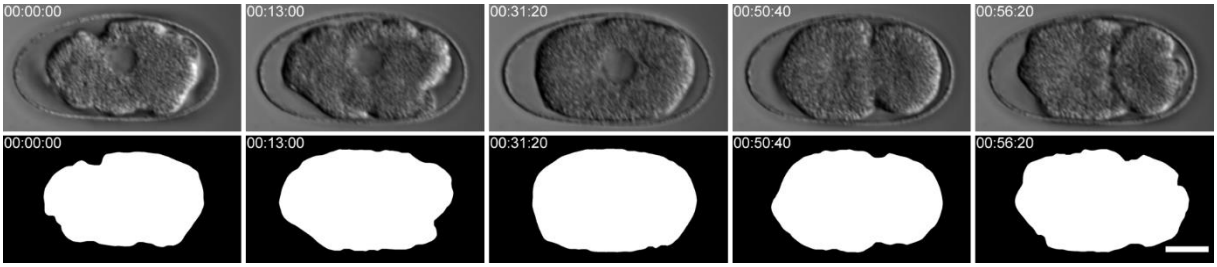

Figure 3.13. Cortical ruffling in *D. pachys* embryos. Top panel: DIC still images of different stages of ACD of *D. pachys* embryos and lower panel are corresponding masks used to calculate deformation.

I then compared the embryo masks with an either/or function where white pixels indicated the presence of a signal in only one of two consecutive frames being compared. In this analysis, the width of the margin of white pixels gave a visualization of contour changes, with a thicker band indicating more variability, thus more cortical activity and deformation. By breaking the stacks down into early ruffling, late ruffling and smoothening phases, a decrease in band thickness could be observed over time as smoothening occurred (going from left to right of top panel in Figure 3.14), but there were no obvious differences in margin thickness when comparing the future posterior and anterior poles. Indeed this was true for a whole population of embryos (N = 25) where plotting margin thickness at the anterior pole versus thickness at the posterior pole during the ruffling phase gave a linear relation with a slope of one (Figure 3.14). So although there was considerable variability in the contours explored by different embryos (margin thicknesses range from one to seven µm), the activity at the posterior and anterior poles was indistinguishable. If the anterior were more active, for example, the line would have had a slope greater than one.

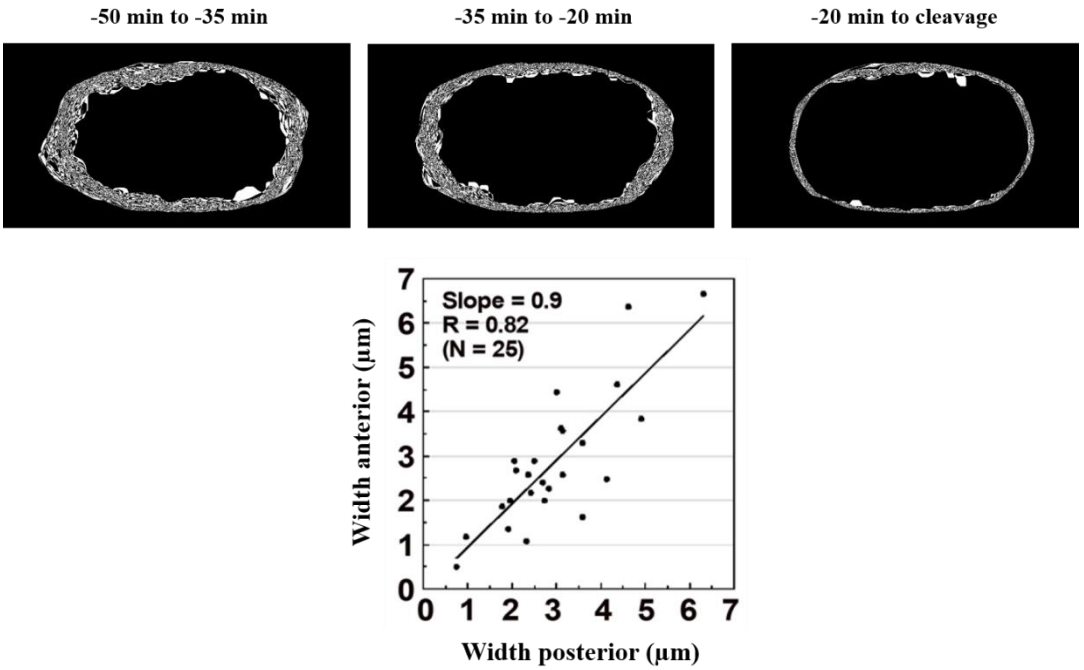

Figure 3.14. Deformation of the contour of *D. pachys* embryos calculated using either/or function. Movies divided into early, late and smoothening stages. White margins indicate unshared pixels between frames. Graph is a plot of anterior versus posterior deformation of embryos until smoothening stage (N=25).

The next step was to observe whether a difference existed in the cytoskeleton between the embryo poles in *D. pachys*. Due to a lack of transgenic techniques in *D. pachys*, I attempted to apply vital dyes for live imaging of cytoskeleton but without success (more details on methods in section 3.3). Therefore, I turned to phalloidin staining of F-actin in fixed embryos, using DNA labeling to stage the embryos. Since for *C. elegans* actin polarization is only evident post-meiotically and then diminishes around cleavage, I focused on *D. pachys* embryos that displayed a clear polar body extrusion indicating that meiosis had already taken place. For post-meiotic *D. pachys* embryos, there was no consistent actin asymmetry at prometaphase, metaphase and anaphase stages (Figure 3.15) (N = 38), whereas in the *C. elegans* control (N = 46), processed for imaging using the same method as for *D. pachys*, there was clear enrichment of actin at the future anterior pole (Figure 3.15). Neither species showed much actin asymmetry in the two-cell stage (Figure 3.15). The fact that the post-meiotic *D. pachys* embryo had a nonpolarized actin cytoskeleton resonated with the homogeneity of cortical activity quantified with live embryos images in DIC (Figure 3.14). However, the lack of polarity was not in agreement with the centrifugation results, which indicated that the nucleus had a clear preference for one pole of the embryo in the steps leading up to ACD. This led to the hypothesis that polarity in *D. pachys* was generated in earlier stages than the ones I had examined by DIC and staining, i.e., during or before beginning of meiosis in the oocyte.

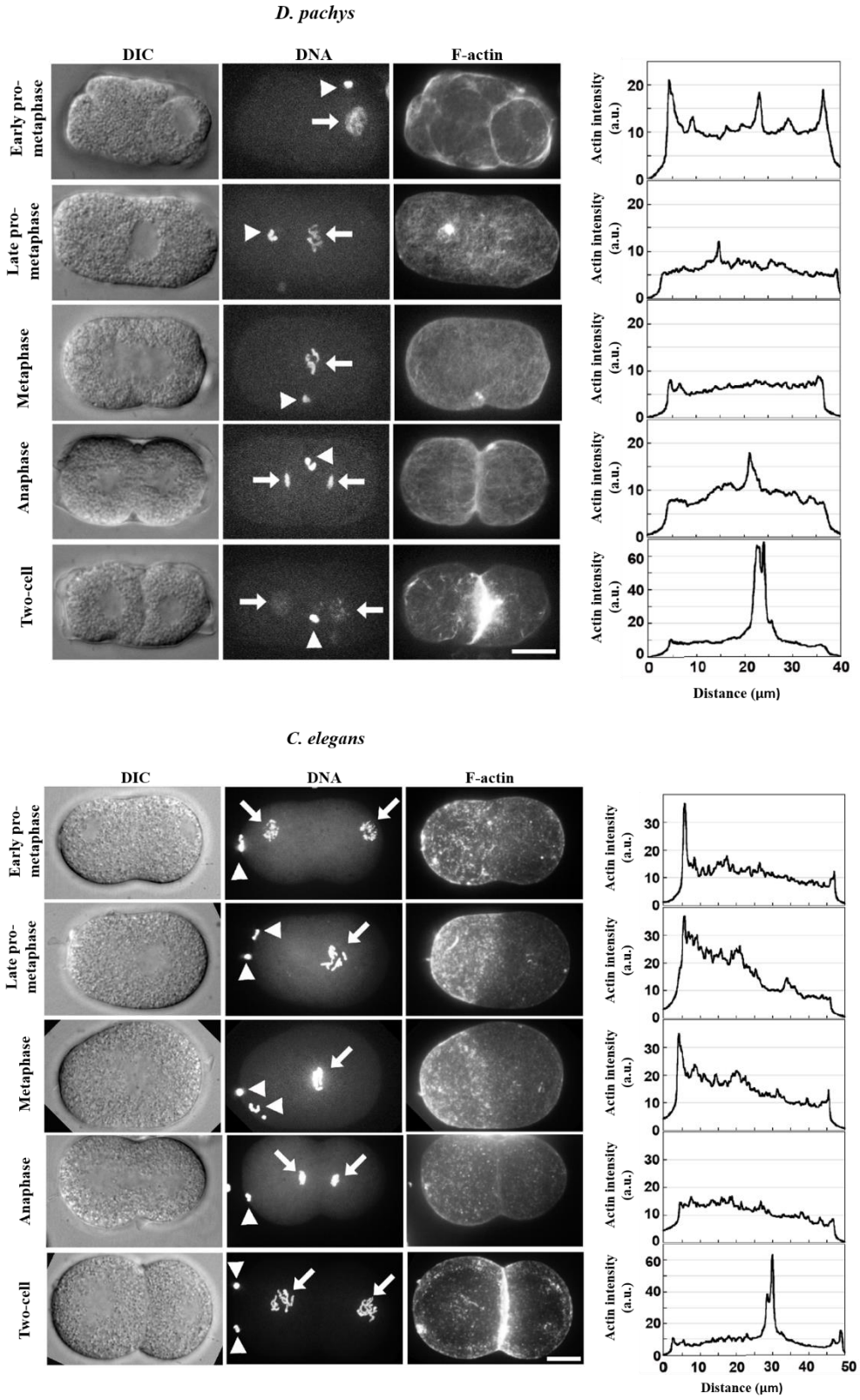

Figure 3.15. Actin cytoskeleton in post-meiotic *D. pachys* and *C. elegans* embryos. Spinning disc images of fixed staining of F-actin (phalloidin Alexa-488) and DNA (Hoechst) of the *D. pachys* and *C. elegans* embryo at different stages of cell division. DNA images are the maximum intensity projection of the embryo stack. Arrows mark nucleus and arrowheads mark polar bodies. F-actin is a sum projection of the stack. On the right are accompanying linescans for each actin image. Scale bar 10 μm.

3.2.4. The meiotic spindle correlates with the future posterior pole in *D. pachys* embryos

As was mentioned previously, the meiotic spindle under certain conditions, has been shown to be able to induce polarity in the *C. elegans* embryo, I therefore looked for a role of the meiotic spindle in symmetry breaking in *D. pachys* by examining the 20% of DIC movies that began early enough to include meiosis. I found that the meiotic spindle was invariably at the lateral side of the oocyte and not at the pole of the cell in contrast to *C. elegans*. Nevertheless, in all nine cases, the meiotic spindle was slightly off centered, and this asymmetric localization correlated with the future posterior pole (Figure 3.16.). As was mentioned in section 3.1., in a previous study on *D. coronatus*, authors came to the conclusion that there was no correlation between the polar body and the posterior pole (Lahl et al., 2006). In the quantification I carried out for *D. pachys*, I only considered the meiotic spindle and not the polar bodies since its position can drift once they are formed. Thus, the results I obtained were compatible with a role for the meiotic spindle in polarity establishment in *D. pachys*.

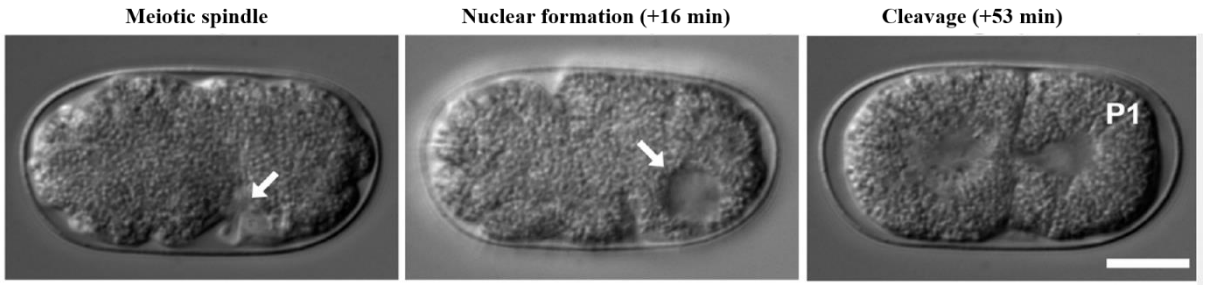

Figure 3.16. DIC still images showing meiotic spindle correlation to posterior cell positioning. Meiotic spindle is always closer to future posterior pole. Arrow points to meiotic spindle and female pronucleus upon formation; P1 marks posterior cell after division. Scale bar 10 µm.

3.2.5. *D. pachys* oocytes display a pre-meiotic microtubule aster and actin asymmetry

If indeed the meiotic spindle played a role in polarity establishment, and based on what was observed with persistent meiotic spindles in *C. elegans*, the next hypothesis to test was that some microtubule structure at the meiotic spindle could transmit a polarity signal to the cell cortex, although the role of microtubules in this process is somewhat controversial (Sonneville and Gonczy, 2004; Wallenfang and Seydoux, 2000). Our collaborator, Marie Delattre, (ENS Lyon) stained oocytes for microtubules, and found that before meiotic spindle formation (pre-meiotic), oocytes exhibited a large microtubule aster between the chromosomes, a structure not observed in *C. elegans* (Figure 3.17). During meiotic division, a cage of microtubules was seen around the chromosomes resembling a *C. elegans* meiotic spindle, but with unusual microtubule extensions reaching out on the side directed toward the cell border (Figure 3.17). Potentially, communication with the cortex during meiotic

division could exist with either one of these structures, delivering an unknown signal and setting the polarity of the embryo.

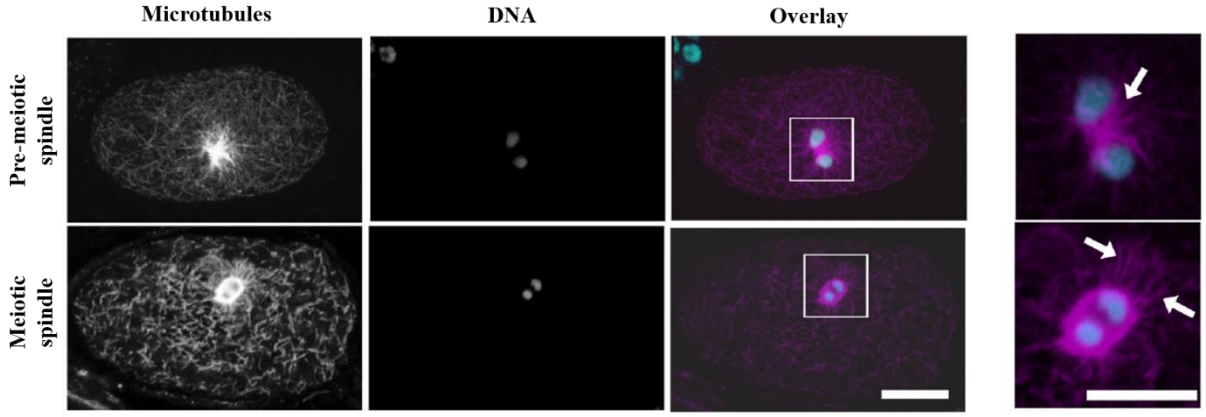

Figure 3.17. Confocal images of immunofluorescence visualization of microtubules on pre-meiotic DNA and nascent meiotic spindle. Maximum intensity projections of embryo stack in microtubules and DNA channels and overlays. Zooms of overlays shown on right. Scale bar 10 µm; 5 µm on zoom images.

To see if there was any manifestation of polarity establishment in the actin cytoskeleton at this stage, I stained and analyzed oocytes that were yet to form a polar body (evaluated by DNA staining). Of a total of 16 pre-meiotic oocytes, nine exhibited a slightly polarized actin cytoskeleton with one hemisphere being richer in actin than the other (Figure 3.18).

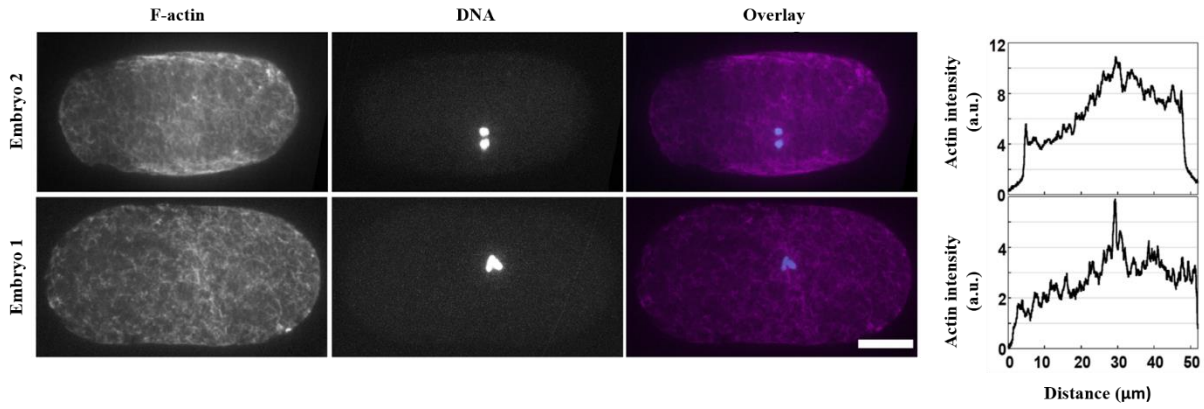

Figure 3.18. Spinning disc images of F-actin in pre-meiotic oocytes. Two examples of embryos with F-actin stained with phalloidin and DNA stained with Hoechst. Brighter F-actin is seen in the region of the DNA in both embryos as shown in left and right columns as well as actin intensity graphs on the right. DNA images are maximum intensity projection of the oocyte stack; F-actin is a sum projection of the stack. Scale bar 10 µm.

In seven cases out of nine, the DNA was in the actin-rich pole of the embryo. Assuming that the location of pre-meiotic DNA corresponded to the site of the future meiotic spindle and given correlation of the meiotic spindle with the posterior pole, my results suggest that actin enrichment was posterior, unlike what is observed in *C. elegans*. Also unlike *C. elegans*, actin polarization was weaker, more fleeting and less consistent in the *D. pachys* embryo so it was difficult to conclude more on the role of actin. In this context, however, it is important to

note that even for *C. elegans*, only certain stages of the first cell division exhibit clear actin asymmetry by phalloidin staining, and that even when asymmetry fades upon cytokinesis, the embryo retains its polarity.

3.3. Other methods tried with *D. pachys*

3.3.1. Genetic manipulation by RNAi feeding

As I mentioned previously, limited genetic tools for *D. pachys* worms exist. One study published in 2017, however, showed that *D. pachys* worms were sensitive to RNAi treatment (Fradin et al., 2017). In the study, RNAi against all five highly conserved *C. elegans* actin genes was applied to the worms. The treatment was successful in two *Diploscapter* species: *D. pachys* (PF1309) and *Diploscapter.* sp. (JU359). The sensitivity to the RNAi treatment was scored by evaluating phenotypic changes 2-3 days after RNAi treatment: larvae began to look transparent and sick, a phenotype similar to *C. elegans* worms treated with RNAi against actin genes. The larvae subsequently died without giving rise to any progeny.

Due to the reported success of this approach, I set out to use RNAi treatment in *D. pachys* for two reasons. First, I wanted to permeablize the eggshell to allow the entry of drugs and dyes as had been done in *C. elegans*, by knocking down the *perm-1* gene, which is conserved in *D. pachys* (Borowiak et al., 2015; Carvalho et al., 2011). This would have allowed me to treat permeabilized embryos with cytoskeleton inhibiting drugs as well as DNA, tubulin and cytoskeleton dyes (SiR tubulin or SiR actin) to observe embryo dynamics. Second and more long-term, I wanted to do a focused screen to knock down genes related to the cytoskeleton and polarity proteins to check how this would affect the process of ACD in single cell embryo.

By protein BLAST searches, I identified the *perm-1* gene in the *D. pachys* genome as well as *mlc-4*, which other members of the lab use routinely as a control to assure that RNAi is working since it gives a very clear phenotype: almost 100% lethal, no eggs lain, no embryos formed inside the mother. For both *perm-1* and *mlc-4*, *D. pachys* homologs were found 45% and 48% identical, respectively, at the protein level. I amplified portions of these sequences up from the *D. pachys* genome, inserted them into the feeding vector and proceeded with RNAi by feeding as per published protocols and as described in the annex at the end of this chapter. I picked 50-60 juveniles to the RNAi feeding plates and observed them every day afterwards for 2 weeks. For worms treated with *mlc-4* RNAi, no phenotype changes were observed. Treated worms laid eggs, which were removed to a fresh RNAi plate in order to follow the progeny. The phenotype of the progeny also remained normal, although this was already around two weeks after RNAi treatment of parents. In parallel I was pursuing RNAi treatment against *perm-1* of *D. pachys* in order to allow entry of vital dyes. Perhaps not surprisingly given the negative result with *mlc-4*, I never observed entry of dyes (membrane dye FM4-64, membrane dye FM1-63 and Hoechst) into *D. pachys* embryos upon dissection of *perm-1* knockdown embryos into dye solutions following the protocols of Carvalho (Carvalho et al., 2011). I subsequently abandoned this approach to follow other avenues of study as it seemed that RNAi efficiency was probe specific and perhaps weak: actin RNAi worked for

Fradin et al., but only after days of treatment, and *perm-1* and *mlc-4* knock-down appeared inefficient.

3.3.2. Live labelling of embryo dynamics

Classic manipulation methods of *C. elegans* also include soaking worms in RNAi probes (Ahringer, 2006), but I was also interested in live labelling of the embryo cytoskeleton in order to characterise *D. pachys* embryo dynamics throughout ACD. Therefore, I wished to use the approach of feeding/soaking for introducing dyes into the worms which would permeate the embryos before egg-shell formation. For proof of concept, I tested different approaches of feeding and soaking using the membrane dye FM4-64.

One method published in 2018 highlighted how the use of liposomes to encapsulate nutrients allows a more effective absorption by the worms in liquid culture due to their feeding mode, which involves filtering out and swallowing small particles rather than liquid (Flavel et al., 2018). I prepared FM4-64-encapsulated liposomes, I either directly added the prepared liposomes to an agar plate with or without OP50 and added worms on these plates, or I put the liposomes in solution with OP50 and added the worms directly into the solution. While I obtained a signal in embryos inside worms using this approach, worms were not healthy, and I did not obtain any viable dissected embryos that had integrated the dye.

In parallel, I tried soaking *D. pachys* worms directly in a solution containing M9 buffer with FM4-64 and OP50 (no liposomes). The FM4-64 dye seemed to integrate both in the cell membrane of the embryo as well as membrane bound or vesicular-like structure inside the embryo (Figure 3.19), however most embryos were not viable. In fact, after soaking, worms did not look healthy, and this could be due to the high concentration of the dye in the soaking solution. Lower concentrations gave no signal. Since the method of soaking the worms directly in M9 solution containing the dye and OP50 showed an integration of the dye in the embryo (although embryos were non-viable), and as SiR-tubulin was already available in the lab, I tried soaking *D. pachys* worms directly in a solution containing SiR-tubulin in hopes of observing live microtubule dynamics. No signal was apparent although this was probably due to the very low concentration of SiR-tubulin used, however, preparing higher SiR-tubulin concentrations was too costly.

To conclude, the approach of soaking and feeding worms with vital dyes did not seem feasible since high concentrations of dyes and drugs were required in order to observe integration into the embryos, but these concentrations were harmful to worms and embryos. The approach was also quite costly, as larger volumes were required since the dye is first ingested by the worm and then integrated into the tissues, gonad and embryos as compared to direct treatment of *perm-1* embryos.

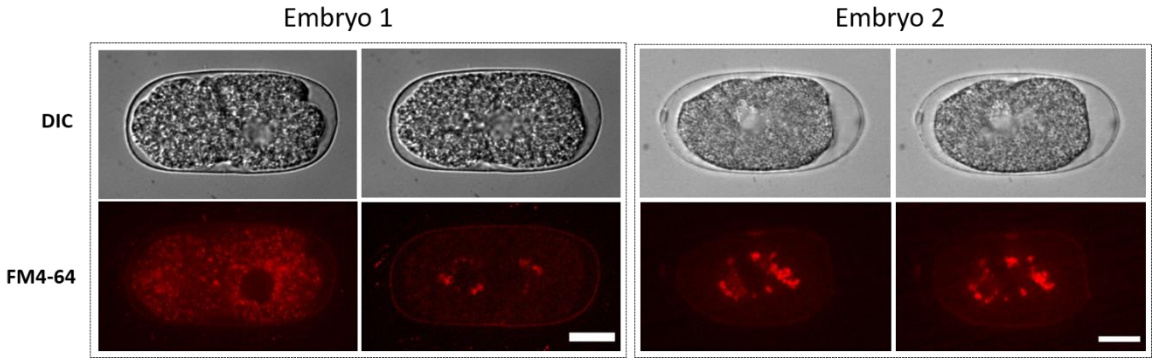

Figure 3.19. Still images from upright spinning disk microscopy films of two membrane stained *D. pachys* embryos. Embryos dissected from worms soaked in FM4-64. Both embryos arrested before cellular cleavage. Scale bar 10 µm.

3.4. Conclusion

A thorough understanding of the dynamics of ACD in the *D. pachys* early embryo ultimately will require live labelling of the cytoskeleton in order to characterize the dynamics of the process. Moreover, in order to test the different roles of the cytoskeleton as well as potential candidates for polarity establishment in the embryo such as AIR-1, PLK-1, PAR proteins etc..., it is imperative to establish genetic tools that allow manipulation of these genes to observe the effects on embryo ACD.

As I have demonstrated in section 4 of this chapter, so far for *D. pachys* worms, tools for live labelling and genetic manipulation are limited. However, successful RNAi feeding of *D. pachys* worms is quite recent and optimization of a new approach in a different lab requires time. During my PhD, optimization of this technique was not feasible; however, I have already solved problems that I was facing while testing RNAi treatment such as consistent plate contamination and lack of enough *D. pachys* worms to work with, thus bringing us closer to better conditions for trying again with RNAi feeding. Obtaining *perm-1 D. pachys* embryos could also be the easiest method for live imaging of the cytoskeleton by adding dyes such as SiR-actin and SiR-tubulin where the concentration would not have to be so high, thus avoiding intoxication of the animal as well as fitting a reasonable lab budget. *perm-1 D. pachys* embryos could then also be treated directly with inhibitory drugs such as microtubule- or actin-inhibitory drugs as well as PAR-inhibitory drugs to test the effect on the process of ACD. Obtaining transgenic lines is of course also the next step, however, especially since the completion of *D. pachys* genome sequencing is recent, different approaches still need to be tested.

The results of my PhD project have shown that the *D. pachys* embryo is polarized very early in development, before mitotic spindle positioning as was shown in the centrifugation experiments where the nucleus remains or moves closer to the preferred pole prior to division and posterior cell positioning. Moreover, the consistent correlation of the meiotic spindle with the posterior pole shows that polarization occurs either during meiosis or even before. Indeed, it would be interesting to find what would happen if the meiotic spindle was shifted by

centrifugation in order to find whether polarity is determined during meiosis, however, so far this has not worked with me. This could most probably be explained by the fragility of early embryos undergoing meiosis and/or the time needed to dissect, mount and centrifuge, thus starting centrifugation after meiosis completion.

My results also shed light on microtubule structures present in the early oocyte that are not observed in *C. elegans*. It could be that the microtubule structures observed at meiosis contribute to the symmetry breaking event. Of course, it cannot be ruled out that something even more upstream involving the oocyte nucleus, and independent of microtubules has a role. In *C. elegans* there are multiple levels of redundancy to ensure polarization is induced via the mature sperm-centrosome (Delattre and Goehring, 2021). In particular PLK-1 and AIR-1 have been shown in *C. elegans* to prevent precocious polarization in oocytes in response to cryptic cues coming from the female pronucleus and the meiotic spindle (Reich et al., 2019) or even from curvature (Klinkert et al., 2019). One hypothesis is that this inhibition is not at work in *D. pachys*, leading to very early polarization.

The question remains as to the exact nature of the polarity cue. It could be coming from the meiotic spindle large aster, be a result of self-organization of PAR proteins (Delattre and Goehring, 2021), or be produced by spontaneous symmetry breaking in curved regions of the embryo due to actomyosin contractility, as has been shown in *in vitro* systems (Carvalho et al., 2013). As concerns the first possibility, the invariably lateral position of the meiotic spindle would seem incompatible with hemispheric polarity. However, in *C. elegans* it has been shown that when polarity emerges off-axis, re-alignment of PAR domains along the long axis can occur (Geßele et al., 2020; Schenk et al., 2010). A similar corrective mechanism could be operational in the *D. pachys* case. As concerns PAR proteins, it has been shown in the sister species *D. coronatus* that PAR-1 is symmetrically distributed in the one-cell embryo just before division (Figure 3.5.) (Brauchle et al., 2009) seemingly shedding doubt on a role for the PAR network in polarity of the *D. pachys* embryo. However it is of note that there are cases in *C. elegans* where PAR-1 is uniform, but normal asymmetric division occurs nonetheless (Folkmann and Seydoux, 2019). It is also entirely possible that the PAR paradigm conceived for *C. elegans* is not the whole story in other species, and that additional PAR regulatory proteins or altogether different polarity proteins play a role (Basham and Rose, 1999; Brauchle et al., 2009; Morton et al., 2012).

Although many open questions remain, the results I obtained on *D. pachys* early oocytes show that already at meiosis, there is a difference between the poles of the *D. pachys* oocyte and this drives the polarity of the embryo. Given that *Diploscapter* is the only genus known to date within the *Rhabditidae* family, which includes *C. elegans*, to polarize independently of a sperm centrosome-derived cue, it is of particular importance to further study self-organization and symmetry breaking in this species. Investigating this will bring to light alternative/redundant pathways for symmetry breaking that are obscured in *C. elegans*, where the sperm centrosome mechanism is dominant.

As part of future perspectives of the project, it would be interesting to follow the position of the oocyte nucleus prior to activation inside the worm to shed light on whether

polarization could be taking place as early as the pre-activated oocyte stage. Although this will help answer my question on how early polarization happens for *D. pachys* embryos, what proteins and molecules are involved in polarization are yet to be discovered. Interesting proteins to investigate in *D. pachys* include PAR-1, PAR-5, PAR-6, AIR-1, PLK-1 and PKC-3 as they show a higher homology with *C. elegans* proteins as compared to other known proteins needed for ACD. As I mentioned above, while RNAi treatment did not work during my attempts in my first year at the lab, I did not get the time to properly test the approach with optimized conditions. Therefore, in future RNAi experiments of *D. pachys* in the lab,) using the better culture conditions of the worm I have established, probes against different target genes can be tested, importantly against actin for control experiments since it has been shown to have an effect on D. pachys worms. Another approach that could be carried out in parallel is injecting dsRNA with lipofectamine into the worm as this has not yet been tested on *D. pachys* worms. Moreover, lipofectamine enhances uptake of RNA and has been shown successful in other non-*C.elegans* species.

To conclude, ACD of the *D. pachys* embryo is a mysterious and interesting phenomenon, even more so when compared to the well-established *C. elegans.* The results of my PhD add to the studies presented in the field on diversity of ACD among early nematode embryos, and to the hypotheses of alternative symmetry breaking cues independent of the sperm centrosome. In-depth analysis of ACD in this species will give insight into this conserved process in cases where the typically dominant sperm centrosome is lacking.

3.5. Materials and methods

Maintenance of worms

Diploscapter pachys strain PF1309 was originally obtained from Hélène Fradin (Fradin et al., 2017). *Caenorhabditis elegans* strain N2 was from the Caenorhabditis Genetics Center. Strains were cultured at 20 °C on 2.5% standard NGM plates for *C. elegans* worms and 5% NGM plates for *D. pachys* worms in order to reduce plate contamination and burrowing. Plates were seeded with the OP50 strain of Escherichia coli as a food source.

Preparation of fresh poly-L-lysine-coated slides

For successful sticking of embryos to slides especially for centrifugation experiments and fixed staining techniques, a good preparation of poly-L-lyisne coated slides is required. Several poly-L-lysine references exist, for the methods described below, the poly-L-lysine, 2.5 mg/mL, Sigma-Aldrich P1524 was used. Upon receiving the bottle from Sigma, the powder-like content is dissolved in 10 ml sterile water and is placed in a rotator at 240 rpm at room temperature for the whole day. At the end of the day, the 10 ml of dissolved poly-L-lysine are divided into 500 µl aliquots in 1.5 ml Eppendorf tubes (smaller or larger aliquots can be prepared as seen fit for optimized volume). The aliquots are then stored at -20°C and each aliquot is thawed at room temperature before use. To prepare a fresh poly-L-lysine coated slide, 20 µl of a thawed and properly mixed aliquot (using vortex) is placed on a cleaned slide (just with kimwipe, no ethanol). The drop of poly-L-lysine is then spread on the entire slide using a rubber-like spreader, this motion is done repeatedly until the surface seems almost dry. The slide is then placed on a heat block set at 200°C for 10-15 seconds. The slide is then removed from the heat block and cooled at room temperature before placing embryos or worms.

DIC microscopy

Gravid adults were cut in a watch glass in M9 buffer and embryos were transferred to a 2% noble agarose pad. Embryos were imaged during asymmetric cell division by DIC microscopy. For time-lapse acquisitions the time between frames was 10 seconds. Long-term time-lapse imaging of egg hatching was acquired at an interval of 10 seconds for capturing first cell division, 30 seconds interval from 2-cell stage until five hours after cleavage and three minute interval for the remainder of the movie. To image embryos in utero, clean gravid worms were transferred to a 4.5% noble agarose pad in 6 µL of M9 buffer containing 0.03% levamisole to immobilize the worms. The time interval for image acquisition was 10 seconds.

Centrifugation of embryos

Clean gravid adults were dissected in 50% M9 on freshly coated poly-L-lysine slides. Embryos were aligned with their AP axis parallel to the long axis of the microscope slide using an eyelash pick as they floated down to the slide surface. Slides were then placed in a 50 mL Falcon tube filled with 50% M9 and centrifuged in a Heraeus Biofuge at 2576 x g (4000 rpm) for 15 minutes.

The slide was then removed from the tube using forceps, and excess liquid around the embryos was removed carefully with a kimwipe before overlaying with a coverslip and sealing with wax. Embryos were immediately imaged by DIC microscopy. A still image was taken of all properly aligned embryos, and then one embryo was filmed until division. Then a second still image was taken of the rest of the embryos to determine the final division positioning.

Image analysis

For nuclear positioning along the AP axis, the distance of the nucleus center to the future posterior pole, as well as the AP length, were measured in Image J every 10 minutes in the DIC movies. The percentage of nuclear position along AP axis was calculated by dividing the nucleus to posterior distance by the AP length. All averages are represented ± the standard deviation.

To quantify morphological dynamics of *D. pachys* embryos, we created training patches to train a 2D U-Net network to create masks from time lapse DIC movies (Ronneberger et al., 2015). An incremental learning approach was used where a model prediction was applied to unseen movies and a Napari correction tool was used to manually correct each frame in order to create more training data for re-training the network. This version of the program was then applied to all raw movies to produce masks. The Logical XOR function of Metamorph was applied to the mask stacks to highlight areas where embryo contours did not match.

Phalloidin staining of F-actin and F-actin imaging

The protocol was a combination of (Munro et al., 2004) and personal communication (François Robin, Institut de Biologie Paris Seine). Briefly, clean gravid worms were dissected on a freshly coated poly-L-lysine (2.5 mg/mL, Sigma-Aldrich P1524) slide and incubated between 0-50 minutes depending on what age embryos were desired. A fixing solution containing 60 mM PIPES, 10 mM EGTA, 25 mM HEPES, 1 mM MgCl2, 0.1 mg/mL lysolecithin (Sigma-Aldrich 62962), 100 mM glucose, 3% paraformaldehyde and 0.2% glutaraldehyde was then added and incubated for 15 minutes. Slides were washed three times with PBS and then incubated overnight at 4°C with 0.66 µM phalloidin Alexa Fluor 488 (Invitrogen 10125092) in PBS. Slides were gently washed with PBS and incubated for 2 hours in PBS + Hoechst (0.5 µg/mL, Fisher Scientific H1399) at room temperature. Samples were washed again in PBS, and then sealed in a drop of Aqua-Poly/Mount (Polysciences 18606) and viewed with a Roper/Zeiss upright spinning disk confocal microscope, equipped with a CoolSnap HQ2 camera and a 100x/1.46 OIL DIC ALPHA PL APO (UV) VIS-IR objective and controlled by Metamorph (Molecular Devices). Z-stack acquisition was obtained at a 0.3 µm step size. Images were processed with Metamorph and ImageJ. Linescans were obtained in Metamorph using a 3 µm line-width in average mode drawn along the AP axis of the embryo, and background was subtracted.

Tubulin staining and imaging

Embryos were freeze-cracked following protocols established for *C. elegans* and other species (Riche et al., 2013). Briefly, gravid females were dissected on poly-L-lysine coated slides and flattened between slide and coverslip before being rapidly frozen on aluminum blocks. After cracking of the coverslip, slides were immersed in -20°C methanol for at least 5 min and later processed for staining. Staining was performed for 45 min in a mouse anti-tubulin antibody DM1a (Sigma-Aldrich) diluted 1:200, followed by 45 min in a secondary donkey anti-mouse antibody DyLight 488 (Jackson 2 Immunoresearch) diluted 1:1000. Slides were then incubated for 5 min in 1µg/ml Hoechst 33342 (Sigma-Aldrich). Images were acquired on Zeiss LSM710 confocal microscope with a 63x oil immersion objective. Images were processed with Metamorph and ImageJ.

Single Worm PCR

This technique was used to amplify DNA fragments from genomic DNA of worms

Preparation of lysis buffer:

For one reaction of 15 µl, following was mixed in order

Ingredient	**Volume (µl)**
H_2O	12.75
Worm PCR buffer (10X)	1.5
Proteinase K (NEB)*	0.75

*enzyme pipetted at the bottom of the solution in the tube several times to clean the tip.

1. *Worm lysis program*

   Run using a standard PCR machine after picking a single worm into each PCR tube containing the single worm PCR lysis buffer described above.

Temperature	**Duration**
65°C	1 hour
95°C	15 minutes
4°C	Hold

2. *PCR Reaction: protocol for one reaction, mixed in order*

   After obtaining genomic DNA from the preceding protocol, a PCR reaction using the gDNA and specific primers was run to amplify the DNA fragments desired.

Ingredient	**Volume (µl)**
H_2O	13.375
10x Taq Buffer	2
dNTPs	0.5
Forward primer	0.5
Reverse primer	0.5
Taq*	0.125
DNA	3

Step	Temperature	Duration (mins:sec)
Initial denaturation	95°C	00:30
35 cycles	95°C 57°C 68°C	00:30 00:30 01:30
Final extension	68°C	05:00
Hold	4°C	

*only basic Taq Polymerase. 'Fancier' polymerases do not work as well for this reaction. Pipetted several times when adding enzyme to clean the tip. Solution is mixed by flicking well closed tubes. Centrifugation for 4 seconds (strip centrifuge) prior to placing in thermocycler.

Primers used for amplification of DNA fragments of mlc-4 and perm-1 from genomic DNA prepared from D. pachys worms.

Name of primer	Sequence (5'-3')
DpaMlc4 F	TTGATATCGAATTCCTGCAGTCGAAGGCAGGAAAGAAG
DpaMlc4 R	ACCGCGGTGGCGGCCGCCTGATCTAACGTTTGACAAATAACC
DpaPerm1 F	TTGATATCGAATTCCTGCAGAAGACGAACCGTCTCTTCGC
DpaPerm1 R	ACCGCGGTGGCGGCCGCCTGCAGAAAACCCTCGCC

Table 3.1. Primer for amplification of DNA fragments for target genes for RNAi feeding preparation. For name of primer: Dpa: *D. pachys* followed by name of gene and F is for forward, R for reverse. Primers were ordered from Eurofins.

Once PCR products of target gene fragments were complete, they were inserted into appropriately digested L4440 plasmids by an InFusion reaction and then transformed into Stellar competent cells for cloning of cells (Miniprep and then Maxiprep for best colony).

Preparing bacteria with probes for feeding

100 µl HT115 competent cells were added into a 1.5 ml tube

150 ng DNA was added to the tube and mixed very gently by hand (tapping on the tube) ensuring no drops were left on the walls. (The DNA is the RNAi probe in the L4440 vector).

Tube was incubated 30 minutes on ice and then treated with a heat shock at 42°C for 2 minutes in a water bath.

1 ml of LB media was then added and the tube was inverted for mixing and then incubated for 1 hour at room temperature.

20 µl and 100 µl were added on to the center of two different ampicillin agar plates pre-treated with tetracycline* and spread on the surface using a glass spreader.

The rest of the bacteria was centrifuged at 20,000 g for 2 minutes at room temperature.

Most of the supernatant was removed leaving 100 µl. This was resuspended and spread on Amp-Tetra plates as described in previous steps.

The plates were incubated overnight at 37°C.

Only colonies closest to the center of the plate were picked (next protocol).

*For tetracycline treatment of plates: 55 µl tetracycline (100 mg/ml) was added to the center on an ampicillin plate and spread evenly on the surface using a glass cell spreader.

RNAi by feeding

A single colony was picked with a 10 µl sterile pipette and grown in 3 ml LB medium + 3 µl of 100 mg/ml ampicillin in a 15 ml culture tube at 37 °C, 220-240 rpm rotation.

After 3 hours, the OD was checked using 100 µl of the culture + 900 µl LB medium after blanking the machine on 900 µl LB.

Once the OD value reads between 0.6 and 0.75, 4 NGM-IPTG plates (protocol below) were spotted with 100 µl for each condition. (If an OD of around 0.4 is measured, it was measured again after 20-25 minutes).

Once the bacteria soaked in, the plates were inverted and incubated at room temperature overnight for inducing expression. For more efficient inducing of expression, the bacteria needed to dry quickly. If after 20 minutes of spotting the plates were not dry, the plates were placed in a hood with the lid of the plates ajar while keeping lab windows closed to avoid contamination.

50-60 *D. pachys* young worms (not yet pregnant) were picked over to each induced plate.

Changes in phenotype such as movement or health of worms were checked for every day.

Preparation of NGM plates that contain IPTG

Once the bacteria containing the probe are prepared, they were poured onto pre-prepared plates that contain IPTG in order to become activated (activation refers to the induction of the T7 promoter in the L4440 plasmid containing the probe).

Ingredient	**Preparation of 1 litre of 5% NGM**
NaCl	3 g
Bacto Agar	51 g
Bacto Peptone	2.5 g
Milli-Q water	950 ml
Bottle contents were mixed by inverting bottle several times prior to autoclaving. This was done quickly in order not to let ingredients sediment, otherwise they will be caramelized in the autoclave. After autoclave (120°C for 20 minutes), bottles were placed in 55°C water bath for at least half an hour before adding salts and antibiotics.	
1M $CaCl_2$	1 ml (for 250 ml: 250 µl)
1M $MgSO_4$	1 ml (for 250 ml: 250 µl)
1M KPO_4 pH 6.0	25 ml (for 250 ml: 6.25 ml)
5 mg/ml cholesterol; solution in ethanol, avoid flame	1 ml (for 250 ml: 250 µl)
For IPTG plate preparation (induction of RNAi)	
IPTG (1M)	For 250 ml: 250 µl
Carbenicillin (100 mg/ml)	For 250 ml: 125 µl

A large volume (1L) of autoclaved NGM was prepared and then divided into smaller (250 ml) bottles without addition of salts and antibiotics and were stored at 4°C. When needed, a bottle of 250 ml NGM was melted in the microwave, supplemented with salts and antibiotics. 250 ml of NGM poured around 25 plates (10 ml per plate).

All plates were stored at 4°C (IPTG in plates is active up to 3-4 days after pouring).

Liposome preparation

Protocol was adapted from (Flavel et al., 2018). Briefly, DOPC (1,2-dioleoyl-sn-glycero-3-phosphocholine) Avanti Polar Lipids was used. Dissolved lipids in chloroform were already available in the lab at 25 mM concentration. 20 µl of the stock was mixed with 480 µl chloroform in glass test tubes to produce lipid concentration of 1 mM. The prepared liposome solution were divided into 100 µl per vial. The chloroform was evaporated in a hood with constant vortexing until a thin film of lipid was formed on the wall of the test tube. The tubes were then dried using a vacuum oven at 20°C for 2 hours. To encapsulate the media in liposomes, I add 2 ml of M9 buffer with FM4-64 (Invitrogen T13320), final concentration 0.33 mM. The tube was then incubated at 37°C for 30 min. This was followed by gentle vortexing to form liposomes.

Soaking worms in dye solution

In brief, in a 1.5 ml tube, I prepared 200 µl M9 solution with FM4-64 at a final concentration of 0.825 mM (optimized after testing different concentrations) and for food, 1 ml of OP50 culture and 3 µl of the pellet were added to the M9/FM4-64 solution. Around 30 *D. pachys* pregnant worms were picked over into the solution and the tube was left to rotate for 2 hours at room temperature. Dissection of worms and imaging at upright spinning disk were carried out as described in methods of section 3.5. The same soaking method was used with SiR-tubulin (Spirochrome SC002) with final concertation of 8 µM.

Chapter 4: Investigating ACD in the *Pristionchus pacificus* embryo: a hermaphroditic nematode evolutionarily distant from *C. elegans*

4.1. Introduction: What we know about *P. pacificus* and goal of the study

4.1.1. General description

As I have highlighted in previous chapters, a new understanding of the mechanisms behind the process of ACD and its regulation can be obtained from establishing comparative models to the well-studied asymmetric division of the single cell *C. elegans* embryo. In addition to investigating ACD in single-cell embryos of the parthenogenetic species *D. pachys*, my PhD project entailed the study of another species called *Pristionchus pacificus* (*P. pacificus*), evolutionarily more distant from *C. elegans* than *D. pachys* (Kiontke and Fitch, 2005) (Figure 2.19). Given that the genome of *P. pacificus* has been sequenced and that genetic tools for manipulation exist, *P. pacificus* presents an important comparative model to the well-studied nematode *C. elegans*. *P. pacificus* like *C. elegans* is a hermaphroditic nematode meaning oocytes undergo self-fertilization inside the worm, or are fertilized by spontaneously occurring males. *P. pacificus* is a free-living nematode that was first isolated in 1996 from Pasadena, California (Sommer et al., 1996). Like *C. elegans, P. pacificus* worms can be grown easily on a plates containing *Escherichia coli* bacteria for food and they have a 4-day generation time, one day longer than that of *C. elegans* (Sommer et al., 1996). Unlike *C. elegans* which is microbivorous, *P. pacificus* worms are omnivorous (Hong and Sommer, 2006). Since the isolation of *P. pacificus*, it has been used in evolutionary, developmental and ecological studies. For example, the development of the vulva in *P. pacificus* has been used to compare it to other nematode species in order to get more insight on the evolution of the process. It was found that in *P. pacificus*, the number of vulva precursor cells was reduced as compared to other rhabditids due to programmed cell death of 7 precursor cells (Sommer and Sternberg, 1996). Genomic comparative studies using *P. pacificus* have been carried out to understand the differences in morphology of this species as compared to other nematode embryos that feed and live differently (Dieterich et al., 2008).

4.1.2. Genetic manipulation of *P. pacificus*

Different techniques have proven successful for genetic manipulation of *P. pacificus* in the last decade including classic transgenesis methods, genome editing by CRISPR/Cas9 and RNAi. I will describe briefly the different methods used for manipulating *P. pacificus* and for what purpose.

Transgenesis in *P. pacificus* has been shown successful by making extrachromosomal arrays using microinjection of transgenic DNA into the gonads (Schlager et al., 2009). Although transformation by microinjection was less efficient than in *C. elegans,* however a dominant mutant locus that gives a roller phenotype was demonstrated as a transformation marker

(Schlager et al., 2009). Making extrachromosomal arrays causes mosaicism, and due to the high-copy numbers of transgenes, silencing of transgenes occurs in the germline and early embryos (Kelly et al., 1997). Moreover, for transgenesis in *C. elegans*, extrachromosomal arrays consist simply of the target transgene and a co-injection marker that drive expression in the somatic cells. This is more complicated in *P. pacificus* as the arrays must consist of: host genomic DNA, the target transgene and a co-injection marker that are all digested with compatible restriction enzymes (Schlager et al., 2009).

Other than making extrachromosomal arrays, a method of transgenes is the CRISPR/Cas9 system. Genetic editing of *C. elegans* using this system has already been established (Dickinson et al., 2013; Friedland et al., 2013) as well as for *P. pacificus* (Witte et al., 2015). In *C. elegans,* CRISPR/Cas9 has been used successfully to insert fluorescent protein to visualize proteins of interest. However, integration of relatively large DNA fragments in *P. pacificus* by CRISPR/Cas9 has been unsuccessful (Namai and Sugimoto, 2018).

Recently, it was shown that inducing RNAi in *P. pacificus*, as well as other non-*C. elegans* species, is effective upon injecting double stranded RNA (dsRNA) with lipofectamine. Microinjection of dsRNA for *par-1* with lipofectamine in the distal end of the *P. pacificus* adult worms resulted in 66% of embryonic lethality (Adams et al., 2019). However, a colleague in another lab in Paris working on nematodes tried injection with lipofectamine in Rhabditophanes species and attempts came to no avail (personal communication with Aurelien Perrier at Institut Jacques Monod). Morpholino (MO) knockdown experiment have also been carried out against different Wnt-pathway components to study the effect on the vulva development of *P. pacificus* (Tian et al., 2008).

A method to integrate low copy number transgenes in the *P. pacificus* genome, especially to construct strains that express fluorescently tagged proteins in the germline and embryos was achieved by a lab in Japan (Namai and Sugimoto, 2018). They were able to successfully obtain *P. pacificus* transgenic lines for GFP-labelled tubulin and histone under a ubiquitous promoter by biolistic bombardment using hygromycin B resistance gene (*HygR*) as a selection marker. They observed strong autofluorescence in the embryo that obscured transgenic fluorescent protein signal (Figure 4.1.A-E). To overcome this they used ethyl methanesulfonate (EMS) mutagenesis and screening for a mutation in autofluorescence (*afl-1*), and in this background, were able to observe the mitotic spindle and DNA in their dividing embryos (Figure 4.1.F-J).

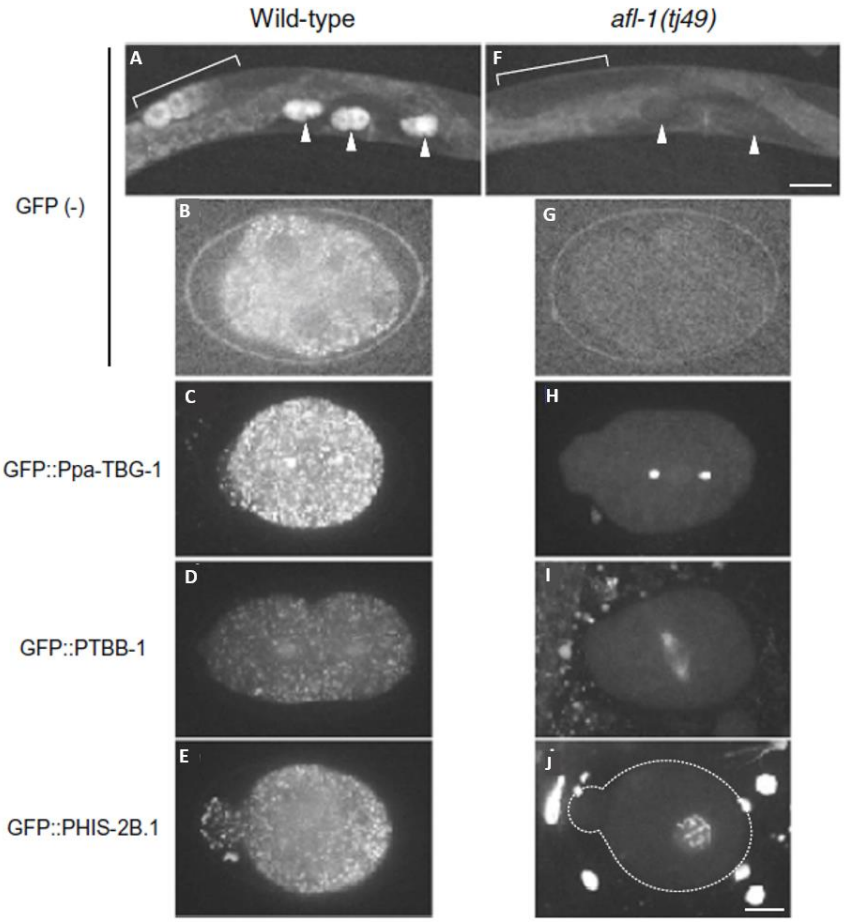

Figure 4.1. Expression of GFP-fusion proteins in the wild type and the afl-1 mutant. A–E Wild type. **F–J** afl-1(tj49) mutant. Oocyte region (brackets) and early embryos (arrowheads) are indicated. **C**, **H** GFP::Ppa-TBG-1 (γ-tubulin, centrosome marker). **D, I** GFP::PTBB-1 (β-tubulin, microtubule marker). **E, J** GFP::PHIS-2B.1 (histone H2B, chromosome marker). Scale bars: **A, F** 50 µm; rest:10 µm. (*Adapted from Namai et al., 2018*).

4.1.3. Goal of the study

Given that the morphological dynamics of the *C. elegans* embryo are well described as concerns the ruffling at the contour of the cell which then breaks towards the anterior due to actomyosin contractility upon breaking symmetry, it is surprising to see that even though *P. pacificus* embryos also get fertilized by sperm, embryo morphology is drastically different. The *P. pacificus* single cell embryo indeed divides to give rise to two asymmetric daughter cells wherein later each cell reproducibly also divides asymmetrically at asynchronous timing. When looking at DIC movies of this species, however, the cellular features of the *P. pacificus* embryo are very different from *C. elegans*, the cell contour dynamics seem more chaotic as well as cytoplasmic streaming and spindle rotation and positioning. Typical features for ACD in DIC as seen and studied in *C. elegans* seem to be lacking in *P. pacificus*, despite this, the *P. pacificus* embryo is still able to successfully divide asymmetrically. The goal of my PhD was to characterize the cytoskeleton of the *P. pacificus* in pursuit of shedding light on different dynamics and regulatory mechanisms of the cytoskeleton that still ensure the cell positions the spindle divides asymmetrically. Given that the genome of *P. pacificus* has been completely

sequenced and genetically amenability of *P. pacificus* has been shown in previous studies, the *P. pacificus* embryo seemed like another promising comparative non-*C. elegans* embryo to fit within the scope of my project.

4.2. Methodology and results

4.2.1. Observations of ACD in *P. pacificus* by DIC

As briefly mentioned in section 2.6, while *P. pacificus* oocytes undergo fertilization just as *C. elegans*, some features such as the cellular contour, constriction an anterior pole and spindle positioning seem exaggerated as compared to *C. elegans* when looking at DIC movies of first ACD (Figure 2.15 and 4.2) (Valfort et al., 2018).

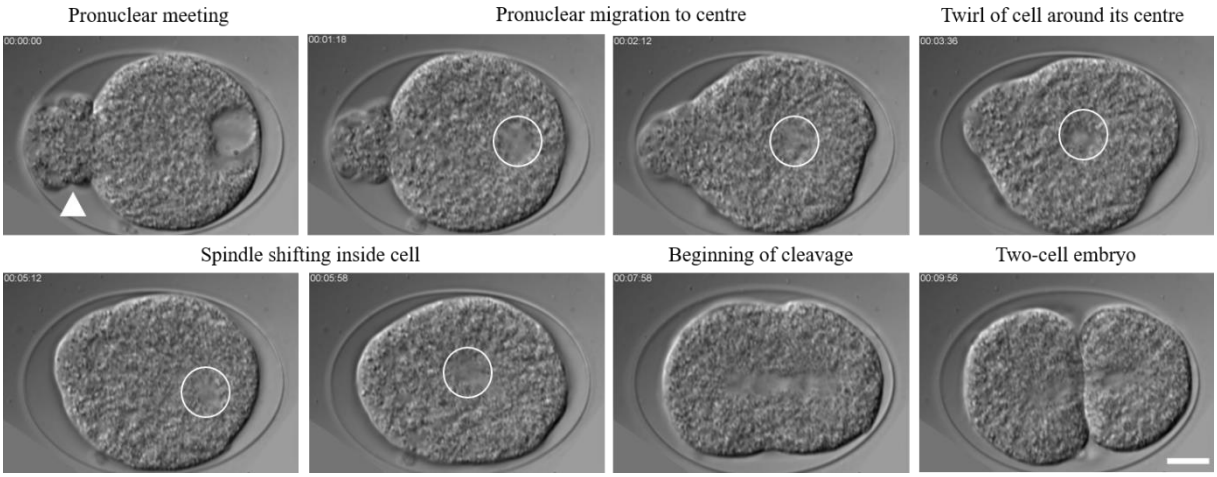

Figure 4.2. Still images of DIC movie of first ACD in *P. pacificus* embryo. Top left to bottom right images showing series of events during ACD of the embryo at 2-second interval acquisition. Arrowhead points to anterior constriction. White empty circles mark pronucleus. Timestamp at top left of each image. Scale is 10 µm.

Pronuclear meeting in the *P. pacificus* embryo occurs at the future posterior pole similar to *C. elegans* (Figure 4.2 and 2.15 for comparison with *C. elegans*). The future anterior pole at this stage is highly constricted forming a bulge-like structure, as if about to extrude a substantially smaller cell. Due to limited movies of *P. pacificus* prior to pronuclear meeting, the development of this anterior constriction could not be assessed enough to say whether it represents the pseudocleavage phenomenon that occurs in *C. elegans*. The anterior constriction in *P. pacificus* remains until pronucleus centering. During pronucleus centering, cytoplasmic flows are directed into the anterior constriction and the pronucleus is also shifted closer in that direction. Although the embryos contour starts to become smooth at this stage, cytoplasmic flows are still chaotic, different from the smooth *C. elegans* embryo during pronucleus centering. The centering of the pronucleus in *P. pacificus* in some embryos is also accompanied by a drifting and turning of the cell around its center. The spindle also seems to shift inside the embryo before being shifted again towards the future posterior pole prior to cleavage. The lack of *C. elegans gpr-1* and *gpr-2* orthologs could probably explain these differences seen in spindle positioning as compared to *C. elegans* (Kraus et al., 2017). The

cleavage furrow takes place at an asymmetric site (closer to the posterior pole) and two asymmetric size daughter cells are produced. Following these observations, although accompanied by more exaggerated movements, given that *P. pacificus* undergoes some main features of ACD that have been well studied in *C. elegans*, I aimed to observe and gain insight of the cytoskeleton of the *P. pacificus* embryo.

4.2.2. Molecular biology for labelling actin cytoskeleton for live imaging

Since the cortical contractility and the development of pseudocleavage in the *C. elegans* is a result of actomyosin contractility that is directed towards the anterior pole, it made sense to think that perhaps the exaggerated morphological dynamics observed in *P. pacificus* embryos are a result of altered actomyosin dynamics as compared to *C. elegans*. Thus, my primary aim was to label the actin cytoskeleton in *P. pacificus* embryos in order to observe and quantify actin dynamics, helping my investigation of whether some regulatory mechanisms of the actin cytoskeleton have been adapted across evolution in order to maintain the conserved process of ACD.

To be able to observe and characterise actin dynamics in the embryo during ACD, my primary PhD goal was to obtain transgenic actin-labelled worm lines. Given the successful transgenesis in *P. pacificus* by biolistic bombardment (Namai and Sugimoto, 2018), I chose to follow this procedure to introduce fluorescent Lifeact into embryos to permit live imaging of actin dynamics. We were lucky in spring of 2018 to have a visit and seminar from Asako Sugimoto, the PI in charge of the successful bombardment in *P. pacificus*. She shared with us her still-unpublished results concerning Lifeact-GFP expression in *P. pacificus*, where she observed interesting actin dynamics including a novel actin patch near the point of detachment of the fused pronuclei from the cortex just as nuclear centering began. She also provided us with her expression plasmids and Lifeact-GFP worms (see Annex to this chapter). She revealed that the study was suffering from low signal, interference from autofluorescence (even in the *afl-1* background) and silencing after a few generations. Therefore, I undertook to produce a different Lifeact strain, labelled with the red fluorescent protein mKate2 instead of GFP to reduce the interference from autofluorescence, which was in the green/yellow range. Also, I decided to use a *mex-5* promoter and 3' untranslated region (UTR), and to include a special linker between the Lifeact label and the mKate2. The choice of promoter, fluorescent protein and linker length had all proved to be very important in *C. elegans* for obtaining healthy worm strains that gave good actin images in the embryo (Reymann et al., 2016). Additionally, it has been shown that synthetic genes for transgenesis that are designed to contain adapted codons from genomic DNA can optimize expression levels of the target gene (Redemann et al., 2011). A good expression of GFP in the animal tail and Lifeact in the early embryo via transgenic methods has been shown successful in *P. pacificus* and *C. elegans*, respectively (Reymann et al., 2016; Schlager et al., 2009). Therefore, different Lifeact genes were prepared for my project: a gene for Lifeact that includes either *P. pacificus* type synthetic

introns (Schlager et al., 2009), or those used traditionally in *C. elegans* or no synthetic introns at all, more details on the use of these designs will follow. Finally, it had been shown that a splice acceptor sequence upstream of the ATG was required to drive the expression of target genes in *P. pacificus* (Schlager et al., 2009), so I also included that splice sequence in all plasmid designs.

To prepare for bombardment, I first needed to prepare the expression vectors that would be used to bombard the worms. The expression vectors needed to carry the *HygR* gene as the selection marker, as well as the *mex-5* promoter sequence and 3'UTR from the *P. pacificus* genome, with the Lifeact::*mkate2* sequence. The lab was accustomed to making complex plasmids via MultiSite Gateway so I first created a destination vector from the plasmid pSNP44 from the Sugimoto lab that contained the *HygR* gene expressed under the ubiquitous *rpl-28* promoter. Between the NotI and PstI sites of the multiple cloning, I inserted via InFusion the attR4-attR3 sequence in order to use this plasmid as the final pDEST-R4-R3 vector. I then extracted DNA from *P. pacificus* worms (worm lysis protocol as described in Chapter 3), and using that as the template, I amplified the *mex-5* promoter and 3'UTR sequences for insertion in the 4,1 and 2,3 positions in the Gateway system, respectively. As an alternative I also amplified the *rps-27* promoter sequence and the *rps-0* 3'UTR sequence from Sugimoto plasmid pSNP52 for insertion in the 4,1 and 2,3 positions in the Gateway system, respectively, since this ubiquitous promoter had worked for them, albeit giving silencing over time as mentioned before. Finally, I constructed different *Lifeact::mkate2* sequences for the expression plasmids, all containing the splice acceptor sequence before the ATG and equipped with the correct sequences for insertion into the 1,2 position in the Gateway system. For the Lifeact gene, as mentioned above, three constructs were prepared: *Lifeact::mkate2* sequence without introns, *Lifeact::mkate2* with *P. pacificus* introns and *Lifeact::mkate2* with *C. elegans* introns. The first two genes were purchased from Eurofins, and the third was amplified in the lab from genomic DNA purified from the worm strain SWG49, a Lifeact_*mKate2 C. elegans* line obtained from Anne-Cecile Reymann (Reymann et al., 2016). All PCR amplified products were verified by running a DNA agarose gel. After carrying out recombination reactions into the entry vectors, plasmids were sequenced in order to make sure they contained the target genes. After recombination into the destination vector diagnostic, digests were performed to verify the correct assembly of the different parts of the constructs. The six constructs I worked with are summarized in Figure A.1. in the annex at the end of the chapter.

4.2.3. Conditions and results of biolistic bombardment 1

An important step for successful biolistic bombardment in *C. elegans* is starting with many synchronized young adult worms. Growing large number of *C. elegans* can be easily done in liquid culture, with worm growth medium (WGM; protocol in Annex at the end of this chapter) and bacteria for food (BL21 furnished in large quantities by a protein purification facility that uses a fermenter). Worm growth in liquid culture for *P. pacificus* proved more challenging than for *C. elegans* for reasons that remain unclear. Overall, the cultures did not thrive, and

after around 10 days from starting the liquid culture for *P. pacificus*, there were still not enough adult worms. Crystals that formed over time in the culture seemed harmful to the worms, particularly the adults and they started dying. This was also experienced in the lab of François Robin (IBPS, personal communication, 2018) Below is a more detailed timeline of worm growth for the first bombardment experiment of *P. pacificus*.

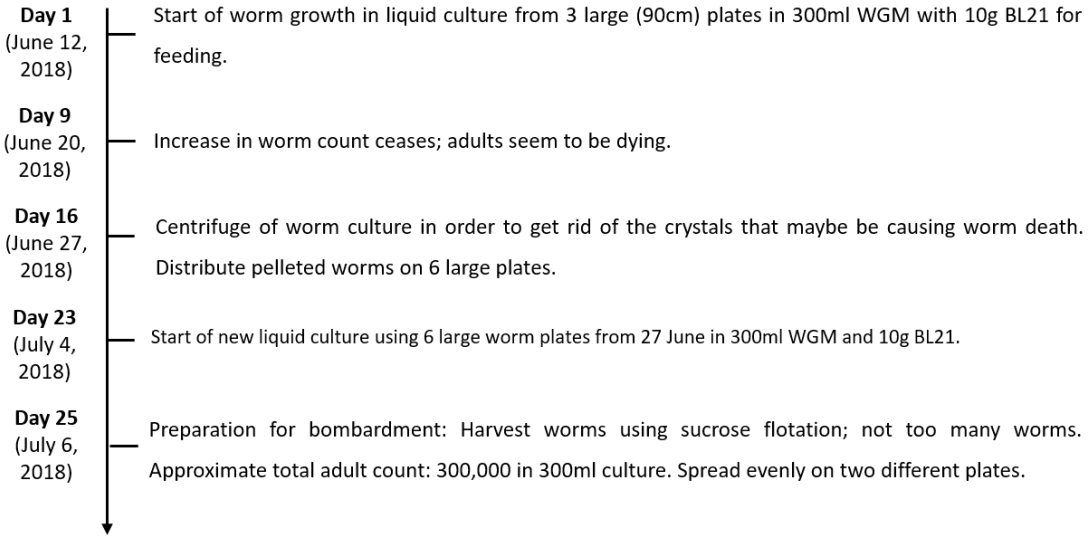

For the first bombardment of *P. pacificus* worms, the standard conditions used for biolistic transgenesis of *C. elegans* were used: 1350 psi rupture discs and 1 µm diameter gold particles. Each plate of worms was bombarded with gold micro particles coated with one expression plasmid; for the first bombardment, expression vector 2 and 5 (Figure A.1 in Annex) were used (both containing the Lifeact::*mKate2* sequence with *P. pacificus* introns).

After carrying out bombardment with both expression vectors, worms were left on the bench for around two hours to recover. Thereafter, worms were washed off the plates and distributed to 20 9-cm NGM OP50-seeded plates. After a day of rest, worms on the plates were treated with hygromycin B with a final concentration of 0.5 mg/ml for each plate. This concentration of hygromycin B treatment was determined after running different concentration tests on the SA1159 *P. pacificus* worm strain that contains the HygR gene. Over the next two weeks, OP50 was added twice to the plates as food had run out. Since there were still some surviving/moving worms (although they looked a bit unhealthy), I picked them over to fresh NGM plates containing hygromycin B. The worms however did not grow well when transferred to the hygromycin B treated plates; most worms died the following day. I therefore concluded that the bombardment had not worked for this attempt. The movers I had on my selection plates were probably animals that had escaped selection due to degradation at 20°C of the antibiotic over time. I therefore started preparing for the next attempt of biolistic bombardment of *P. pacificus*, described in the next section.

4.2.4. Conditions and results of biolistic bombardment 2

In order to grow a large number of worms for the second bombardment, a different approach was carried out in order to minimize time in liquid culture. The details of the worm growth timeline are described below.

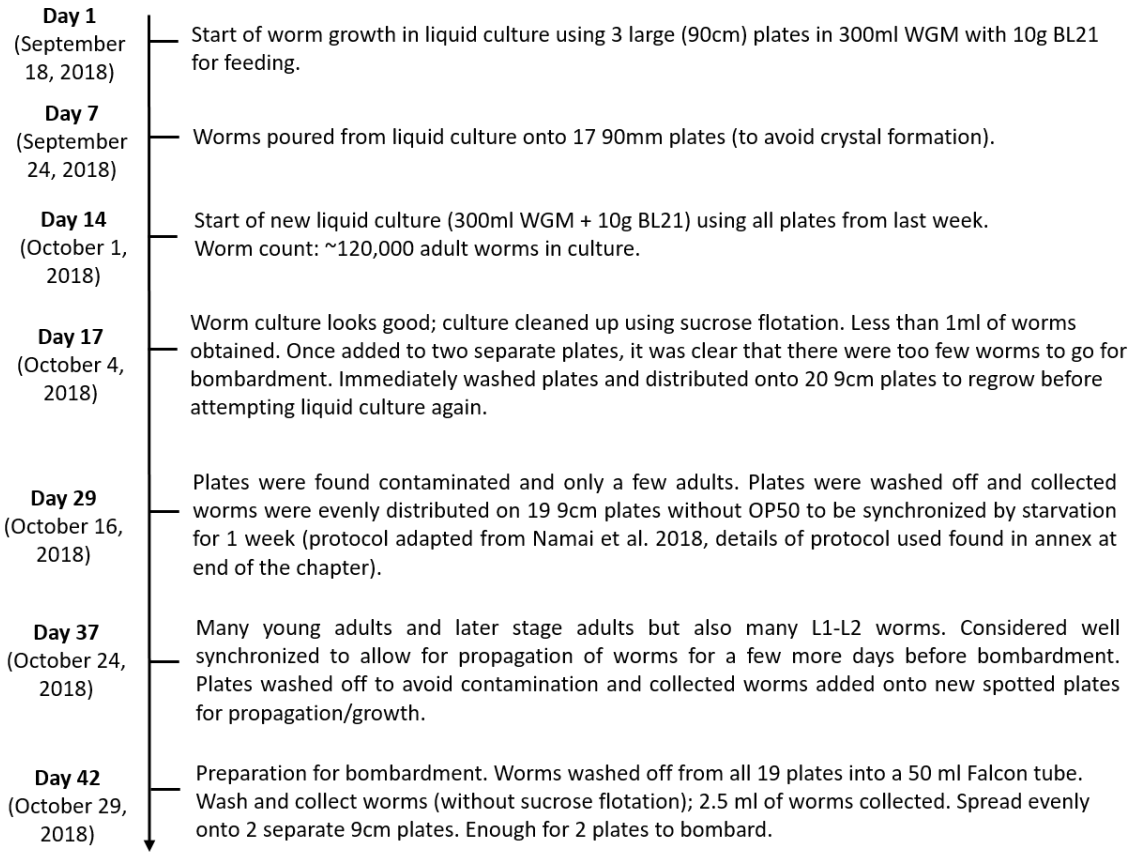

Conditions for the second bombardment in *P. pacificus* were carried out according to the Sugimoto lab protocol, which involved using tougher rupture discs (1500 psi) and larger gold micro-particles (1.6 µm diameter) than what I had used for the first bombardment and what the lab had used successfully with *C. elegans* in the past. The same expression plasmids (expression vector 2 and 5) were used again for bombardment 2.

After bombardment, worm plates were left for 2 hours on the bench to recover. The worms were then washed off the plates with M9 buffer and distributed evenly on 9 cm NGM plates seeded with OP50. The plates were left overnight in order to dry properly. The following day, mainly healthy adult worms were found so the plates were turned over and incubated at 20°C. Plates were treated with hygromycin B the next day at a final concentration of 0.4 mg/ml this time, taking into consideration that perhaps the 0.5 mg/ml concentration used the first time was too high. Two weeks later, there were some healthy, young worms although no surviving adults were found. The moving worms were isolated on plates containing 0.4 mg/ml hygromycin B. Survivors were picked over to fresh hygromycin-containing plates two more times to verify resistance the treatment. Upon isolating moving worms to new plates, each

time 3/5 worms would die, and the surviving worms would grow normally and produce progeny.

4.2.5. Imaging transformants from bombardment 2

Since I consistently obtained worms that survived antibiotic treatment, I set out to image them to see if fluorescence was observable. Worms were mounted on 4.5% Noble agar pads, immobilized using 15 mM sodium azide and observed by epifluorescence microscopy. I examined early embryos in both the red channel for mKate2 and in the green channel for autofluorescence.

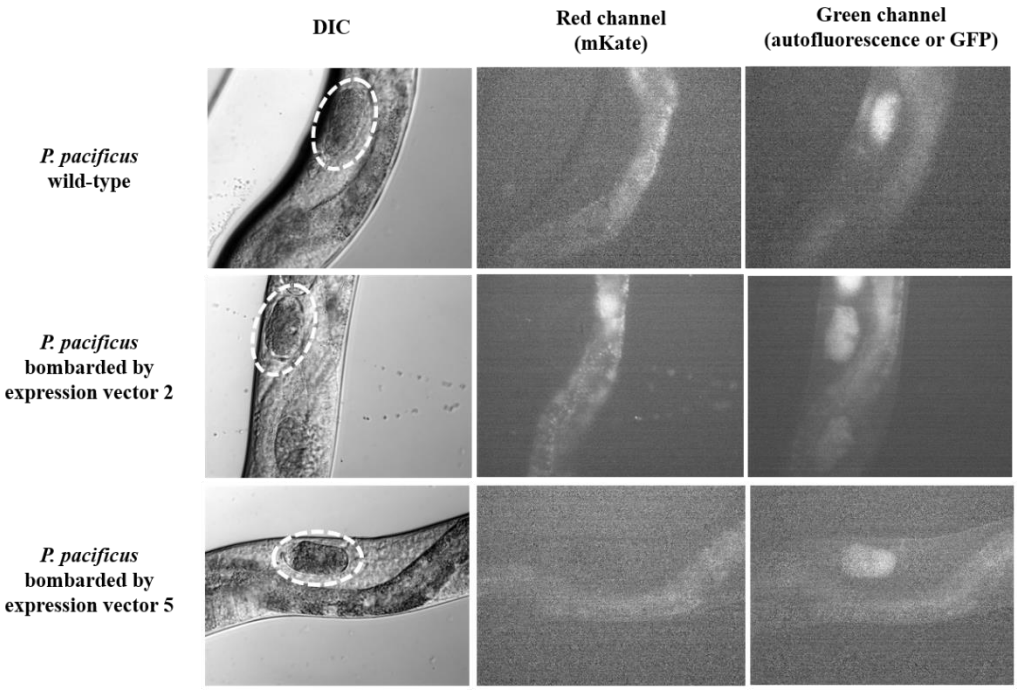

Figure 4.3. Checking for fluorescence in embryos of *P. pacificus* survivors after hygromycin B treatment using an epifluorescence microscope. White dashed lines mark the embryos inside the worm being checked for fluorescence. Images taken using epifluorescence microscope. All images are auto-scaled in ImageJ.

Wild-type *P. pacificus* showed as expected a strong signal in the green channel corresponding to autofluorescence and no signal in the red channel (Figure 4.3). For my transformants, under both embryo specific and ubiquitous promoters (expression vector 2 and 5, respectively) no fluorescence in the red channel corresponding to mKate2 was detected, although autofluorescence in the green channel was strong (Figure 4.3, two lower panels).

4.2.6. PCR analysis of transformants from bombardment 2

Since the worms did not show red fluorescence, but seemed nevertheless resistant to the antibiotic, it was possible that the worms were transformed, but that the *mKate2* gene was silenced. To check this, I singled out survivors after another hygromycin B treatment. Once singled onto regular NGM + OP50 plates, if the worms survived the 'move', I lysed the worm

(worm lysis protocol in Chapter 3) and ran a single worm PCR using *mkate2*-specific primers I included a negative control containing no DNA, along with a positive control from a lysed SWG49 worm (the Lifeact_*mKate2 C. elegans* line mentioned earlier). The *mKate2* PCR product size is 389 bp. None of my transgenic lines displayed a band, while SWG49 did (Figure 4.4). The lack of fluorescence combined with the lack of a band showed that indeed isolated *P. pacificus* 'survivors' were not transgenic worms.

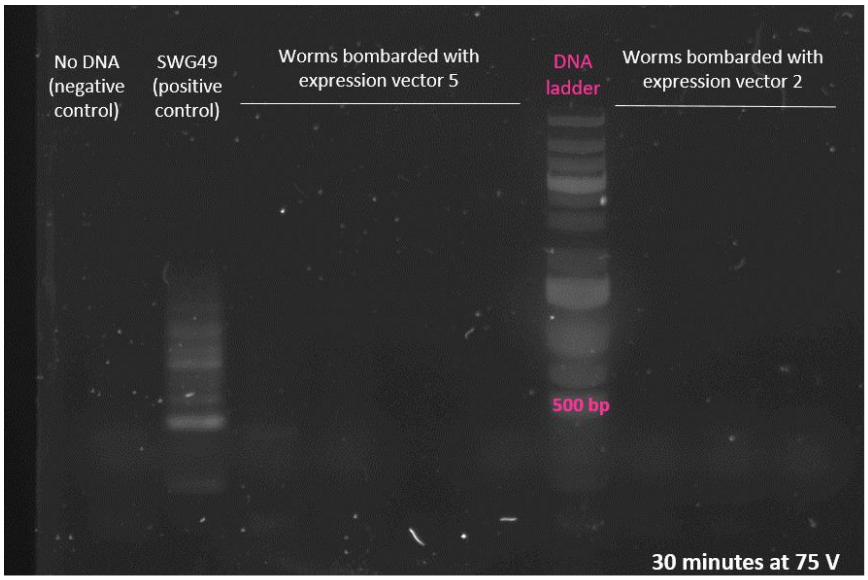

Figure 4.4. DNA agarose gel for diagnostic check for presence or absence of *mKate2* gene in *P. pacificus* bombarded worms. Negative control shows no band while SWG49 *C. elegans* worms (Lifeact::*mKate2)* show DNA band close to 500 bp mark (*mKate2* is 389 bp). *P. pacificus* worms bombarded either by expression vector 5 or expression vector 2 show no DNA band for *mKate2*.

4.2.7. Obstacles and suggestions for future attempts

There were two major problems with *P. pacificus* bombardment: difficulty obtaining a large amount of young synchronized adults and leakiness of the hygromycin B selection system. As concerns the first point, *P. pacificus* worms seem to be sensitive to growth in liquid culture. They have a peak growth rate within a week in liquid culture and then start to die. Starting from a liquid culture and then growing the worms on plates seems to be the best protocol. However an even more important problem is the existence of many false positives with hygromycin B selection, as all of my "transformants" that had survived hygromycin B turned out not to be carrying the rescue gene. In the future, it will be necessary to screen many more worms by PCR, or ideally, find a better selection system. The efficiency of bombardment in *C. elegans* lies in the use of selection via the *unc-119* gene, which prevents non transformants from being able to enter dauer and survive starvation. Although *P. pacificus* has an unc-119 gene and mutants are available, preliminary tests in the lab before my arrival indicated that *P. pacificus* is highly resistant to starvation in juvenile stages, so adapting the *unc-119* selection system to *P. pacificus* does not seem promising.

4.3. Conclusion

Due to the novelty of the *P. pacificus* early embryo as a system to study development, genetic manipulation and live cytoskeleton labelling are yet to be optimized and standardized. Although transgenesis in *P. pacificus* was previously proven successful, lack of sufficient adult worms and a stringent selection marker for transgenics made this project unfeasible during my PhD. Revealing the mechanisms regulating ACD in the *P. pacificus* embryo would augment our understanding of polarity establishment, spindle positioning and cleavage as compared to the classic *C. elegans* embryo. Given that *P. pacificus* is also a self-fertilizing worm, one would expect that the sperm delivers the polarity cue and initiates cortical contractility that we observe in DIC imaging. Why the morphological changes, flows and spindle movements differ so much between the two species are just a few of the many questions to ask based on looking at DIC images.

Annex: Chapter 4

Materials

Reagents obtained for the Sugimoto lab

Plasmid pSNP44	*Ppa-rpl-28p::HygR::Ppa-rpl-23 3' UTR*
Plasmid pSNP52	*Ppa-rps-27p::Lifeact::GFP::Ppa-rps-0_3'UTR,HygR*
P. pacificus worm line SA1159	*afl-1(tj49);tjIs364[rps-27p::lifeact::gfp::rps-0 3'UTR,HygR]*

In-Fusion primers for amplifying and inserting the R4-R3 MultiSite Gateway consensus sequence into pSNP44 HygR vector

Primer	Sequence (5' -3')
InFusR4-R3 Forward	ACCGCGGTGGCGGCCGCCAGGAAACAGCTATGACCATG
InFusR4-R3 Reverse	TTGATATCGAATTCCTGCAGGTAAAACGACGGCCAGTG

Primers designed with att sites for PCR amplification of target genes in preparation for Gateway recombination reactions.

Name of Oligo	Sequence (5'-3')
attB4 Pmex-5 F	GGGG ACA ACT TTG TAT AGA AAA GTT GCA GGC TCG TAT CTC TCG
attB1r Pmex-5 R	GGGG AC TGC TTT TTT GTA CAA ACT TGC AAT GTT TAG ACA AGT AAA CG
attB1 LA-mkate F (*with splice acceptor)*	GGGG ACA AGT TTG TAC AAA AAA GCA GGC TTT TTT TTT TTC AGA TGG GAG
attB2 LA-mkate R	GGGG AC CAC TTT GTA CAA GAA AGC TGG GTT TAA CGG TGT CCG AGC
attB2r mex-5 UTR F	GGGGACAGCTTTCTTGTACAAAGTGGTTAATATATATTTAATGAATACATTTAATAAATG
attB3 mex-5 UTR R	GGGGACAACTTTGTATAATAAAGTTGATGAATTTGTCAACAGTAATATC
attB4 rps-27P F	GGGG ACA ACT TTG TAT AGA AAA GTT G TCG AGC TTG TTG AGA CGA C
attB1r rps-27P R	GGGG AC TGC TTT TTT GTA CAA ACT TG CTT GTT TTA ACC AGT TGA GCG
attB2r rps-0 UTR F	GGGG ACA GCT TTC TTG TAC AAA GTG G AGA GAA ACA TGC GGA AGC
attB3 rps-0 UTR R	GGGG AC AAC TTT GTA TAA TAA AGT TG GTC TCT GAA ATG GGA GGA G

Left column are names of primers including what *att* site is included in the sequence. The F in the name of primer is for forward primer and R is for reverse primer.

Primers for running PCR diagnostic check of mKate2 presence in gDNA of HygB survivor bombarded worms (DNA on gel shown in Figure 4.4).

Primer	Sequence (5'-3')
mKate2 Forward	TTCATGTACGGATCCAAGACC
mKate2 Reverse	AGGTTGCAGATGAGGTGTCC

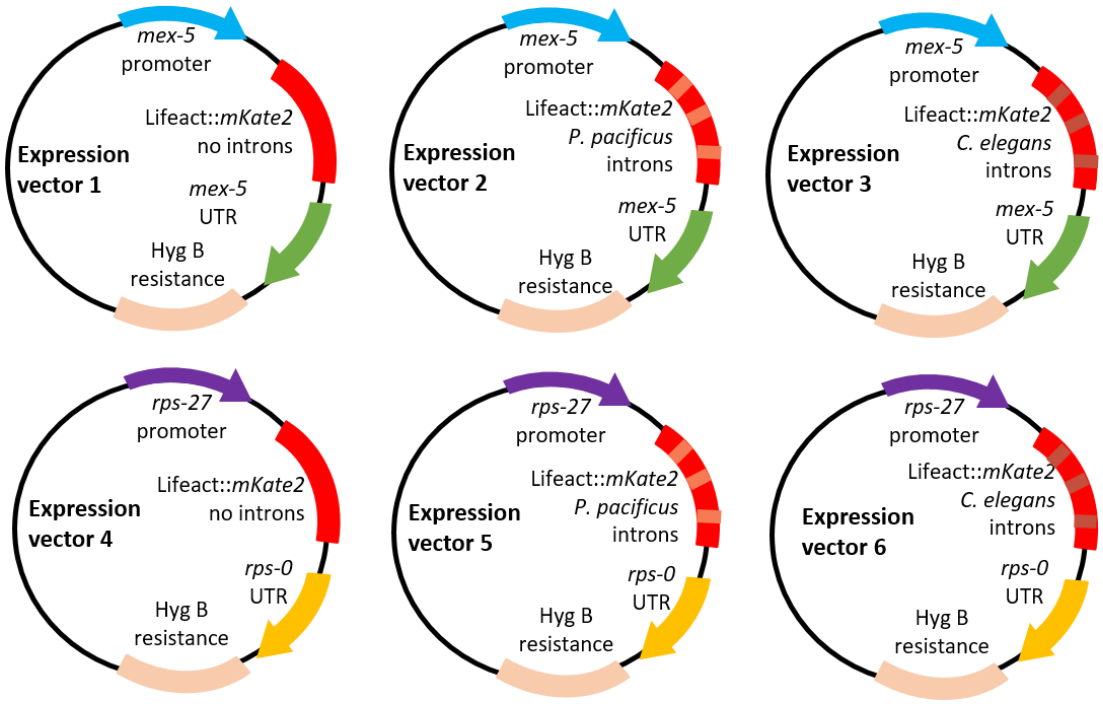

Figure A.1. Final expression vectors prepared by Gateway recombination reactions for Lifeact::*mKate2* labelling in *P. pacificus* embryos. Top panel: expression vectors prepared to contain the *mex-5* promoter (blue) and *mex-5* 3' UTR (green) sequences amplified from genomic DNA of *P. pacificus*. Lower panel: expression vectors prepared to contain the *rps-27* promoter (purple) and *rps-0* 3'UTR (yellow) amplified from the pSNP52 plasmid. Lifeact sequence and *mKate2* (red) were included in all vectors, either without any introns (first column), with introns from *P. pacificus* (second column) or with introns from *C. elegans* (third column). All vectors also contained the hygromycin B resistance gene (*HygR*) (beige).

Protocols

Preparation of worm growth media (WGM)

Ingredients added to bottle next to a flame except cholesterol which is added using a filter syringe since it is dissolved in ethanol and highly flammable.

Ingredient	Volume (millilitres)
NaCl (5 M)	2
H_2O	950
KH_2PO_4 (1 M) pH 6	10
K citrate (1 M) pH 6.1	10
Trace Metals (100 x)	10
$CaCl_2$ (1 M)	3
$MgSO_4$	3
Fill to 1 litre with H_2O using sterile filter	
Cholesterol (5 mg/ml) in EtOH	1

Washing of plates and worm synchronization protocol adapted from Namai et al., 2018

1) Worms were washed off the plates gently with M9 solution into 2 15-ml Falcon tubes using a Pasteur pipette.
2) Tubes were left for 5 minutes on the bench until all worms sedimented. The M9 supernatant was replaced with fresh M9, inverted for mixing and then left again at 5 minutes for sedimentation of worms. This was repeated 2 more times until M9 supernatant solution was cleared of bacteria.
3) Worms were then transferred to a new 15-ml tube and centrifuged at 2000 xg for 1 minute. The supernatant was discarded.
4) Fresh M9 was added and the tube was inverted. Worms were evenly distributed on 19 9-cm plates without food in order to starve worms for synchronization.
5) After one week of starvation, worms were collected from all 19 plates and washed using method of step 3 to avoid contamination. Collected worms were placed on seeded plates to allow for growth of worms.

General Conclusion

During the past few decades, many achievements have been made with the nematode *C. elegans* as concerns the development of advanced manipulation techniques, thus making it a popular model system for everything from ageing to neurogenesis and including embryogenesis. The thorough understanding of *C. elegans* developmental biology, and the similar body plan and general physiology of nematodes as a whole has made them an attractive group of organisms for comparative evolutionary studies. A detailed comparative analysis of ACD between the well-studied *C. elegans* embryo and its close relatives is a way to answer fundamental questions about the conservation of the ACD process. Marked phenotypic differences exist during early steps of embryogenesis in different nematodes, even though they all lead to the same result after the first cell division: daughter cells that are of different size, fate and division timing. Indeed, studies on non-*C. elegans* early embryogenesis have been conducted for decades, but these nematodes are less amenable to genetic manipulation, limiting the results obtained. However, recent completion of genome sequencing and improvements in genetic tools are bringing us closer to more insight on the process of ACD in non-*C. elegans* nematodes. The species I chose to study during my PhD held promise in this regard, which is one of the reasons I chose them, but in the end, the genetic techniques available were not efficient enough for what I wanted to do. Nevertheless these approaches will continue to be refined by my host lab and others, and in that context, my studies provide a basis to expand on for future, more molecular, discoveries.

My main scientific result during my PhD was to show that the parthenogenetic single-cell *D. pachys* embryo was polarized early in embryogenesis presumably via an interaction with the meiotic spindle or nucleus of the oocyte. This result adds to the evidence that polarity cues independent from the sperm exist. The fact that *D. pachys* one-cell embryos are polarized despite the lack of asymmetric cortical ruffling and asymmetric organization of the actin cytoskeleton highlights differences in ACD regulation as compared to *C. elegans* where actin asymmetry is well maintained and anterior cortical ruffling exist until metaphase.

The main technical contribution that I made during my PhD was to show that, while genetic manipulation techniques for *D. pachys* and *P. pacificus* have recently been shown successful, optimization of these techniques is still required. My thesis describes the obstacles that must be anticipated, and how to solve them in the hopes of making these experiments more efficient in the future.

All together, my PhD work adds to the field of ACD in general, and to the field of non-*C. elegans* nematode embryos in particular, where little is yet known as compared to *C. elegans*. As such I have contributed to the field of developmental biology by enlarging the choice of available model system, and thus diversifying the scientific ecosystem in order to expand our view of the fundamental process of ACD.

References

Aceto, D., M. Beers, and K.J. Kemphues. 2006. Interaction of PAR-6 with CDC-42 is required for maintenance but not establishment of PAR asymmetry in C. elegans. *Developmental Biology*. 299:386-397.

Adams, S., P. Pathak, H. Shao, J.B. Lok, and A. Pires-daSilva. 2019. Liposome-based transfection enhances RNAi and CRISPR-mediated mutagenesis in non-model nematode systems. *Scientific Reports*. 9:483.

Ahringer, J. 2006. Reverse genetics. *WormBook*. doi/10.1895/wormbook.1.47.1.

Atwood, S.X., and K.E. Prehoda. 2009. aPKC phosphorylates Miranda to polarize fate determinants during neuroblast asymmetric cell division. *Current Biology*. 19:723–729.

Barker, N., R.A. Ridgway, J.H. van Es, M. van de Wetering, H. Begthel, M. van den Born, E. Danenberg, A.R. Clarke, O.J. Sansom, and H. Clevers. 2009. Crypt stem cells as the cells-of-origin of intestinal cancer. *Nature*. 457:608-611.

Basham, S.E., and L.S. Rose. 1999. Mutations in ooc-5 and ooc-3 disrupt oocyte formation and the reestablishment of asymmetric PAR protein localization in two-cell *Caenorhabditis elegans* embryos. *Developmental Biology*. 215:253-263.

Berkowitz, L.A., and S. Strome. 2000. MES-1, a protein required for unequal divisions of the germline in early C. elegans embryos, resembles receptor tyrosine kinases and is localized to the boundary between the germline and gut cells. *Development*. 127:4419–4431.

Borowiak, M., W. Nahaboo, M. Reynders, K. Nekolla, P. Jalinot, J. Hasserodt, M. Rehberg, M. Delattre, S. Zahler, A. Vollmar, D. Trauner, and O. Thorn-Seshold. 2015. Photoswitchable inhibitors of microtubule dynamics optically control mitosis and cell death. *Cell*. 162:403-411.

Bossinger, O., and E. Schierenberg. 1992. Transfer and tissue-specific accumulation of cytoplasmic components in embryos of Caenorhabditis elegans and Rhabditis dolichura: in vivo analysis with a low-cost signal enhancement device. *Development*. 114:317-330.

Brauchle, M., K. Kiontke, P. MacMenamin, D.H. Fitch, and F. Piano. 2009. Evolution of early embryogenesis in rhabditid nematodes. *Developmental Biology*. 335:253–262.

Bringmann, H., and A.A. Hyman. 2005. A cytokinesis furrow is positioned by two consecutive signals. *Nature*. 436:731-734.

Broadus, J., and C.Q. Doe. 1997. Extrinsic cues, intrinsic cues and microfilaments regulate asymmetric protein localization in Drosophila neuroblasts. *Current Biology*. 7:827-835.

Cabernard, C., and C.Q. Doe. 2009. Apical/basal spindle orientation is required for neuroblast homeostasis and neuronal differentiation in Drosophila. *Developmental Cell*. 17:134-141.

Cabernard, C., K.E. Prehoda, and C.Q. Doe. 2010. A mitotic spindle-independent cleavage furrow positioning pathway. *Nature*. 467:91-94.

Carvalho, A., S.K. Olson, E. Gutierrez, K. Zhang, L.B. Noble, E. Zanin, A. Desai, A. Groisman, and K. Oegema. 2011. Acute drug treatment in the early *C. elegans* embryo. *PLoS One*. 6:e24656.

Carvalho, K., J. Lemiere, F. Faqir, J. Manzi, L. Blanchoin, J. Plastino, T. Betz, and C. Sykes. 2013. Actin polymerization or myosin contraction: two ways to build up cortical tension for symmetry breaking. *Philosophical transactions of the Royal Society of London. Series B, Biological sciences*. 368:20130005.

Caussinus, E., and C. Gonzalez. 2005. Induction of tumor growth by altered stem-cell asymmetric division in Drosophila melanogaster. *Nature Genetics*. 37:1125-1129.

Cicalese, A., G. Bonizzi, C.E. Pasi, M. Faretta, S. Ronzoni, B. Giulini, C. Brisken, S. Minucci, P.P. Di Fiore, and P.G. Pelicci. 2009. The tumor suppressor p53 regulates polarity of self-renewing divisions in mammary stem cells. *Cell*. 138:1083–1095.

Colombo, K., S.W. Grill, R.J. Kimple, F.S. Willard, D.P. Siderovski, and P. Gonczy. 2003. Translation of polarity cues into asymmetric spindle positioning in Caenorhabditis elegans embryos. *Science*. 300:1957-1961.

Costa, M.R., G. Wen, A. Lepier, T. Schroeder, and M. Gotz. 2008. Par-complex proteins promote proliferative progenitor divisions in the developing mouse cerebral cortex. *Development*. 135:11-22.

Couwenbergs, C., J.C. Labbe, M. Goulding, T. Marty, B. Bowerman, and M. Gotta. 2007. Heterotrimeric G protein signaling functions with dynein to promote spindle positioning in *C. elegans*. *Journal of Cell Biology*. 179:15–22.

Cowan, C.R., and A.A. Hyman. 2004. Asymmetric cell division in *C. elegans*: cortical polarity and spindle positioning. *Annual Review of Cell and Developmental Biology*. 20:427–453.

Cowan, C.R., and A.A. Hyman. 2006. Cyclin E-Cdk2 temporally regulates centrosome assembly and establishment of polarity in Caenorhabditis elegans embryos. *Nature Cell Biology*. 8:1441-1447.

Cuenca, A., A. Schetter, D. Aceto, K. Kemphues, and G. Seydoux. 2003. Polarization of the *C. elegans* zygote proceeds via distinct establishment and maintenance phases. *Development*. 130:1255–1265.

D'Avino, P.P., M.S. Savoian, and D.M. Glover. 2005. Cleavage furrow formation and ingression during animal cytokinesis: a microtubule legacy. *Journal of Cell Science*. 118:1549-1558.

De Henau, S., M. Pages-Gallego, W.J. Pannekoek, and T.B. Dansen. 2020. Mitochondria-derived H2O2 promotes symmetry breaking of the *C. elegans* zygote. *Developmental Cell*. 53:263–271.

De Simone, A., F. Nedelec, and P. Gonczy. 2016. Dynein transmits polarized actomyosin cortical flows to promote centrosome separation. *Cell Reports*. 14:2250–2262.

Delattre, M., and N.W. Goehring. 2021. The first steps in the life of a worm: themes and variations in asymmetric division in *C. elegans* and other nematodes. *Current Topics in Developmental Biology*. 144:269-308.

Descovich, C.P., D.B. Cortes, S. Ryan, J. Nash, L. Zhang, P.S. Maddox, F. Nedelec, and A.S. Maddox. 2018. Cross-linkers both drive and brake cytoskeletal remodeling and furrowing in cytokinesis. *Molecular Biology of the Cell*. 29:622-631.

Dickinson, D.J., F. Schwager, L. Pintard, M. Gotta, and B. Goldstein. 2017. A single-cell biochemistry approach reveals PAR complex dynamics during cell polarization. *Developmental Cell*. 42:416-434.

Dickinson, D.J., J.D. Ward, D.J. Reiner, and B. Goldstein. 2013. Engineering the Caenorhabditis elegans genome using Cas9-triggered homologous recombination. *Nature Methods*. 10:1028-1034.

Dieterich, C., S.W. Clifton, L.N. Schuster, A. Chinwalla, K. Delehaunty, I. Dinkelacker, L. Fulton, R. Fulton, J. Godfrey, P. Minx, M. Mitreva, W. Roeseler, H. Tian, H. Witte, S.P. Yang, R.K. Wilson, and R.J. Sommer. 2008. The Pristionchus pacificus genome provides a unique perspective on nematode lifestyle and parasitism. *Nature Genetics*. 40:1193-1198.

Dolinski, C., J.G. Baldwin, and W.K. Thomas. 2001. Comparative survey of early embryogenesis of Secernentea (Nematoda), with phylogenetic implications. *Canadian Journal of Zoology*. 79:82-94.

Etienne-Manneville, S. 2004. Cdc42-the centre of polarity. *Journal of Cell Science*. 117:1291-1300.

Fielmich, L.E., R. Schmidt, D.J. Dickinson, B. Goldstein, A. Akhmanova, and S. van den Heuvel. 2018. Optogenetic dissection of mitotic spindle positioning in vivo. *eLife*. 7:e38198.

Flavel, M.R., A. Mechler, M. Shahmiri, E.R. Mathews, A.E. Francks, W. Chen, D. Zanker, B. Xian, S. Gao, J. Luo, S. Tegegne, C. Doneski, and M. Jois. 2018. Growth of *Caenorhabditis elegans* in defined media is dependent on presence of particulate matter. *G3*. 8:567-575.

Folkmann, A.W., and G. Seydoux. 2019. Spatial regulation of the polarity kinase PAR-1 by parallel inhibitory mechanisms. *Development*. 146:dev171116.

Fradin, H., K. Kiontke, C. Zegar, M. Gutwein, J. Lucas, M. Kovtun, D.L. Corcoran, L.R. Baugh, D.H.A. Fitch, F. Piano, and K.C. Gunsalus. 2017. Genome architecture and evolution of a unichromosomal asexual nematode. *Current Biology* 27:2928-2939.

Friedland, A.E., Y.B. Tzur, K.M. Esvelt, M.P. Colaiacovo, G.M. Church, and J.A. Calarco. 2013. Heritable genome editing in C. elegans via a CRISPR-Cas9 system. *Nature Methods*. 10:741–743.

Gallo, C.M., J.T. Wang, F. Motegi, and G. Seydoux. 2010. Cytoplasmic partitioning of P granule components is not required to specify the germline in *C. elegans*. *Science*. 330:1685–1689.

Geßele, R., J. Halatek, L. Würthner, and E. Frey. 2020. Geometric cues stabilise long-axis polarisation of PAR protein patterns in C. elegans. *Nature Communications*. 11:539.

Glotzer, M. 2004. Cleavage furrow positioning. *Journal of Cell Biology*. 164:347–351.

Goehring, N.W. 2014. PAR polarity: from complexity to design principles. *Experimental Cell Research*. 328:258-266.

Goehring, N.W., C. Hoege, S.W. Grill, and A.A. Hyman. 2011. PAR proteins diffuse freely across the anterior-posterior boundary in polarized C. elegans embryos. *Journal of Cell Biology*. 193:583–594.

Goldstein, B. 2001. On the evolution of early development in the Nematoda. *Philosophical Transactions of the Royal Society B*. 356:1521-1531.

Goldstein, B., L.M. Frisse, and W.K. Thomas. 1998. Embryonic axis specification in nematodes: evolution of the first step in development. *Current Biology*. 8:157-160.

Goldstein, B., and S.N. Hird. 1996. Specification of the anterioposterior axis in *Caenorhabditis elegans*. *Development*. 122:1467-1474.

Gonczy, P. 2008. Mechanisms of asymmetric cell division: flies and worms pave the way. *Nature Reviews: Molecular Cell Biology*. 9:355-366.

Gönczy, P., S. Pichler, M. Kirkham, and A.A. Hyman. 1999. Cytoplasmic dynein is required for distinct aspects of MTOC positioning, including centrosome separation, in the one cell stage Caenorhabditis elegans embryo. *Journal of Cell Biology*. 147:135–150.

Gotta, M., and J. Ahringer. 2001. Distinct roles for Gα and Gβγ in regulating spindle position and orientation in *Caenorhabditis elegans* embryos. *Nature Cell Biology*. 3:297-300.

Gotta, M., Y. Dong, Y.K. Peterson, S.M. Lanier, and J. Ahringer. 2003. Asymmetrically distributed *C. elegans* homologs of AGS3/PINS control spindle position in the early embryo. *Current Biology*. 13:1029–1037.

Govindan, J.A., H. Cheng, J.E. Harris, and D. Greenstein. 2006. Galphao/i and Galphas signaling function in parallel with the MSP/Eph receptor to control meiotic diapause in *C. elegans*. *Current Biology*. 16:1257-1268.

Grosmaire, M., C. Launay, M. Siegwald, T. Brugière, L. Estrada-Virrueta, D. Berger, C. Burny, L. Modolo, M. Blaxter, P. Meister, M.-A. Félix, P.-H. Gouyon, and M. Delattre. 2019. Males as somatic investment in a parthenogenetic nematode. *Science*. 363:1210-1213.

Gross, P., K.V. Kumar, N.W. Goehring, J.S. Bois, C. Hoege, F. Julicher, and S.W. Grill. 2019. Guiding self-organized pattern formation in cell polarity establishment. *Nature Physics*. 15:293–300.

Guo, S., and K.J. Kemphues. 1996. A non-muscle myosin required for embryonic polarity in Caenorhabditis elegans. *Nature*. 382:455-458.

Hall, D.H., V.P. Winfrey, G. Blaeuer, L.H. Hoffman, O. Hobert, and D. Greenstein. 1999. Ultrastructural features of the adult hermaphrodite gonad of Caenorhabditis elegans: relations between the germ line and soma. *Developmental Biology*. 212:101-123.

Hamill, D.R., A.F. Severson, J.C. Carter, and B. Bowerman. 2002. Centrosome maturation and mitotic spindle assembly in C. elegans require SPD-5, a protein with multiple coiled-coil domains. *Developmental Cell*. 3:673–684.

Hao, Y., L. Boyd, and G. Seydoux. 2006. Stabilization of cell polarity by the C. elegans RING protein PAR-2. *Developmental Cell*. 10:199–208.

Hiraki, H., H. Kagoshima, C. Kraus, P.H. Schiffer, Y. Ueta, M. Kroiher, E. Schierenberg, and Y. Kohara. 2017. Genome analysis of Diploscapter coronatus: insights into molecular peculiarities of a nematode with parthenogenetic reproduction. *BMC Genomics*. 18:478.

Hirata, J., H. Nakagoshi, Y.-i. Nabeshima, and F. Matsuzaki. 1995. Asymmetric segregation of the homeodomain protein Prospero during Drosophila development. *Nature*. 377:627-630.

Hong, R.L., and R.J. Sommer. 2006. Pristionchus pacificus: a well-rounded nematode. *Bioessays*. 28:651-659.

Huelgas-Morales, G., and D. Greenstein. 2018. Control of oocyte meiotic maturation in C. elegans. *Seminars in Cell and Developmental Biology*. 84:90–99.

Jankele, R., R. Jelier, and P. Gonczy. 2021. Physically asymmetric division of the C. elegans zygote ensures invariably successful embryogenesis. *eLife*. 10:e61714.

Jantsch-Plunger, V., P. Gönczy, A. Romano, H. Schnabel, D. Hamill, R. Schnabel, A.A. Hyman, and M. Glotzer. 2000. CYK-4: A rho family GTPase activating protein (GAP) required for central spindle formation and cytokinesis. *Journal of Cell Biology*. 149:1391–1404.

Januschke, J., and C. Gonzalez. 2010. The interphase microtubule aster is a determinant of asymmetric division orientation in Drosophila neuroblasts. *Journal of Cell Biology*. 188:693–706.

Jaworska, A.M., N.A. Wlodarczyk, A. Mackiewicz, and P. Czerwinska. 2020. The role of TRIM family proteins in the regulation of cancer stem cell self-renewal. *Stem Cells*. 38:165–173.

Jenkins, N., J.R. Saam, and S.E. Mango. 2006. CYK-4/GAP provides a localized cue to initiate anteroposterior polarity upon fertilization. *Science*. 313:1298-1301.

Johnston, D.S. 1995. The intracellular localization of messenger RNAs. *Cell*. 81:161-170.

Kaltschmidt, J.A., C.M. Davidson, N.H. Brown, and A.H. Brand. 2000. Rotation and asymmetry of the mitotic spindle direct asymmetric cell division in the developing central nervous system. *Nature Cell Biology*. 2:7-12.

Kapoor, S., and S. Kotak. 2019. Centrosome Aurora A regulates RhoGEF ECT-2 localisation and ensures a single PAR-2 polarity axis in C. elegans embryos. *Development*. 146:dev174565.

Keerthivasan, G., A. Wickrema, and J.D. Crispino. 2011. Erythroblast enucleation. *Stem Cells International*. 2011:139851.

Kelly, W.G., S. Xu, M.K. Montgomery, and A. Fire. 1997. Distinct requirements for somatic and germline expression of a generally expressed Caenorhabditis elegans gene. *Genetics*. 146:227-238.

Kemphues, K.J., J.R. Priess, D.G. Morton, and N. Cheng. 1988. Identification of genes required for cytoplasmic localozation in early C. elegans embryo. *Cell*. 52:311-320.

Kimura, K., and A. Kimura. 2020. Cytoplasmic streaming drifts the polarity cue and enables posteriorization of the Caenorhabditis elegans zygote at the side opposite of sperm entry. *Molecular Biology of the Cell*. 31:1651-1821.

Kiontke, K., and D.H.A. Fitch. 2005. The phylogenetic relationships of *Caenorhabditis* and other rhabditids. *Wormbook*. doi: 10.1895/wormbook.1.11.1.

Kitajima, A., N. Fuse, T. Isshiki, and F. Matsuzaki. 2010. Progenitor properties of symmetrically dividing Drosophila neuroblasts during embryonic and larval development. *Developmental Biology*. 347:9-23.

Kiyomitsu, T. 2019. The cortical force-generating machinery: how cortical spindle-pulling forces are generated. *Current Opinion in Cell Biology*. 60:1-8.

Klinkert, K., N. Levernier, P. Gross, C. Gentili, L. von Tobel, M. Pierron, C. Busso, S. Herrman, S.W. Grill, K. Kruse, and P. Gonczy. 2019. Aurora A depletion reveals centrosome-independent polarization mechanism in Caenorhabditis elegans. *eLife*. 8:e44552.

Knoblich, J.A., L.Y. Jan, and Y.N. Jan. 1995. Asymmetric segregation of Numb and Prospero during cell division. *Nature*. 377:624–627.

Kotak, S. 2019. Mechanisms of spindle positioning: lessons from worms and mammalian cells. *Biomolecules*. 9:80.

Koury, S.T., M.J. Koury, and M.C. Bondurant. 1989. Cytoskeletal distribution and function during the maturation and enucleation of mammalian erythroblasts. *Journal of Cell Biology*. 109:3005-3013.

Kraus, C., P.H. Schiffer, H. Kagoshima, H. Hiraki, T. Vogt, M. Kroiher, Y. Kohara, and E. Schierenberg. 2017. Differences in the genetic control of early egg development and reproduction between C. elegans and its parthenogenetic relative D. coronatus. *EvoDevo*. 8.

Kwon, C.H., D. Zhao, J. Chen, S. Alcantara, Y. Li, D.K. Burns, R.P. Mason, E.Y. Lee, H. Wu, and L.F. Parada. 2008. Pten haploinsufficiency accelerates formation of high-grade astrocytomas. *Cancer Research*. 68:3286-3294.

Kwon, M., M. Bagonis, G. Danuser, and D. Pellman. 2015. Direct microtubule-binding by myosin-10 orients centrosomes toward retraction fibers and subcortical actin clouds. *Developmental Cell*. 34:323-337.

Lahl, V., B. Sadler, and E. Schierenberg. 2006. Egg development in parthenogenetic nematodes: variations in meiosis and axis formation. *International Journal of Developmental Biology*. 50:393-398.

Lahl, V., J. Schulze, and E. Schierenberg. 2009. Differences in embryonic pattern formation between Caenorhabditis elegans and its close parthenogenetic relative Diploscapter coronatus. *International Journal of Developmental Biology*. 53:507-515.

Lang, C.F., and E. Munro. 2017. The PAR proteins: from molecular circuits to dynamic self-stabilizing cell polarity. *Development*. 144:3405-3416.

Launay, C., M.A. Felix, J. Dieng, and M. Delattre. 2020. Diversification and hybrid incompatibility in auto-pseudogamous species of Mesorhabditis nematodes. *BMC Evolutionary Biology*. 20.

Lechler, T., and E. Fuchs. 2005. Asymmetric cell divisions promote stratification and differentiation of mammalian skin. *Nature*. 437:275–280

Leite, J., F.-Y. Chan, D.S. Osório, J. Saramago, A.F. Sobral, A.M. Silva, R. Gassmann, and A.X. Carvalho. 2020. Equatorial non-muscle myosin II and plastin cooperate to align and compact F-actin bundles in the cytokinetic ring. *Frontiers in Cell and Developmental Biology*. 8.

Li, R. 2013. The art of choreographing asymmetric cell division. *Developmental Cell*. 25:439-450.

Longo, F.J., and D.-Y. Chen. 1985. Development of cortical polarity in mouse eggs: involvement of the meiotic apparatus. *Developmental Biology*. 107:382-394.

Lord, M., E. Laves, and T.D. Pollard. 2005. Cytokinesis depends on the motor domains of myosin-II in fission yeast but not in budding yeast. *Molecular Biology of the Cell*. 16:5346–5355.

Loyer, N., and J. Januschke. 2020. Where does asymmetry come from? Illustrating principles of polarity and asymmetry establishment in Drosophila neuroblasts. *Current Opinion in Cell Biology*. 62:70–77.

Ma, X., M. Kovacs, M.A. Conti, A. Wang, Y. Zhang, J.R. Sellers, and R.S. Adelstein. 2012. Nonmuscle myosin II exerts tension but does not translocate actin in vertebrate cytokinesis. *Proceedings of the National Academy of Sciences of the United States of America*. 109:4509–4514.

Mangal, S., J. Sacher, T. Kim, D.S. Osorio, F. Motegi, A.X. Carvalho, K. Oegema, and E. Zanin. 2018. TPXL-1 activates Aurora A to clear contractile ring components from the polar cortex during cytokinesis. *Journal of Cell Biology*. 217:837-848.

Maro, B., and M.H. Verlhac. 2002. Polar body formation: new rules for asymmtric divisions. *Nature Cell Biology*. 4:E281–E283.

Matsui, W.H. 2016. Cancer stem cell signaling pathways. *Medicine*. 95:S8-S19.

McCarter, J., B. Bartlett, T. Dang, and T. Schedl. 1999. On the control of oocyte meiotic maturation and ovulation in Caenorhabditis elegans. *Developmental Biology*. 205:111-128.

McNally, F.J. 2013. Mechanisms of spindle positioning. *J Cell Biol*. 200:131-140.

McNally, K.L., A.S. Fabritius, M.L. Ellefson, J.R. Flynn, J.A. Milan, and F.J. McNally. 2012. Kinesin-1 prevents capture of the oocyte meiotic spindle by the sperm aster. *Dev Cell*. 22:788-798.

McNally, K.L., J.L. Martin, M. Ellefson, and F.J. McNally. 2010. Kinesin-dependent transport results in polarized migration of the nucleus in oocytes and inward movement of yolk granules in meiotic embryos. *Dev Biol*. 339:126-140.

Mendes Pinto, I., B. Rubinstein, A. Kucharavy, J.R. Unruh, and R. Li. 2012. Actin depolymerization drives actomyosin ring contraction during budding yeast cytokinesis. *Developmental Cell*. 22:1247-1260.

Mittasch, M., P. Gross, M. Nestler, A.W. Fritsch, C. Iserman, M. Kar, M. Munder, A. Voigt, S. Alberti, S.W. Grill, and M. Kreysing. 2018. Non-invasive perturbations of intracellular flow reveal physical principles of cell organization. *Nature cell biology*. 20:344-351.

Morin, X., and Y. Bellaiche. 2011. Mitotic spindle orientation in asymmetric and symmetric cell divisions during animal development. *Developmental Cell*. 21:102-119.

Morita, K., K. Hirono, and M. Han. 2005. The Caenorhabditis elegans ect-2 RhoGEF gene regulates cytokinesis and migration of epidermal P cells. *EMBO Reports*. 6:1163-1168.

Morrison, S.J., and J. Kimble. 2006. Asymmetric and symmetric stem-cell divisions in development and cancer. *Nature*. 441:1068–1074.

Morton, D.G., W.A. Hoose, and K.J. Kemphues. 2012. A genome-wide RNAi screen for enhancers of *par* mutants reveals new contributors to early embryonic polarity in *Caenorhabditis elegans*. *Genetics*. 192:929-942.

Motegi, F., and A. Sugimoto. 2006. Sequential functioning of the ECT-2 RhoGEF, RHO-1 and CDC-42 establishes cell polarity in Caenorhabditis elegans embryos. *Nature Cell Biology*. 8:978-985.

Motegi, F., N.V. Velarde, F. Piano, and A. Sugimoto. 2006. Two phases of astral microtubule activity during cytokinesis in C. elegans embryos. *Developmental Cell*. 10:509–520.

Motegi, F., S. Zonies, Y. Hao, A.A. Cuenca, E. Griffin, and G. Seydoux. 2011. Microtubules induce self-organization of polarized PAR domains in Caenorhabditis elegans zygotes. *Nature Cell Biology*. 13:1361–1367.

Munro, E., J. Nance, and J.R. Priess. 2004. Cortical flows powered by asymmetrical contraction transport PAR proteins to establish and maintain anterior-posterior polarity in the early C. elegans embryo. *Developmental Cell*. 7:413-424.

Namai, S., and A. Sugimoto. 2018. Transgenesis by microparticle bombardment for live imaging of fluorescent proteins in Pristionchus pacificus germline and early embryos. *Development Genes and Evolution*. 228:75-82.

Neumuller, R.A., and J.A. Knoblich. 2009. Dividing cellular asymmetry: asymmetric cell division and its implications for stem cells and cancer. *Genes and Development*. 23:2675-2699.

Nguyen-Ngoc, T., K. Afshar, and P. Gönczy. 2007. Coupling of cortical dynein and Gα proteins mediates spindle positioning in *Caenorhabditis elegans*. *Nature Cell Biology*. 9:1294-1302.

Nishikawa, M., S.R. Naganathan, F. Julicher, and S.W. Grill. 2017. Controlling contractile instabilities in the actomyosin cortex. *eLife*. 6:e19595.

O'Connell, K.F., K.N. Maxwell, and J.G. White. 2000. The spd-2 gene is required for polarization of the anteroposterior axis and formation of the sperm asters in the Caenorhabditis elegans zygote. *Developmental Biology*. 222:55-70.

Ohno, S. 2001. Intercellular junctions and cellular polarity: the PAR–aPKC complex, a conserved core cassette playing fundamental roles in cell polarity. *Current Opinion in Cell Biology*. 13:641-648.

Olson, S.K., G. Greenan, A. Desai, T. Muller-Reichert, and K. Oegema. 2012. Hierarchical assembly of the eggshell and permeability barrier in C. elegans. *Journal of Cell Biology*. 198:731-748.

Osorio, D.S., F.Y. Chan, J. Saramago, J. Leite, A.M. Silva, A.F. Sobral, R. Gassmann, and A.X. Carvalho. 2019. Crosslinking activity of non-muscle myosin II is not sufficient for embryonic cytokinesis in C. elegans. *Development*. 146:dev179150.

Ou, G., N. Stuurman, M. D'Ambrosio, and R.D. Vale. 2010. Polarized myosin produces unequal-size daughters during asymmetric cell division. *Science*. 330:677-680.

Pacquelet, A. 2017. Asymmetric cell division in the one-cell C. elegans embryo: multiple steps to generate cell size asymmetry. *Results and Problems in Cell Differentiation*. 61:115-140.

Pacquelet, A., M. Jousseaume, J. Etienne, and G. Michaux. 2019. Simultaneous regulation of cytokinetic furrow and nucleus positions by cortical tension contributes to proper DNA segregation during late mitosis. *Current Biology*. 29:3766-3777.

Panzica, M.T., H.C. Marin, A.C. Reymann, and F.J. McNally. 2017. F-actin prevents interaction between sperm DNA and the oocyte meiotic spindle in C. elegans. *Journal of Cell Biology*. 216:2273-2282.

Park, D.H., and L.S. Rose. 2008. Dynamic localization of LIN-5 and GPR-1/2 to cortical force generation domains during spindle positioning. *Developmental Biology*. 315:42-54.

Pilz, G.-A., S. Bottes, M. Betizaeu, D.J. Jorg, S. Carta, B.D. Simons, F. Helmchen, and S. Jessberger. 2018. Live imaging of neurogenesis in the adult mouse hippocampus. *Science*. 359:658-662.

Prehoda, K.E. 2009. Polarization of Drosophila neuroblasts during asymmetric division. *Cold Spring Harbor Perspectives in Biology*. 1:a001388.

Quyn, A.J., P.L. Appleton, F.A. Carey, R.J. Steele, N. Barker, H. Clevers, R.A. Ridgway, O.J. Sansom, and I.S. Nathke. 2010. Spindle orientation bias in gut epithelial stem cell compartments is lost in precancerous tissue. *Cell Stem Cell*. 6:175-181.

Redemann, S., S. Schloissnig, S. Ernst, A. Pozniakowsky, S. Ayloo, A.A. Hyman, and H. Bringmann. 2011. Codon adaptation-based control of protein expression in C. elegans. *Nature Methods*. 8:250-252.

Reich, J.D., L. Hubatsch, R. Illukkumbura, F. Peglion, T. Bland, N. Hirani, and N.W. Goehring. 2019. Regulated activation of the PAR polarity network ensures a timely and specific response to spatial cues. *Current Biology*. 29:1911–1923.

Reymann, A.C., F. Staniscia, A. Erzberger, G. Salbreux, and S.W. Grill. 2016. Cortical flow aligns actin filaments to form a furrow. *eLife*. 5.

Rhyu, M.S., L.Y. Jan, and Y.N. Jan. 1994. Asymmetric distribution of Numb protein during division of the sensory organ precursor cell confers distinct fates to daughter cells. *Cell*. 76:477-4791.

Riche, S., M. Zouak, F. Argoul, A. Arneodo, J. Pecreaux, and M. Delattre. 2013. Evolutionary comparisons reveal a positional switch for spindle pole oscillations in Caenorhabditis embryos. *Journal of Cell Biology*. 201:653-662.

Rodriguez-Garcia, R., L. Chesneau, S. Pastezeur, J. Roul, M. Tramier, and J. Pecreaux. 2018. The polarity-induced force imbalance in Caenorhabditis elegans embryos is caused by asymmetric binding rates of dynein to the cortex. *Molecular Biology of the Cell*. 29:3093-3104.

Rodriguez, J., F. Peglion, J. Martin, L. Hubatsch, J. Reich, N. Hirani, A.G. Gubieda, J. Roffey, A.R. Fernandes, D. St Johnston, J. Ahringer, and N.W. Goehring. 2017. aPKC cycles between functionally distinct PAR protein assemblies to drive cell polarity. *Developmental Cell*. 42:400-415.

Ronneberger, O., P. Fischer, and T. Brox. 2015. U-Net: convolutional networks for biomedicalImage segmentation. *MICCAI*. 9351:234–241.

Rose, L., and P. Gonczy. 2014. Polarity establishment, asymmetric division and segregation of fate determinants in early *C. elegans* embryos. *WormBook*. doi: 10.1895/wormbook.1.30.2.

Roubinet, C., A. Tsankova, T.T. Pham, A. Monnard, E. Caussinus, M. Affolter, and C. Cabernard. 2017. Spatio-temporally separated cortical flows and spindle geometry establish physical asymmetry in fly neural stem cells. *Nature Communications*. 8:1383.

Sadler, P.L., and D.C. Shakes. 2000. Anucleate Caenorhabditis elegans sperm can crawl, fertilize oocytes and direct anterior-posterior polarization of the 1-cell embryo. *Development*. 127:355-366.

Schenk, C., H. Bringmann, A.A. Hyman, and C.R. Cowan. 2010. Cortical domain correction repositions the polarity boundary to match the cytokinesis furrow in *C. elegans* embryos. *Development*. 137:1743-1753.

Schierenberg, E. 1996. Developmental strategies during early embryogenesis of Caenorhabditis elegans. *Journal of Embryology and Experimental Morphology*. 97:31-44.

Schlager, B., X. Wang, G. Braach, and R.J. Sommer. 2009. Molecular cloning of a dominant roller mutant and establishment of DNA-mediated transformation in the nematode Pristionchus pacificus. *Genesis*. 47:300-304.

Schlicht, P., and E. Schierenberg. 1991. Altered establishment of cell lineages in the Caenorhabditis elegans embryo after suppression of the first cleavage supports a concentration-dependent decision mechanism. *Roux's Archives of Developmental Biology*. 199:437-448.

Schmidt, R., L.E. Fielmich, I. Grigoriev, E.A. Katrukha, A. Akhmanova, and S. van den Heuvel. 2017. Two populations of cytoplasmic dynein contribute to spindle positioning in C. elegans embryos. *Journal of Cell Biology*. 216:2777-2793.

Schonegg, S., and A.A. Hyman. 2006. CDC-42 and RHO-1 coordinate acto-myosin contractility and PAR protein localization during polarity establishment in C. elegans embryos. *Development*. 133:3507-3516.

Schulze, J., and E. Schierenberg. 2011. Evolution of embryonic development in nematodes. *EvoDevo*. 2:18.

Shinin, V., B. Gayraud-Morel, D. Gomes, and S. Tajbakhsh. 2006. Asymmetric division and cosegregation of template DNA strands in adult muscle satellite cells. *Nature Cell Biology*. 8:677-687.

Siegrist, S.E., and C.Q. Doe. 2006. Extrinsic cues orient the cell division axis in Drosophila embryonic neuroblasts. *Development*. 133:529-536.

Siegrist, S.E., and C.Q. Doe. 2007. Microtubule-induced cortical cell polarity. *Genes and Development*. 21:483-496.

Simpson, C.F., and J.M. Kling. 1967. The mechanism of denucleation in circulating erythroblasts. *Journal of Cell Biology*. 35:237-245.

Skiba, F., and E. Schierenberg. 1992. Cell lineages, developmental timing, and spacial pattern formation in embryos of free-living soil nematodes. *Developmental Biology*. 151:597-610.

Small, L.E., and A.T. Dawes. 2017. PAR proteins regulate maintenance-phase myosin dynamics during Caenorhabditis elegans zygote polarization. *Molecular Biology of the Cell*. 28:2220-2231.

Sommer, R.J., L.K. Carta, S.-Y. Kim, and P.W. Sternberg. 1996. Morphological, genetic and molecular description of Pristionchus pacificus sp. n. (Nematoda : Neodiplogastridae). *Fundamental and Applied Nematology*. 19:511-521.

Sommer, R.J., and P.W. Sternberg. 1996. Evolution of nematode vulval fate patterning. *Developmental Biology*. 173:396-407.

Sonneville, R., and P. Gonczy. 2004. Zyg-11 and cul-2 regulate progression through meiosis II and polarity establishment in C. elegans. *Development*. 131:3527-3543.

Srinivasan, D.G., R.M. Fisk, H. Xu, and S. van den Heuvel. 2003. A complex of LIN-5 and GPR proteins regulates G protein signaling and spindle function in *C. elegans*. *Genes and Development*. 17:1225–1239.

Strome, S. 1986. Fluorescence visualization of the distribution of microfilaments in gonads and early embryos of the nematode *Caenorhabditis elegans*. *Journal of Cell Biology*. 103:2241-2252.

Strome, S., and W.B. Wood. 1983. Generation of asymmetry and segregation of germ-Line granules in early C. elegans embryos. *Cell*. 35:15-25.

Strome, S.S., P. Martin, E.S. Schierenberg, and J. Paulsen. 1995. Transformation of the germ line into muscle in mes-1 mutant embryos of C. elegans. *Developmant*. 121:2961-2972.

Sulston, J.E., E. Schierenberg, J.G. White, and J.N. Thomson. 1983. The embryonic cell lineage of the nematode Caenorhabditis elegans. *Developmental Biology*. 100:64-119.

Suzuki, A., and S. Ohno. 2006. The PAR-aPKC system: lessons in polarity. *Journal of Cell Science*. 119:979-987.

Takizawa, P.A., A. Sil, J.R. Swedlow, I. Herskowitz, and R.D. Vale. 1997. Actin-dependent localization of an RNA encoding a cell-fate determinant in yeast. *Nature*. 389:90-93.

Tanaka, T., N. Tani, and A. Nakamura. 2021. Receptor-mediated yolk uptake is required for oskar mRNA localization and cortical anchorage of germ plasm components in the Drosophila oocyte. *PLoS Biology*. 19:e3001183.

Thompson, B.J. 2021. Par-3 family proteins in cell polarity & adhesion. *The FEBS Journal*. doi: 10.1111/febs.15754.

Tian, H., B. Schlager, H. Xiao, and R.J. Sommer. 2008. Wnt signaling induces vulva development in the nematode Pristionchus pacificus. *Current Biology*. 18:142-146.

Tsai, M.C., and J. Ahringer. 2007. Microtubules are involved in anterior-posterior axis formation in C. elegans embryos. *Journal of Cell Biology*. 179:397-402.

Tse, Y.C., A. Piekny, and M. Glotzer. 2011. Anillin promotes astral microtubule-directed cortical myosin polarization. *Molecular Biology of the Cell*. 22:165-175.

Uemura, T., S. Shepherd, L. Ackerman, L.Y. Jan, and Y.N. Jan. 1989. numb, a gene required in determination of cell fate during sensory organ in Drosophila embryos. *Cell*. 58:349-360.

Valfort, A.C., C. Launay, M. Semon, and M. Delattre. 2018. Evolution of mitotic spindle behavior during the first asymmetric embryonic division of nematodes. *PLoS Biology*. 16:e2005099.

Verlhac, M.H., C. Lefebvre, P. Guilaud, P. Rassinier, and B. Maro. 2000. Asymmetric division in mouse oocytes: with or without Mos. *Current Biology*. 10:1303-1306.

von Dassow, G., K.J. Verbrugghe, A.L. Miller, J.R. Sider, and W.M. Bement. 2009. Action at a distance during cytokinesis. *Journal of Cell Biology*. 187:831-845.

Wallenfang, M.R., and G. Seydoux. 2000. Polarization of the anterior–posterior axis of *C. elegans* is a microtubule-directed process. *Nature*. 408:89-92.

Wang, J., L. Wang, G. Feng, Y. Wang, Y. Li, X. Li, C. Liu, G. Jiao, C. Huang, J. Shi, T. Zhou, Q. Chen, Z. Liu, W. Li, and Q. Zhou. 2018. Asymmetric expression of LincGET biases cell fate in two-cell mouse embryos. *Cell*. 175:1887-1901

Wang, J.T., and G. Seydoux. 2013. Germ cell specification. *Advances in Experimental Medicine and Biology*. 757:17–39.

Wang, S.C., T.Y.F. Low, Y. Nishimura, L. Gole, W. Yu, and F. Motegi. 2017. Cortical forces and CDC-42 control clustering of PAR proteins for Caenorhabditis elegans embryonic polarization. *Nature Cell Biology*. 19:988–995.

Wang, X., J.W. Tsai, J.H. Imai, W.N. Lian, R.B. Vallee, and S.H. Shi. 2009. Asymmetric centrosome inheritance maintains neural progenitors in the neocortex. *Nature*. 461:947-955.

Wirtz-Peitz, F., T. Nishimura, and J.A. Knoblich. 2008. Linking cell cycle to asymmetric division: Aurora-A phosphorylates the Par complex to regulate Numb localization. *Cell*. 135:161-173.

Witte, H., E. Moreno, C. Rodelsperger, J. Kim, J.S. Kim, A. Streit, and R.J. Sommer. 2015. Gene inactivation using the CRISPR/Cas9 system in the nematode Pristionchus pacificus. *Developmental Genes and Evolution*. 225:55-62.

Wu, M., H.Y. Kwon, F. Rattis, J. Blum, C. Zhao, R. Ashkenazi, T.L. Jackson, N. Gaiano, T. Oliver, and T. Reya. 2007. Imaging hematopoietic precursor division in real time. *Cell Stem Cell*. 1:541-554.

Yamada, L., K. Kobayashi, Y. Satou, and N. Satoh. 2005. Microarray analysis of localization of maternal transcripts in eggs and early embryos of the ascidian, Ciona intestinalis. *Developmental Biology*. 284:536-550.

Zhao, P., X. Teng, S.N. Tantirimudalige, M. Nishikawa, T. Wohland, Y. Toyama, and F. Motegi. 2019. Aurora-A breaks symmetry in contractile actomyosin networks independently of its role in centrosome maturation. *Developmental Cell*. 48:631–645.

Zhu, R., S. Antoku, and G.G. Gundersen. 2017. Centrifugal displacement of nuclei Reveals multiple LINC complex mechanisms for homeostatic nuclear positioning. *Current Biology.* 27:3097–3110.

Zhuravlev, Y., S.M. Hirsch, S.N. Jordan, J. Dumont, M. Shirasu-Hiza, and J.C. Canman. 2017. CYK-4 regulates Rac, but not Rho, during cytokinesis. *Molecular Biology of the Cell*. 28:1258–1270.

Zonies, S., F. Motegi, Y. Hao, and G. Seydoux. 2010. Symmetry breaking and polarization of the C. elegans zygote by the polarity protein PAR-2. *Development*. 137:1669-1677.

Annex: Review article International Journal of Molecular Science 2020

Title: Role of actin in morphogenesis of early *Caenorhabditis elegans* embryo
Authors: Dureen Samandar Eweis and Julie Plastino

My contribution: I wrote and re-read the manuscript with Julie.

International Journal of
Molecular Sciences

MDPI

Review

Roles of Actin in the Morphogenesis of the Early *Caenorhabditis elegans* Embryo

Dureen Samandar Eweis [1,2] and Julie Plastino [1,2,*]

[1] Laboratoire Physico-Chimie Curie, Institut Curie, PSL Research University, CNRS, 75005 Paris, France; dureen.samandar-eweis@curie.fr
[2] Sorbonne Université, 75005 Paris, France
* Correspondence: julie.plastino@curie.fr

Received: 6 April 2020; Accepted: 19 May 2020; Published: 21 May 2020

Abstract: The cell shape changes that ensure asymmetric cell divisions are crucial for correct development, as asymmetric divisions allow for the formation of different cell types and therefore different tissues. The first division of the *Caenorhabditis elegans* embryo has emerged as a powerful model for understanding asymmetric cell division. The dynamics of microtubules, polarity proteins, and the actin cytoskeleton are all key for this process. In this review, we highlight studies from the last five years revealing new insights about the role of actin dynamics in the first asymmetric cell division of the early *C. elegans* embryo. Recent results concerning the roles of actin and actin binding proteins in symmetry breaking, cortical flows, cortical integrity, and cleavage furrow formation are described.

Keywords: actin cytoskeleton; myosin; *C. elegans* embryo; asymmetric cell division

1. Introduction

Actin is one of the most abundant proteins in the cell, existing as globular monomers (G-actin) that polymerize into helical filaments (F-actin). F-actin is polar with a fast-growing, dynamic 'barbed end' and a slow-growing, less dynamic 'pointed end'. The dynamic assembly and disassembly of F-actin, as well as the myosin molecular motors that associate with actin, produce forces within the cell and between cells that drive cellular and tissue reorganization. Actin dynamics are controlled by actin-binding proteins, which variously activate or inhibit F-actin formation, stabilize/destabilize existing actin structures, or bind actin monomers [1]. One of the most important actin regulators is the Arp2/3 complex that nucleates the formation of new actin filaments as branches off the sides of existing filaments. Another important class of actin polymerization nucleators is the formin family of proteins. Formins create new unbranched filaments, and also associate with the barbed end of the actin filament, enhancing actin assembly. Once formed, F-actin is remodeled by actin bundling and cross-linking proteins—such as fascin, plastin/fimbrin, and filamin—which promote the formation of parallel and antiparallel bundles of F-actin or cross-linked arrays, respectively. Additionally, myosin remodels F-actin structures, using actin filaments as tracks, sliding antiparallel filaments in relation to each other to create contraction. G-actin binding proteins include profilin, which is key for actin dynamics in the cell, as it reduces spontaneous nucleation and also prevents pointed end polymerization thus allowing for controlled, directed actin assembly in vivo. Capping proteins, which bind barbed ends and prevent further polymerization, and ADF/cofilin proteins, which sever actin filaments, are also important for in vivo actin dynamics and function [2]. Many actin binding proteins, including the main polymerization nucleators and myosin, are regulated by the small GTPases Rho, Rac, and Cdc42, which are in turn controlled by guanine-nucleotide-exchange factors (GEFs) and GTPase-activating proteins (GAPs) downstream of extracellular signals.

The diversity of actin-binding proteins leads to a diversity of actin architectures in the cell, adapted to different functions [1]. The actomyosin cortex is a thin layer of cross-linked actin filaments interspersed by myosin, attached to the inner face of the cell membrane. In the moving cell, the cortex at the back of the cell contracts to squeeze the cell forward, while protrusive actin structures, lamellipodia and filopodia, form at the front. Blebs, another type of cell protrusion, occur when the cell membrane detaches from the cytoskeleton and balloons outward, initially devoid of actin, due to actomyosin contractility in the cortex.

Caenorhabditis elegans has been used as a model organism to investigate the regulation and dynamics of actin networks in developmental processes [3]. In particular, the first asymmetric division of the *C. elegans* single cell embryo has been studied extensively in order to understand symmetry breaking, polarity establishment, microtubule assembly, spindle positioning, and the cell shape changes that accompany asymmetric cell division [4,5]. Briefly, as concerns the actin cytoskeleton and related proteins, in the just-fertilized zygote, cortical ruffles are evident all around the circumference of the embryo due to the highly dynamic and contractile cortical actomyosin layer. Symmetry is broken when the sperm contents approach the future posterior pole, locally downregulating contractility there and initiating the retraction of the actomyosin cortex to the future anterior pole [6,7]. This flow of actomyosin density towards the anterior pole leads to an invagination at the boundary between high and low actomyosin activity similar to ruffles but much deeper, called the pseudocleavage furrow. Anterior-directed cortical flow is concomitant with the segregation of the polarity proteins PAR-3, PAR-6, and PKC-3 to the anterior of the embryo, while PAR-1 and PAR-2 are recruited to the posterior cortex [8].

The result of this polarization phase in the embryo is the formation of two cortical domains that have different actomyosin activity and different PAR protein occupancy. During this period, known as the maintenance phase, a complex network of reciprocally supportive and antagonistic interactions between PAR proteins exists reinforcing their localization at the poles of the embryo. This also includes effects on actomyosin wherein PAR-1 and PAR-2 at the posterior pole have a role in inhibiting the posterior localization of non-muscle myosin II (NMY-2), while anterior PARs—PAR-3 and PAR-6/PKC-3—lead to the accumulation of NMY-2 at the anterior, establishing and maintaining a more contractile anterior pole [9]. During the maintenance phase, in a series of steps that are largely microtubule dependent, the maternal pronucleus joins the paternal pronucleus at the future posterior side of the cell, the complex recenters and then forms the spindle, which is pulled posteriorly again during anaphase to give the final asymmetry in division. Importantly, the positioning of the cleavage furrow and site of division is highly dependent on the positioning of the spindle [10], and it is the cortical polarity of the embryo that controls the mitotic spindle shift since cortical pulling forces are more pronounced at the posterior pole [6,11].

Although the first cell division of the *C. elegans* embryo has been studied for decades, many open questions remain. Here we review results from the last five years that address some of the outstanding questions in the field and demonstrate the multitude of roles played by the actin cytoskeleton in the *C. elegans* embryo.

2. Role of Actin in the Just-Fertilized Embryo during Completion of Meiosis

As for many organisms, *C. elegans* oocytes complete meiosis upon fertilization. While meiotic divisions are occurring at what will become the anterior pole of the embryo, the sperm contents, including genetic material, are retained at the site of sperm entry at the posterior pole, despite cytoplasmic streaming in the embryo.

A recent finding reported that the actin cytoskeleton was what was confining sperm DNA to the posterior pole of the embryo, and keeping it from getting captured by the meiotic spindle [12]. In embryos where actin polymerization was reduced, either by interfering with the profilin/formin mode of actin assembly or via application of inhibitory drugs, sperm DNA was distributed throughout the embryo due to cytoplasmic flows. This study further showed that the sperm contents were not

restricted to the posterior cortex by cytoplasmic actin via a sieving effect as could have been expected. Rather, the study suggested that it was the cortical actin pool that was important for sperm content confinement by an as-yet-unidentified mechanism. Although most studies on the one-cell embryo pay particular attention to actin structures and functions during and after polarity establishment, this work showed that F-actin was an important player prior to these events.

3. Actomyosin Dynamics in Symmetry Breaking

The morphological and biochemical changes defining the anteroposterior axis of the embryo occur downstream of sperm entry, which has been shown to break the symmetry of the embryo and define its future posterior pole [6,7,13]. At the moment of fertilization, actomyosin foci are present over the entire embryo surface, along with actomyosin-based cortical contractions. At the end of meiosis II and just as mitosis is beginning, the sperm centrosome moves close to the embryo cortex at the future posterior pole. As described in the introduction, this produces an immediate cessation of cortical activity and a flow of actomyosin foci away from this region. As reviewed recently [6], this local transformation in the actomyosin cytoskeleton is known to be due to the removal of the RhoGEF ECT-2 from the cortex.

Until recently, the molecular nature of the cue delivered by the sperm centrosome to downregulate posterior actomyosin activity and initiate cortical flow was unknown. Novel studies in the past year have identified the mitotic kinase Aurora A (AIR-1) as the previously unidentified centrosome component (Figure 1). One study showed that the phosphorylated, active form of AIR-1 was released from the centrosomes into the cytoplasm, driving the inhibition of posterior cortical actomyosin networks in the vicinity of the centrosomes [14]. This was discovered based on the finding that the GFP-tagged version of AIR-1 was not completely wild-type. GFP-labeled AIR-1 embryos performed AIR-1-dependent processes normally, including centrosome maturation, but failed to correctly clear actomyosin from the future posterior pole during symmetry breaking. It was hypothesized that this effect was due to a defect in diffusion of the GFP-labeled protein. This hypothesis was supported by experiments that manipulated the position of the centrosome, moving it closer and further away from the cortex, improving and exacerbating, respectively, the actomyosin clearing defect [14]. Another recent study came to a similar conclusion concerning the identity of the centrosome-derived cue [15]. Both studies showed that AIR-1's role in symmetry breaking was a result of its effect on ECT-2, altering its localization and perhaps its GEF activity by an unknown mechanism. AIR-1 could also be downregulating myosin activity via its phosphorylation of other RHO-1 pathway effectors that are upstream of ECT-2.

In addition to its centrosomal role in initiating cortical flow, non-centrosomal AIR-1 has been shown in recent studies to globally downregulate cortical actomyosin activity during polarity establishment. Embryos lacking AIR-1 showed hypercontractility of the cortex, and became bipolar, with NMY-2-poor/PAR-2-rich domains at both poles of the embryo, and weak cortical flows directed toward the embryo center from both sides [14–17]. One study further showed that this bipolarization could occur even in wild-type embryos when fertilized with acentrosomal sperm [16]. Putting all this together, it seemed that there was a basal activity of non-centrosomal AIR-1, which kept actomyosin downregulated globally and prevented spontaneous bipolarization events, while centrosomal AIR-1 downregulated actomyosin locally to initiate the polarizing cortical flows that establish embryo polarity. Why PAR-2 domains form in a bipolar manner was unclear, but it was proposed that curvature could be the determining factor [16]. This hypothesis was tested by placing *air-1* depleted embryos in triangular chambers. It was observed that PAR-2 domains emerged in regions with the highest curvature. PAR-2 accumulation at curved regions could be biochemically driven by lipid affinities or due to geometrical considerations, where the curved surface of the poles restricts diffusion out of the immediate vicinity [16]. An additional function for AIR-1 was recently observed in the steps leading up to fertilization and symmetry breaking in the oocyte, where AIR-1 was shown to play a role via another cell cycle kinase PLK-1 (polo-like kinase) in regulating anterior PAR loading and activation at the membrane, although the details of the actomyosin cortex are not addressed in this study [17].

This regulation prevents premature polarization of the embryo, and enforces the dependence on the centrosome cue.

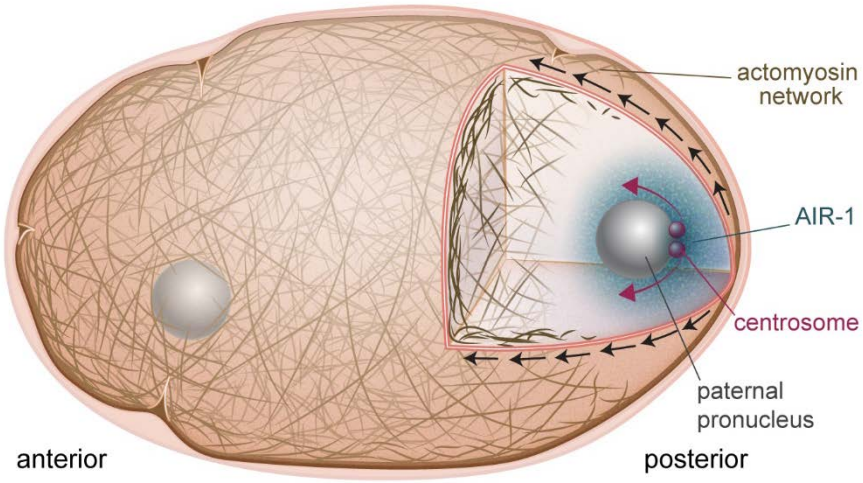

Figure 1. Symmetry breaking in the one-cell embryo. AIR-1 (blue cloud) is the cue that initiates polarization of the embryo. AIR-1 diffuses from the centrosome (red spheres) and downregulates actomyosin at the adjacent cortex. This causes a local weakening, and produces cortical flows (black arrows) directed away from this point, which also serve to separate the centrosomes (red arrows).

4. Cortical Flows during Polarity Establishment

Anterior-directed actomyosin contractility creates cortical flow, which sets up the polarity axis of the embryo as concerns both actin cytoskeleton and PAR proteins. Several recent studies have shed light on the precise details of how actomyosin-driven dynamics are coupled to PAR protein polarization. One study showed that cortical actomyosin tension facilitates the clustering of PAR-3 perhaps by inducing conformational changes that allow oligomerization [18]. Indeed, embryos lacking cortical tension molecules like NMY-2 did not exhibit PAR-3 clusters, but clusters could be rescued by artificial increases in cortical tension applied via osmotic shock for example. PAR-3 clustering induced clustering of PKC-3, and the clustering of both proteins was important for their proper transport to the anterior pole. A coincident study concurred, proposing that either clustering reduced the effective diffusion of membrane-associated anterior PARs, or the larger size of clusters allowed them to interact more effectively with the cortical actomyosin layer, both of which would favor advective transport by flows [19]. Another study came to a similar conclusion, showing via a single-cell extract technique that PAR-3 clusters were more efficiently transported by cortical flow due to the longer residence time of the PAR-3 oligomers at the cortex [20]. These and other findings concerning the roles of PLK-1 and CDC-42 in PAR protein clustering and cortical transport to the anterior pole are nicely reviewed in [21].

Another recent study showed the very clear link between cortical flows and PAR domain location. In this work, they used a novel focused-light-induced cytoplasmic streaming (FLUCS) system to induce controllable cytoplasmic flows in the embryo via temperature changes [22]. Cytoplasmic flows were shown to drive cortical flows, which were exactly mirrored by PAR protein domain relocation [22]. Compellingly, when the PAR-2 domain was moved to the anterior pole by flow, the embryo divided with an inverted size asymmetry (smaller anterior cell). All together, recent work confirms and extends the importance of actomyosin cortical flow for PAR domain establishment in the embryo.

The studies discussed above were principally about how flows driven by actomyosin contractility play a role in PAR protein localization, however the converse is also true: PAR proteins affect NMY-2 recruitment to the cortex and thus control flows. This complex interplay was investigated in a recent study where the kinetics of NMY-2 association and dissociation from the posterior and anterior cortex were measured [23]. It was observed that NMY-2 association with the cortex was identical for the posterior and anterior domains. Dissociation on the other hand was twice as high in the

posterior domain as compared to the anterior region. This was shown to depend on PAR-6 specifically, where increases in PAR-6 were accompanied by decreases in the dissociation of NMY-2. It was proposed that this mechanochemical feedback between actomyosin localization and PAR proteins ensured robustness of embryo polarity.

A previously unidentified role for cortical flow was highlighted in a recent study demonstrating that flow contributed to centrosome separation [24]. The centrosome pair present on the paternal pronucleus must be separated to correctly form the bipolar mitotic spindle necessary for the first cell division. The authors showed that cortical dynein, imbedded in the actomyosin cortex, and also bound to microtubules emanating from the centrosomes, was the main player in this process. Cortical dynein was swept anteriorly by actomyosin flows, pulling with it the centrosomes. When cortical flow was impaired by depletion of NMY-2 or RHO-1, centrosome separation was retarded although there was no effect on cell cycle progression. Since AIR-1 on the centrosome is what is responsible for breaking the symmetry of the embryo and triggering cortical flow, centrosomes are perfectly positioned to harness flow for separation (Figure 1).

PAR proteins control flows, but actin-binding proteins are also known to affect flows, presumably by modifying the organization and mechanical properties of the cortex. This point was addressed by carefully characterizing flow velocities, flow pulsatility and myosin foci size and density in *C. elegans* embryos upon depletion of different actin-binding proteins and myosin regulators [25]. Many were found to affect the measured parameters in sometimes subtle ways. One general result that came out of this analysis was that bigger, more sparsely-distributed myosin foci were correlated with slower average flow velocities. However, the main point of this study was that data clustering revealed classes of proteins with sometimes dissimilar molecular activities that nevertheless affected cortical properties in similar ways. This pointed to a degeneracy in the molecular components needed to produce a given phenotype. A related paper specifically examined the origins of pulsatility, asking why this did not lead to instability and collapse of the system [26]. They showed evidence that Rho activity oscillated, thus damping down myosin foci contraction and preventing collapse of the cortex. Although not pertaining to the one-cell embryo, another study came to a similar conclusion about the presence of a Rho oscillator [27]. These studies all together illustrate that actomyosin contractility and resulting flows are robustly controlled in the *C. elegans* embryo.

5. Cortical Actin Architecture and Dynamics

Many proteins that affect flows in the polarizing embryo also have effects on the stability of the actomyosin cortex in the maintenance phase, for example, the actin filament bundling protein plastin (PLST-1) [28]. Deletion of *plst-1* led to smaller and more dispersed NMY-2 foci as well as weaker and less coherent directed cortical flows suggesting a need for PLST-1 for proper NMY-2 coalescence and resulting flows. Predictably, since PAR protein organization depends in part on cortical flows, there was also a defect in the polarity of PAR proteins in embryos lacking PLST-1. Via laser ablations and measurements of cortex recoil velocity, lack of PLST-1 was shown to decrease the tension of the anterior cortex of the embryo during the maintenance phase, indicating reduced cortical stiffness. Overall, the authors proposed that, by controlling actin network connectivity, PLST-1 regulated the mechanical properties of the cortex. Imaging techniques that allow visualization of nanoscale structures of the actin cortex in the presence and absence of PLST-1 would be very interesting to obtain in order to get a molecular picture of connectivity differences.

Another interesting study on cortical stability addressed the functions of cadherin (HMR-1) in the *C. elegans* embryo [29]. HMR-1 is normally involved in cell-cell adhesions, but these are not present in the one-cell embryo. It was further shown that HMR-1's ability to interact with the permeability barrier surrounding the plasma membrane of the embryo was not important for HMR-1's role at this stage, so it appeared that HMR-1 was playing an adhesion-independent role. The observation was that clusters of HMR-1 formed during the polarity establishment phase of the single cell embryo, and associated with cortical F-actin. Clusters were transported to the anterior pole by flows where, during the maintenance

phase, they appeared to antagonize cortical NMY-2. Indeed, upon depletion of *hmr-1*, the level of anterior cortical NMY-2 significantly increased while there was no significant effect on the global concentration of NMY-2 or cortical F-actin. Non-junctional HMR-1 clusters appeared to control cortical NMY-2 via its upstream regulator, RHO-1: the amount of active cortical RHO-1 increased upon *hmr-1* depletion. Finally, in conditions of depleted *hmr-1*, cortical flows were accentuated and the actin cortex was observed to tear away from the cell membrane, probably due to the combined effect of increased flow/contractility and loss of stabilizing linkages conferred by HMR-1, which bridges the cell membrane to the actin network. Overall, this study brought to light a role for non-adhesive cadherin clusters in regulating actomyosin cortex stability and flows, and attachment to the cell membrane.

While much of the work reviewed here deals with the actomyosin cortex, which is attached to the cell membrane, not many studies have investigated the involvement of the cell membrane itself in the *C. elegans* embryo. A new study showed that the lipid phosphatidylinositol 4,5-bisphosphate (PIP2) was non-uniform in the polarized embryo. It was enriched at the anterior pole where it controlled actin dynamics and PAR protein recruitment [30]. However, this study conflicts with another recent work, which demonstrated that the increased formation of membrane folds at the anterior pole lead to an enrichment of lipids in general, not just PIP2 [31]. In fact, these membrane folds were shown to be filopodia, dependent on the formin CYK-1 and the Arp2/3 complex. The existence of PIP2 membrane microdomains in the *C. elegans* zygote therefore does not appear likely.

Overall, these recent studies detail the molecular regulation of the structure and dynamics of the actomyosin cortex during the post-polarization phase, expanding what is already known for symmetry breaking and polarity establishment.

6. Contractile Ring Formation and Positioning

Once polarity is triggered and established, the main steps preceding cytokinesis are contractile ring formation and spindle positioning, which is what defines the position of the cleavage furrow [10]. The ring is comprised of F-actin, myosin and accessory proteins and it accomplishes cytokinesis of the single cell embryo. Detailed, up-to-date reviews of the players needed for ensuring proper formation of the cytokinetic ring and furrow ingression have been published [6,32].

Insight as to how the contractile ring is constructed was provided by a recent study, where it was shown that F-actin alignment due to converging cortical flow at the cell equator was sufficient to drive ring formation (Figure 2) [33]. No localized actin polymerization was necessary, and in fact did not exist for ring formation during pseudocleavage, although such mechanisms exist for contractile ring formation during cleavage. Reducing flow rates by perturbing myosin machinery had predictable effects on the pseudocleavage furrow: slight reductions still permitted actin filaments to align to create a furrow while drastic reductions abolished furrow formation. A related work showed that mechanical compression of embryos inhibited longitudinal flows, but favoured rotational flows, which had the same end result of efficiently aligning filaments to create a contractile ring [34]. This study further showed that myosin flow characteristics were not quite the same as actin flows. In particular, NMY-2 flows were more long-ranged, a difference explained by the fact that actin was disassembled by compression as it flowed to the equator while myosin was not [34]. Cortical flows were also shown to be important for ring dynamics during constriction [35]. This study found that new cortex, including NMY-2, was being pulled into the ring due to myosin activity and polar relaxation. The added myosin in turn led to increased flow into the ring, and an exponential increase in the amount of ring components. This was counterbalanced by disassembly-coupled ring shortening. The end result was that, although NMY-2 levels and the levels of other ring components appeared to remain constant during ring constriction, the ring was in fact undergoing dramatic restructuring. These recent studies emphasize the robustness of cortical flows for creating and maintaining a proper furrow structure.

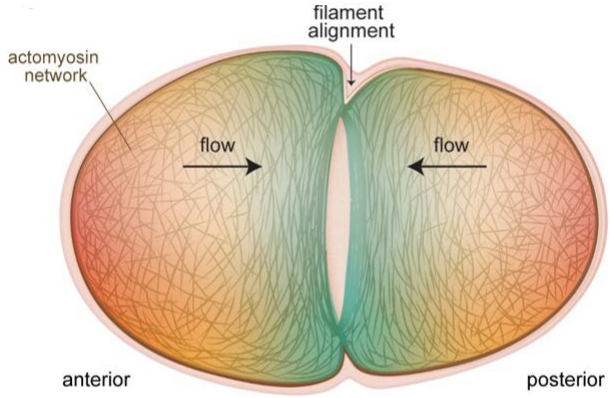

Figure 2. Cortical flows align filaments to form the contractile ring for cytokinesis of the one-cell embryo. The actomyosin cortex at the poles flows toward the equator of the embryo (black arrows), and these flows progressively transform the unorganized actin filament network at the poles (red shading) into the aligned structure of the cytokinetic ring (blue shading). In cases where actin-binding proteins are perturbed, thus altering cortical properties and flows, the formation and ingression of the contractile ring are impacted (see text).

One recent study revealed that both the Arp2/3 complex and the formin CYK-1 were important for the kinetics of cytokinesis even though the Arp2/3 complex did not localize to the cleavage furrow [36]. CYK-1 was shown to be enriched in the contractile ring and essential to elongate filaments to form it: *cyk-1* depletion led to a decrease in actin bundles at the equatorial cortex, and a furrow that initiated and ingressed more slowly. However, the Arp2/3 complex was also found to positively regulate the kinetics of contractile ring assembly and ring constriction, although it had the opposite effect on furrow initiation. Intriguingly, the slowing down of cytokinesis upon Arp2/3 complex inhibition was a result of an increase in CYK-1-mediated actin polymerization at the cell cortex and in the contractile ring. The conclusion was that Arp2/3 complex activity was required in the cortex to temper CYK-1-based polymerization, possibly via a competition for actin monomers as has been shown in other systems [37]. Too much cortical actin could be supposed to interfere with the cell shape changes accompanying cell division, while excessive actin in the furrow could inhibit contraction by impeding ring disassembly.

Proteins that affect cortical flows in the polarization phase and actomyosin cortex integrity in the maintenance phase also affect the speed of contractile ring formation and its contraction, due to the dependence of all these processes on similar parameters. The new studies concerning PLST-1 and HMR-1, mentioned previously in the context of cortex integrity, showed that these proteins also play roles in furrow formation. Lack of PLST-1 resulted in furrows that formed more slowly, although once formed, they ingressed at the normal speed, while lack of HMR-1 produced faster ingression than wild-type although with a tendency for the cortex to peel away from the cell membrane at the anterior pole [28,29].

As concerns furrow ingression, some studies have shown evidence that it is not myosin motor activity that drives contraction of the cytokinetic ring, but rather myosin's actin cross-linking activity coupled with depolymerization [38–40]. New studies in the *C. elegans* embryo have demonstrated unequivocally that NMY-2 motor activity was required throughout the formation and constriction of the actomyosin ring [41]. During ring assembly, the activity of NMY-2, rather than its F-actin cross-linking ability, were shown to control proper densification and alignment of actin in the cytokinetic ring, and timely deformation of the cell equator. In general, however, actin cross-linking activity is known to play a role in modulating contractility, and it was shown that for the *C. elegans* cytokinetic ring, an optimal degree of cross-linking existed, while too much or too little cross-linking activity was deleterious to contraction [42].

Contractile ring formation is important, but so is its correct positioning in the cell. Although positioning is mostly determined by astral microtubule dynamics, two recent papers

show the importance of the downregulation of actomyosin contractility at the embryo cortex for correct placement of the furrow. One study brought to light the essential role of AIR-1 in clearing contractile ring proteins such as anillin, but also actin, from the poles of the embryo [43]. At the onset of anaphase, a conserved activator of AIR-1, TPXL-1, became localized to astral microtubules, and it was shown that its capacity to bind and activate AIR-1 was key for polar clearing. The hypothesis was that activated AIR-1 promoted clearing of contractile ring proteins from the poles of the embryo via phosphorylation of target proteins, but this mechanism has yet to be investigated in detail. Taken all together with results described previously in this review, this study provides another example of the AIR-1's varied roles in the regulation of the actin cytoskeleton during the development of the early *C. elegans* embryo.

The role of cortical dynamics in furrow positioning was also demonstrated in another recent study, which described a role for bleb formation in releasing cortical tension in mutant embryos that had excessive anterior myosin contractility [44]. In these embryos, the furrow initially formed in an anterior position, however DNA segregation defects were avoided by a posterior shift of the furrow concomitant with an anterior shift of the anterior nucleus. These shifts were shown to be produced by bleb formation near the anterior side of the furrow. The release of tension due to bleb formation allowed repositioning of the nascent cleavage furrow, and also created cytoplasmic flows that contributed to moving the nucleus posteriorly.

7. Conclusions

The *C. elegans* embryo is a powerful model system for understanding the many roles of the actomyosin cytoskeleton in asymmetric cell division. Results obtained using this model over the last five years have answered outstanding questions, as summarized in this review. In particular, the nature of the centrosomal cue for symmetry breaking has at last been identified. Moreover, other recent studies have delved deeper into the molecular mechanisms of how actomyosin dynamics drives morphological changes in the embryo. In the past, the microtubule cytoskeleton and PAR proteins have taken center stage in the *C. elegans* embryo. Our summary in this review shows the importance of the actin cytoskeleton in polarity establishment of the *C. elegans* zygote as well as the cellular shape changes that ensure the first asymmetric division of the embryo.

Funding: J.P. acknowledges financial support from the Fondation ARC (Grant PJA 20191209604) and the program "Investissements d'Avenir" launched by the French Government and implemented by ANR (ANR-10-LABX-0038 and ANR-10-IDEX-0001-02 PSL). D.S.E. received funding from the European Union's Horizon 2020 research and innovation program under the Marie Skłodowska-Curie grant agreement N° 666003.

Acknowledgments: We acknowledge Agnieszka Kawska at IlluScientia.com for graphical design of the figures.

Conflicts of Interest: The authors declare no conflict of interest.

References

1. Blanchoin, L.; Boujemaa-Paterski, R.; Sykes, C.; Plastino, J. Actin dynamics, architecture and mechanics in cell motility. *Physiol. Rev.* **2014**, *94*, 235–263. [CrossRef] [PubMed]
2. Plastino, J.; Blanchoin, L. Dynamic stability of the actin ecosystem. *J. Cell Sci.* **2018**, *132*, jcs219832. [CrossRef]
3. Agarwal, P.; Zaidel-Bar, R. Principles of actomyosin regulation in vivo. *Trends Cell Biol.* **2019**, *29*, 150–163. [CrossRef] [PubMed]
4. Cowan, C.R.; Hyman, A.A. Asymmetric cell division in *C. elegans*: Cortical polarity and spindle positioning. *Annu. Rev. Cell Dev. Biol.* **2004**, *20*, 427–453. [CrossRef]
5. Begasse, M.L.; Hyman, A.A. The first cell cycle of the *Caenorhabditis elegans* embryo: Spatial and temporal control of an asymmetric cell division. *Results Probl. Cell Differ.* **2011**, *53*, 109–133. [PubMed]
6. Pacquelet, A. Asymmetric cell division in the one-cell *C. elegans* embryo: Multiple steps to generate cell size asymmetry. *Results Probl. Cell Differ.* **2017**, *61*, 115–140. [PubMed]

7. Rose, L.; Gonczy, P. Polarity establishment, asymmetric division and segregation of fate determinants in early *C. elegans* embryos. *WormBook* **2014**. Available online: http://www.wormbook.org/chapters/www_asymcelldiv.2/asymcelldiv.2.html (accessed on 21 May 2020). [CrossRef]
8. Munro, E.; Nance, J.; Priess, J.R. Cortical flows powered by asymmetrical contraction transport PAR proteins to establish and maintain anterior-posterior polarity in the early *C. elegans* embryo. *Dev. Cell* **2004**, *7*, 413–424. [CrossRef]
9. Lang, C.F.; Munro, E. The PAR proteins: From molecular circuits to dynamic self-stabilizing cell polarity. *Development* **2017**, *144*, 3405–3416. [CrossRef]
10. Glotzer, M. Cleavage furrow positioning. *J. Cell Biol.* **2004**, *164*, 347–351. [CrossRef]
11. Gonczy, P. Mechanisms of asymmetric cell division: Flies and worms pave the way. *Nat. Rev. Mol. Cell Biol.* **2008**, *9*, 355–366. [CrossRef] [PubMed]
12. Panzica, M.T.; Marin, H.C.; Reymann, A.C.; McNally, F.J. F-actin prevents interaction between sperm DNA and the oocyte meiotic spindle in *C. elegans*. *J. Cell Biol.* **2017**, *216*, 2273–2282. [CrossRef] [PubMed]
13. Cowan, C.R.; Hyman, A.A. Acto-myosin reorganization and PAR polarity in *C. elegans*. *Development* **2007**, *134*, 1035–1043. [CrossRef] [PubMed]
14. Zhao, P.; Teng, X.; Tantirimudalige, S.N.; Nishikawa, M.; Wohland, T.; Toyama, Y.; Motegi, F. Aurora-A breaks symmetry in contractile actomyosin networks independently of its role in centrosome maturation. *Dev. Cell* **2019**, *48*, 631–645. [CrossRef] [PubMed]
15. Kapoor, S.; Kotak, S. Centrosome Aurora A regulates RhoGEF ECT-2 localisation and ensures a single PAR-2 polarity axis in *C. elegans* embryos. *Development* **2019**, *146*, dev174565. [CrossRef]
16. Klinkert, K.; Levernier, N.; Gross, P.; Gentili, C.; von Tobel, L.; Pierron, M.; Busso, C.; Herrman, S.; Grill, S.W.; Kruse, K.; et al. Aurora A depletion reveals centrosome-independent polarization mechanism in *Caenorhabditis elegans*. *eLife* **2019**, *8*, e44552. [CrossRef]
17. Reich, J.D.; Hubatsch, L.; Illukkumbura, R.; Peglion, F.; Bland, T.; Hirani, N.; Goehring, N.W. Regulated activation of the PAR polarity network ensures a timely and specific response to spatial cues. *Curr. Biol.* **2019**, *29*, 1911–1923. [CrossRef]
18. Wang, S.C.; Low, T.Y.F.; Nishimura, Y.; Gole, L.; Yu, W.; Motegi, F. Cortical forces and CDC-42 control clustering of PAR proteins for *Caenorhabditis elegans* embryonic polarization. *Nat. Cell Biol.* **2017**, *19*, 988–995. [CrossRef]
19. Rodriguez, J.; Peglion, F.; Martin, J.; Hubatsch, L.; Reich, J.; Hirani, N.; Gubieda, A.G.; Roffey, J.; Fernandes, A.R.; St Johnston, D.; et al. aPKC cycles between functionally distinct PAR protein assemblies to drive cell polarity. *Dev. Cell* **2017**, *42*, 400–415. [CrossRef]
20. Dickinson, D.J.; Schwager, F.; Pintard, L.; Gotta, M.; Goldstein, B. A single-cell biochemistry approach reveals PAR complex dynamics during cell polarization. *Dev. Cell* **2017**, *42*, 416–434. [CrossRef]
21. Munro, E. Protein clustering shapes polarity protein gradients. *Dev. Cell* **2017**, *42*, 309–311. [CrossRef] [PubMed]
22. Mittasch, M.; Gross, P.; Nestler, M.; Fritsch, A.W.; Iserman, C.; Kar, M.; Munder, M.; Voigt, A.; Alberti, S.; Grill, S.W.; et al. Non-invasive perturbations of intracellular flow reveal physical principles of cell organization. *Nat. Cell Biol.* **2018**, *20*, 344–351. [CrossRef] [PubMed]
23. Gross, P.; Kumar, K.V.; Goehring, N.W.; Bois, J.S.; Hoege, C.; Julicher, F.; Grill, S.W. Guiding self-organized pattern formation in cell polarity establishment. *Nat. Phys.* **2019**, *15*, 293–300. [CrossRef] [PubMed]
24. De Simone, A.; Nedelec, F.; Gonczy, P. Dynein transmits polarized actomyosin cortical flows to promote centrosome separation. *Cell Rep.* **2016**, *14*, 2250–2262. [CrossRef] [PubMed]
25. Naganathan, S.R.; Furthauer, S.; Rodriguez, J.; Fievet, B.T.; Julicher, F.; Ahringer, J.; Cannistraci, C.V.; Grill, S.W. Morphogenetic degeneracies in the actomyosin cortex. *eLife* **2018**, *7*, e37677. [CrossRef]
26. Nishikawa, M.; Naganathan, S.R.; Julicher, F.; Grill, S.W. Controlling contractile instabilities in the actomyosin cortex. *eLife* **2017**, *6*, e19595. [CrossRef]
27. Michaux, J.B.; Robin, F.B.; McFadden, W.M.; Munro, E.M. Excitable RhoA dynamics drive pulsed contractions in the early *C. elegans* embryo. *J. Cell Biol.* **2018**, *217*, 4230–4252. [CrossRef]
28. Ding, W.Y.; Ong, H.T.; Hara, Y.; Wongsantichon, J.; Toyama, Y.; Robinson, R.C.; Nedelec, F.; Zaidel-Bar, R. Plastin increases cortical connectivity to facilitate robust polarization and timely cytokinesis. *J. Cell Biol.* **2017**, *216*, 1371–1386. [CrossRef]

29. Padmanabhan, A.; Ong, H.T.; Zaidel-Bar, R. Non-junctional E-cadherin clusters regulate the actomyosin cortex in the *C. elegans* zygote. *Curr. Biol.* **2017**, *27*, 103–112. [CrossRef]
30. Scholze, M.J.; Barbieux, K.S.; De Simone, A.; Boumasmoud, M.; Suess, C.C.N.; Wang, R.; Gonczy, P. PI(4,5)P2 forms dynamic cortical structures and directs actin distribution as well as polarity in *Caenorhabditis elegans* embryos. *Development* **2018**, *145*, dev164988. [CrossRef]
31. Hirani, N.; Illukkumbura, R.; Bland, T.; Mathonnet, G.; Suhner, D.; Reymann, A.C.; Goehring, N.W. Anterior-enriched filopodia create the appearance of asymmetric membrane microdomains in polarizing *C. elegans* zygotes. *J. Cell Sci.* **2019**, *132*, jcs230714. [CrossRef] [PubMed]
32. Leite, J.; Osorio, D.S.; Sobral, A.F.; Silva, A.M.; Carvalho, A.X. Network contractility during cytokinesis-from molecular to global views. *Biomolecules* **2019**, *9*, 194. [CrossRef] [PubMed]
33. Reymann, A.C.; Staniscia, F.; Erzberger, A.; Salbreux, G.; Grill, S.W. Cortical flow aligns actin filaments to form a furrow. *eLife* **2016**, *5*, e17807. [CrossRef]
34. Singh, D.; Odedra, D.; Dutta, P.; Pohl, C. Mechanical stress induces a scalable switch in cortical flow polarization during cytokinesis. *J. Cell Sci.* **2019**, *132*, jcs231357. [CrossRef]
35. Khaliullin, R.N.; Green, R.A.; Shi, L.Z.; Gomez-Cavazos, J.S.; Berns, M.W.; Desai, A.; Oegema, K. A positive-feedback-based mechanism for constriction rate acceleration during cytokinesis in *Caenorhabditis elegans*. *eLife* **2018**, *7*, e36073. [CrossRef]
36. Chan, F.Y.; Silva, A.M.; Saramago, J.; Pereira-Sousa, J.; Brighton, H.E.; Pereira, M.; Oegema, K.; Gassmann, R.; Carvalho, A.X. The ARP2/3 complex prevents excessive formin activity during cytokinesis. *Mol. Biol. Cell* **2019**, *30*, 96–107. [CrossRef] [PubMed]
37. Burke, T.A.; Christensen, J.R.; Barone, E.; Suarez, C.; Sirotkin, V.; Kovar, D.R. Homeostatic actin cytoskeleton networks are regulated by assembly factor competition for monomers. *Curr. Biol.* **2014**, *24*, 579–585. [CrossRef]
38. Lord, M.; Laves, E.; Pollard, T.D. Cytokinesis depends on the motor domains of myosin-II in fission yeast but not in budding yeast. *Mol. Biol. Cell* **2005**, *16*, 5346–5355. [CrossRef]
39. Ma, X.; Kovacs, M.; Conti, M.A.; Wang, A.; Zhang, Y.; Sellers, J.R.; Adelstein, R.S. Nonmuscle myosin II exerts tension but does not translocate actin in vertebrate cytokinesis. *Proc. Natl. Acad. Sci. USA* **2012**, *109*, 4509–4514. [CrossRef]
40. Mendes Pinto, I.; Rubinstein, B.; Kucharavy, A.; Unruh, J.R.; Li, R. Actin depolymerization drives actomyosin ring contraction during budding yeast cytokinesis. *Dev. Cell* **2012**, *22*, 1247–1260. [CrossRef]
41. Osorio, D.S.; Chan, F.Y.; Saramago, J.; Leite, J.; Silva, A.M.; Sobral, A.F.; Gassmann, R.; Carvalho, A.X. Crosslinking activity of non-muscle myosin II is not sufficient for embryonic cytokinesis in *C. elegans*. *Development* **2019**, *146*, dev179150. [CrossRef] [PubMed]
42. Descovich, C.P.; Cortesa, D.B.; Ryan, S.; Nash, J.; Zhang, L.; Maddox, P.S.; Nedelec, F.; Maddox, A.S. Cross-linkers both drive and brake cytoskeletal remodeling and furrowing in cytokinesis. *Mol. Biol.Cell* **2018**, *29*, 622–631. [CrossRef] [PubMed]
43. Mangal, S.; Sacher, J.; Kim, T.; Osorio, D.S.; Motegi, F.; Carvalho, A.X.; Oegema, K.; Zanin, E. TPXL-1 activates Aurora A to clear contractile ring components from the polar cortex during cytokinesis. *J. Cell Biol.* **2018**, *217*, 837–848. [CrossRef] [PubMed]
44. Pacquelet, A.; Jousseaume, M.; Etienne, J.; Michaux, G. Simultaneous regulation of cytokinetic furrow and nucleus positions by cortical tension contributes to proper DNA segregation during late mitosis. *Curr. Biol.* **2019**, *29*, 3766–3777. [CrossRef] [PubMed]

Annex: Research article manuscript *submitted*

Title: Asymmetry is defined during meiosis in the oocyte of the parthenogenetic nematode *Diploscapter pachys*
Authors: Dureen Samandar Eweis, Marie Delattre and Julie Plastino

Contribution: I performed all experiments, except tubulin fixed staining of embryos, and all image analysis. I wrote and re-read the manuscript with Julie.

Asymmetry is defined during meiosis in the oocyte of the parthenogenetic nematode *Diploscapter pachys*

Dureen Samandar Eweis[1,2], Marie Delattre[3] and Julie Plastino[1,2,4]
[1] Physico Chimie Curie, Institut Curie, PSL Research University, CNRS UMR168, 75005 Paris, France.
[2] Sorbonne Université, 75005 Paris, France.
[3] Laboratory of Biology and Modeling of the Cell, Ecole Normale Supérieure de Lyon, CNRS, Inserm, UCBL, 69007 Lyon, France
[4] Corresponding author: julie.plastino@curie.fr, +33 156246484

KEY WORDS: asymmetric cell division, actin, microtubule aster, parthenogenesis, symmetry breaking, nuclear positioning, polarity, myosin

ABSTRACT

Asymmetric cell division is an essential feature of normal development and certain pathologies. The process and its regulation have been studied extensively in the *Caenorhabditis elegans* embryo, particularly how symmetry of the actomyosin cortical cytoskeleton is broken by a sperm-derived signal at fertilization, upstream of polarity establishment. *Diploscapter* pachys is the closest parthenogenetic relative to *C. elegans*, and *D. pachys* one-cell embryos also divide asymmetrically. However how polarity is triggered in the absence of sperm remains unknown. In post-meiotic embryos, we find that the nucleus inhabits principally one embryo hemisphere, the future posterior pole. When forced to one pole by centrifugation, the nucleus returns to its preferred pole, although poles appear identical as concerns cortical ruffling and actin cytoskeleton. The location of the meiotic spindle also correlates with the future posterior pole and slight actin enrichment is observed at that pole in some early embryos along with unusual microtubule structures emanating from the meiotic spindle. Our results show that polarity of the *D. pachys* embryo is attained during meiosis, perhaps via the meiotic spindle, by a mechanism that may be present but suppressed in *C. elegans*.

INTRODUCTION

Asymmetric cell division produces daughter cells of different fate and usually of different size, and as such, it promotes cellular diversity. The mechanisms ensuring asymmetric cell division have been studied and understood using a relatively limited range of model systems, including the first cell division of the *Caenorhabditis elegans* embryo (Gönczy, 2008; Knoblich, 2010).

C. elegans embryos are arrested at prometaphase of meiosis I until fertilization. Upon sperm entry and towards the end of meiosis II, the network of actin and myosin that underlies the embryo membrane, known as the cortex, begins contracting all around the embryo (Munro et al., 2004). The discrimination of one pole of the embryo from the other, or symmetry breaking, is a fundamental prerequisite for asymmetric cell division (Gan and Motegi, 2021). In the fertilized *C. elegans* embryo, symmetry breaking has been shown to depend on a sperm centrosome-derived kinase AIR-1 (Kapoor and Kotak, 2019; Klinkert et al., 2019; Zhao et al., 2019). This kinase locally weakens the actomyosin cortex, triggering a contraction away from the sperm centrosome at the presumptive posterior pole. This produces directed cytoplasmic streaming and anterior-directed actomyosin cortical flows, which are accompanied by intense cortical ruffling and a traveling deep invagination, known as the pseudocleavage furrow that separates a smooth posterior cortex from a dynamic anterior cortex (Hird and White, 1993; Munro et al., 2004). As a result of actomyosin symmetry breaking, an actin-rich anterior domain is formed and the PAR polarity proteins are segregated differentially with anterior localization of PAR-3, PAR-6, and PKC-3 while PAR-1 and PAR-2 are recruited to the posterior cortex (Munro et al., 2004). During cortical polarity establishment, the maternal and paternal pronuclei meet at the posterior pole, and migrate to the cell center in a microtubule-dependent manner. During anaphase, the mitotic spindle is subsequently off-centered as a result of an imbalance of microtubule pulling forces from the anterior versus the posterior cortex, resulting in unequally-sized daughter cells (Rose and Gönczy, 2014).

Despite sometimes vast evolutionary distances, a conserved feature of nematodes studied so far is embryo polarization as early as the first cell cycle (Brauchle et al., 2009; Schulze and Schierenberg, 2011; Valfort et al., 2018). The manifestation of this early polarization is as follows: i) an asymmetric first division giving rise to a large anterior cell (AB) and a small posterior cell (P1), although the asymmetry is in some cases very subtle (Valfort et al., 2018), ii) an asynchrony of division between AB and P1 with AB being either first or second depending on species, iii) an asymmetric division of P1 whereas AB divides symmetrically (Delattre and Goehring, 2021).

Despite the importance of the sperm centrosome in symmetry breaking in *C. elegans*, other species have been found to polarize independently of sperm, either because there is no sperm, as in parthenogenetic species, or because sperm is not the polarity cue (Goldstein et al., 1998; Lahl et al., 2006). What acts as the polarity cue and how symmetry is broken in these cases remains an open question, one which we address in this study using the parthenogenetic nematode *Diploscapter pachys*. By a combination of live embryo imaging and dynamics

analysis, cytoskeleton fixed staining at different stages and perturbing centrifugation experiments, we observe that, while many features of the asymmetric division process are conserved between *D. pachys* and *C. elegans*, the timing of polarity establishment and the correlation of the posterior pole with the location of the meiotic spindle are unique to *D. pachys*.

RESULTS/DISCUSSION

Evidence of symmetry breaking in the one-cell embryo of D. pachys

D. pachys is an asexual nematode, but nevertheless a close relative to the sexually reproducing *C. elegans* (Fradin et al., 2017). *D. pachys* carries a single chromosome pair, and oocytes appear to skip meiosis I and undergo a single meiosis II-type nuclear division to separate sister chromatids, forming a polar body and a diploid oocyte, which becomes an embryo without fertilization (Fradin et al., 2017).

Most embryos dissected from gravid *D. pachys* females were at the one-cell stage, meaning that they were laid before their first mitotic division. Moreover 80% were post-meiotic as evidenced by a clearly delimited round shape of the nucleus (n = 34/43) while the remainder were just before or undergoing meiotic division. Most post-meiotic embryos we filmed took about 50 minutes to proceed to cleavage, passing through four recognizable stages in DIC microscopy: membrane ruffling, membrane smoothening, cleavage start and scission (Figure 1A and Supplementary Movie 1). Ruffling was the longest stage, lasting 20-45 minutes depending on the specimen. About 15 minutes before the onset of cytokinesis, recognizable as membrane invagination, and about five minutes before nuclear envelope breakdown (NEBD), membrane ruffling abated and the embryo contour became smooth. From the start to finish of cleavage took about five minutes (Figure 1A). As compared to *C. elegans*, the overall impression obtained from these films, which will be detailed more in the following, was that *D. pachys* embryos displayed more membrane activity in general than *C. elegans*, but that the asymmetric smoothening of one pole was lacking in *D. pachys*, there was no identifiable pseudocleavage furrow and cytoplasmic flows were chaotic.

D. pachys embryos were also able to hatch between slide and coverslip, displaying recognizable stages as compared to *C. elegans*, but taking around 38 hours to hatch from the time of cleavage initiation of the first cell division, as opposed to nine hours for *C. elegans* (Supplementary Figure S1A and Supplementary Movie 2). As previously reported for closely related *Diploscapter coronatus* (Lahl et al., 2009), at the 2-cell stage of *D. pachys* embryos, one blastomere was slightly smaller than the other, and the smaller cell went on to divide before the other in an asymmetric manner, revealing that the embryo was polarized. By analogy with *C. elegans* and other nematodes, this cell was thus considered the posterior cell P1. In *D. pachys*, as in other members of the *Diploscapter* genus, the mitotic spindle in both AB and P1 oriented along the longitudinal axis of the embryo (Goldstein, 2001; Lahl et al., 2009) (Supplementary Figure S1A). Observing females that retained their embryos for longer in the uterus and/or examining egg-laying of anesthetized females, we followed cell division and confirmed, like for *D. coronatus*, that there was no correlation between oocyte orientation in the uterus and the location of the posterior cell: 50% of embryos had their posterior pole adjacent to the vulva and 50% had their anterior pole towards the vulva (N = 11) (Lahl et al., 2006). Taking all of this information together, the fact that there was no uterine cue and that the smaller cell systematically gave rise to the P1 lineage indicated that the asymmetry found at the first division was sufficient to define the future posterior side of the embryo in this species which lacked a paternal contribution.

More in detail we found that at the start of filming, the position of the maternal nucleus was variable although it was often positioned in the future posterior half of the embryo. Without exception by the end of smoothening, the nucleus had traveled to the part of the embryo that would become the posterior pole, and positioned itself at 46 ± 3% (N = 43) of the total length of the embryo by the onset of metaphase (Figure 1B). Indeed outlier embryos in both the anterior and posterior directions showed the most dramatic movements toward the 46% mark just before and during the smoothening period, and ended up dividing asymmetrically like the others (Figure 1B). This result showed a strict correlation between the position of the post-meiotic nucleus and the position of the posterior pole.

The posterior pole is not determined by the position of the post-meiotic nucleus

The question was then if this were causal: did proximity of the nucleus define the posterior pole? To test this, we perturbed the initial position of the female pronucleus by centrifugation of live embryos adhered to microscope slides in order to shift the nucleus to one side of the embryo and see if that pole became the posterior. Only embryos that were positioned with their long anterior-posterior (AP) axis parallel to the centrifugation force were considered. Due to the duration of the centrifugation treatment, most (90%) of the embryos were post-meiotic. Just after centrifugation, these post-meiotic nuclei were, in the majority of cases, found at the pole opposite to the centrifugal force (24/27 embryos) (Figure 1C). This was unanticipated, but indicated that most nuclei were less dense than other contents of the embryo. We then observed subsequent embryo development, and evaluated which end of the embryo became the posterior pole. In 13/24 embryos, the nucleus remained at its post-centrifugation pole, and that became the posterior cell as evaluated by both size and by P1 cell division (dividing before AB) (Figure 1C and Supplementary Movie 3). However in the remaining 11 embryos, the nucleus moved to the opposite pole, and that became the posterior cell (Figure 1C Supplementary Movie 4). However taking the main population of post-meiotic embryos, the data suggested that polarity of the embryo was set upstream of post-meiotic nuclear positioning since the initial location of the nucleus after centrifugation did not correlate with the future posterior pole of the embryo. Early pole definition also explained the behavior of anteriorly-positioned outliers, which migrated directionally toward the future posterior pole (Figure 1B).

Cortical ruffling and actin cytoskeleton are not polarized in post-meiotic embryos

This result echoed what was known for the *C. elegans* embryo where polarity is established well before nuclear positioning for division. As discussed in the introduction, polarization is typified by dissimilar cortical dynamics at the two embryo poles, visible by live DIC microscopy as enhanced ruffling at the anterior pole during pronuclear meeting and centering, as well as by live or fixed actin cytoskeleton labelling, which shows enrichment of actin and myosin at the anterior pole (Strome, 1986; Munro et al., 2004; Reymann et al., 2016). We therefore looked for some indication that the *D. pachys* embryo had polarized cortical activity by first assessing DIC movies. We created masks via machine learning to automatically detect embryo contours over time, and compared them with an either/or function where white pixels indicated presence of signal in only one of two consecutive frames being compared (Figure 2A and Supplementary Movie 5 and 6). In this analysis the width of the margin of

white pixels gave a visualization of contour changes, with a thicker band indicating more variability and thus more cortical activity. Breaking the stacks down into early ruffling, late ruffling and smoothening phases, we observed a decrease in band thickness over time as smoothening occurred (going from left to right in Figure 2B), but there were no obvious differences in margin thickness when comparing the future posterior and anterior poles. Indeed this was true for a whole population of embryos (N = 25) where plotting margin thickness at the anterior pole versus thickness at the posterior pole during the ruffling phase gave a linear relation with a slope of one (Figure 2B). So although there was considerable variability in the contours explored by different embryos (margin thicknesses range from one to seven μm), the activity at the posterior and anterior poles was indistinguishable. If the anterior were more active, for example, the line would have had a slope greater than one.

We next sought to observe a difference in actin cytoskeleton between the embryo poles in *D. pachys*. Due to a lack of transgenic techniques in *D. pachys*, we attempted to apply vital dyes such as SirActin by different means, including feeding loaded liposomes (Flavel et al., 2018) and *perm-1* RNAi (Fradin et al., 2017) without success. We therefore turned to phalloidin staining of F-actin in fixed embryos, using DNA labeling to stage the embryos. Since for *C. elegans* actin polarization is only evident post-meiotically and then diminishes around cleavage, we initially focused on *D. pachys* embryos that displayed a clear polar body extrusion indicating that meiosis had already taken place. For post-meiotic *D. pachys* embryos, we observed no consistent actin asymmetry at prometaphase, metaphase and anaphase stages (N = 38), whereas in the *C. elegans* control (N = 46), processed for imaging via the same method as used for *D. pachys*, there was clear enrichment of actin at the future anterior pole (Figure 2C, 2D). Neither species showed much actin asymmetry in the two-cell stage (Figure 2C, 2D). The fact that the post-meiotic *D. pachys* embryo had a nonpolarized actin cytoskeleton resonated with the homogeneity of cortical activity quantified with live embryos (Figure 2A, 2B). However this lack of polarity was not in keeping with our centrifugation results, which indicated that the nucleus had a clear preference for one pole of the embryo post-meiotically. This led us to the hypothesis that polarity in *D. pachys* was generated early, during or before meiosis in the oocyte.

The meiotic spindle correlates with the future posterior pole in D. pachys embryos

In *C. elegans*, the meiotic spindle is usually at the anterior pole but the relationship is not causal. The real polarity signal is released by the sperm centrosome, and the posterior pole is therefore defined by its location (Goldstein and Hird, 1996; Bienkowska and Cowan, 2012; Kimura and Kimura, 2020). However in mutant cases in *C. elegans* where there is a persistent meiotic spindle, it has been shown that signaling from the spindle can establish polarity and define the posterior pole, so this role is not unique to the sperm centrosome (Wallenfang and Seydoux, 2000). Given this context we looked for a role of the meiotic spindle in symmetry breaking in *D. pachys* by examining the 20% of our DIC movies that began early enough to include meiosis. The meiotic spindle was invariably found on the lateral side of the oocyte and not at the pole of the cell in contrast to *C. elegans*. Nevertheless in all nine cases, the meiotic spindle was found slightly off centered, and this asymmetric localization correlated with the future posterior pole (Figure 3A). In a previous study on a

sister parthenogenetic species, *Diplosapter coronatus*, the authors came to the conclusion that there was no correlation between the polar body and the posterior pole (Lahl et al., 2006), however we were looking at meiotic spindle formation as opposed to polar bodies whose position can drift once they are formed. Our result was compatible with a role for the meiotic spindle in polarity establishment in *D. pachys*.

D. pachys embryos display a pre-meiotic microtubule aster and actin asymmetry

If this were the case, and based on what was observed with persistent meiotic spindles in *C. elegans*, we would expect to find evidence of a microtubule structure that could potentially serve as a polarity cue, although the role of microtubules in this process is somewhat controversial (Wallenfang and Seydoux, 2000; Sonneville and Gönczy, 2004). We therefore stained oocytes for microtubules, and found that, before meiotic spindle formation, embryos exhibited a large microtubule aster between the chromosomes, a structure not observed in *C. elegans* (Figure 3B). During meiotic division, we observed a cage of microtubules around the chromosomes resembling a *C. elegans* meiotic spindle, but with unusual microtubule extensions reaching out on the side directed toward the cell border (Figure 3B). Either one of these structures could potentially communicate with the cortex during meiotic division, delivering an unknown signal and setting the polarity of the embryo.

To see if there was any manifestation of polarity establishment in the actin cytoskeleton at this stage, we phalloidin stained pre-meiotic embryos, before polar body formation as evaluated by DNA staining. Of a total of 16 pre-meiotic embryos, we observed nine that exhibited a slightly polarized actin cytoskeleton with one hemisphere being richer in actin than the other (Figure 3C). In seven cases out of nine, the DNA was in the actin-rich pole of the embryo. Assuming that the location of pre-meiotic DNA corresponded to the site of the future meiotic spindle and given correlation of the meiotic spindle with the posterior pole, we concluded from this that actin enrichment was posterior, unlike what is observed in *C. elegans*. Also unlike *C. elegans*, actin polarization was weaker, more fleeting and less consistent in the *D. pachys* embryo so it was difficult to conclude. However in this context, it is important to note that even for *C. elegans*, only certain stages of the first cell division exhibit clear actin asymmetry by phalloidin staining, and that even when asymmetry fades upon cytokinesis, the embryo retains its polarity.

Conclusion

Putting all the data together, we conclude that the *D. pachys* embryo is polarized very early in development, at or before the unique meiotic division of the oocyte. The microtubule structures observed at meiosis could contribute to the symmetry breaking event, but we cannot rule out something even more upstream involving the oocyte nucleus, and independent of microtubules. Indeed in *C. elegans* there are multiple levels of redundancy to ensure polarization via the sperm (Delattre and Goehring, 2021). In particular PLK-1 and AIR-1 have been shown in *C. elegans* to prevent precocious polarization in oocytes in response to cryptic cues coming from the female pronucleus and the meiotic spindle (Reich et al., 2019) or even from curvature (Klinkert et al., 2019). We hypothesize that this inhibition is not at work in *D. pachys*, leading to very early polarization.

The question remains as to the exact nature of the polarity cue. It could be coming from the meiotic spindle large aster, be a result of self-organization of PAR proteins (Delattre and Goehring, 2021), or be produced by spontaneous symmetry breaking in curved regions of the embryo due to actomyosin contractility, as has been shown in *in vitro* systems (Carvalho et al., 2013). As concerns the first possibility, the invariably lateral position of the meiotic spindle would seem incompatible with hemispheric polarity. However in *C. elegans* it has been shown that when polarity emerges off-axis, re-alignment of PAR domains along the long axis can occur (Schenk et al., 2010; Gessele et al., 2020). A similar corrective mechanism could be operational in the *D. pachys* case. As concerns PAR proteins, it has been shown in the sister species *D. coronatus* that PAR-1 is symmetrically distributed in the one-cell embryo just before division (Brauchle et al., 2009) seemingly shedding doubt on a role for the PAR network in polarity of the *D. pachys* embryo. However it is of note that there are cases in *C. elegans* where PAR-1 is uniform, but normal asymmetric division occurs nonetheless (Folkmann and Seydoux, 2019). Furthermore it is entirely possible the PAR paradigm conceived for *C. elegans* is not the whole story in other species, and that additional PAR regulatory proteins or altogether different polarity proteins play a role (Basham and Rose, 1999; Brauchle et al., 2009; Morton et al., 2012).

To conclude although many open questions remain, what is clear from this study is that already at meiosis, there is a difference between the poles of the *D. pachys* oocyte, which drives polarity of the embryo. *Diploscapter* is the only genus known to date within the *Rhabditidae* family, which includes *C. elegans*, to polarize independently of a sperm centrosome-derived cue. It is therefore of particular importance to further study self-organization and symmetry breaking in this species in order to bring to light alternative/redundant pathways for symmetry breaking that are obscured in *C. elegans*, where the sperm centrosome mechanism is dominant.

MATERIALS AND METHODS

Worm cultivation

Diploscapter pachys strain PF1309 was originally obtained from Hélène Fradin (Fradin et al., 2017). *Caenorhabditis elegans* strain N2 was from the Caenorhabditis Genetics Center. Strains were cultured at 20 °C on 2.5% standard NGM plates for *C. elegans* worms and 5% NGM plates for *D. pachys* worms in order to reduce plate contamination and burrowing. Plates were seeded with the OP50 strain of *Escherichia coli* as a food source.

DIC microscopy

Gravid adults were cut in a watch glass in M9 buffer and embryos were transferred to a 2% noble agarose pad. Embryos were imaged during asymmetric cell division by DIC microscopy. For time-lapse acquisitions the time between frames was 10 seconds. Long-term time-lapse imaging of egg hatching was acquired at an interval of 10 seconds for capturing first cell division, 30 seconds interval from 2-cell stage until five hours after cleavage and three minute interval for the remainder of the movie. To image embryos *in utero,* clean gravid worms were transferred to a 4.5% noble agarose pad in 6 μL of M9 buffer containing 0.03% levamisole to immobilize the worms. The time interval for image acquisition was 10 seconds.

Centrifugation of embryos

Clean gravid adults were dissected in 50% M9 on freshly coated poly-L-lysine slides. Embryos were aligned with their AP axis parallel to the long axis of the microscope slide using an eyelash pick as they floated down to the slide surface. Slides were then placed in a 50 mL Falcon tube filled with 50% M9 and centrifuged in a Heraeus Biofuge at 2576 x g (4000 rpm) for 15 minutes. The slide was then removed from the tube, and excess liquid around the embryos was removed before overlaying with a coverslip. Embryos were immediately imaged by DIC microscopy. A still image was taken of all properly aligned embryos, and then one embryo was filmed until division. Then a second still image was taken of the rest of the embryos to determine the final division positioning.

Image analysis

For nuclear positioning along the AP axis, the distance of the nucleus center to the future posterior pole, as well as the AP length, were measured in Image J every 10 minutes in the DIC movies. The percentage of nuclear position along AP axis was calculated by dividing the nucleus to posterior distance by the AP length. All averages are represented ± the standard deviation.

To quantify morphological dynamics of *D. pachys* embryos, we created training patches to train a 2D U-Net network to create masks from time lapse DIC movies (Ronneberger et al., 2015). We used an incremental learning approach where we applied the model prediction to unseen movies and used a Napari correction tool to manually correct each frame to create more training data for re-training the network. This version of the program was then applied to all raw movies to produce masks. The Logical XOR function of Metamorph was applied to the mask stacks to highlight areas where embryo contours did not match.

Phalloidin staining of F-actin and F-actin imaging

The protocol was a combination of (Munro et al., 2004) and personal communication (François Robin, Institut de Biologie Paris Seine). Briefly clean gravid worms were dissected on a freshly coated poly-L-lysine (2.5 mg/mL, Sigma-Aldrich P1524) slide and incubated between 0-50 minutes depending on what age embryos were desired. A fixing solution containing 60 mM PIPES, 10 mM EGTA, 25 mM HEPES, 1 mM MgCl2, 0.1 mg/mL lysolecithin (Sigma-Aldrich 62962), 100 mM glucose, 3% paraformaldehyde and 0.2% glutaraldehyde was then added and incubated for 15 minutes. Slides were washed three times with PBS and then incubated overnight at 4°C in a 0.66 μM phalloidin Alexa Fluor 488 (Invitrogen 10125092) in PBS. Slides were gently washed with PBS and incubated for 2 hours in PBS + Hoechst (0.5 μg/mL, Fisher Scientific H1399) at room temperature. Samples were washed again in PBS, and then sealed in a drop of Aqua-Poly/Mount (Polysciences 18606) and viewed with a Roper/Zeiss upright spinning disk confocal microscope, equipped with a CoolSnap HQ2 camera and a 100x/1.46 OIL DIC ALPHA PL APO (UV) VIS-IR objective and controlled by Metamorph (Molecular Devices). Z-stack acquisition was obtained at a 0.3 μm step size. Images were processes with Metamorph and ImageJ. Linescans were obtained in Metamorph using a 3 μm line-width in average mode drawn along the AP axis of the embryo, and background was subtracted.

Tubulin staining and imaging

Embryos were freeze-cracked following protocols established for *C. elegans* and other species (Riche et al., 2013). Briefly, gravid females were dissected on poly-L-lysine coated slides and flattened between slide and coverslip before being rapidly frozen on aluminum blocks. After cracking of the coverslip, slides were immersed in -20°C methanol for at least 5 min and later processed for staining. Staining was performed for 45 min in a mouse anti-tubulin antibody DM1a (Sigma-Aldrich) diluted 1:200, followed by 45 min in a secondary donkey anti-mouse antibody DyLight 488 (Jackson 2 Immunoresearch) diluted 1:1000. Slides were then incubated for 5 min in 1μg/ml Hoechst 33342 (Sigma-Aldrich). Images were acquired on Zeiss LSM710 confocal microscope with a 63x oil immersion objective. Images were processes with Metamorph and ImageJ.

Acknowledgments
We warmly acknowledge Olivier Renaud and Olivier Leroy of the Cell and Tissue Imaging Platform (member of France BioImaging, ANR-10-INBS-04) of the Genetics and Developmental Biology Department (UMR3215/U934) of Institut Curie for help with light microscopy. We also thank Varun Kapoor for developing the script for the machine learning for embryo masks. We also thank François Robin (Institut de Biologie Paris Seine) for help with phalloidin staining and Jean-Léon Maître (Institut Curie) for discussions.

Funding information
J.P. acknowledges financial support for this work from the Fondation pour la Recherche Médicale (Grant DEQ20120323737) and the Fondation ARC (Grant PJA 20151203487 and Grant PJA 20191209604). This work also received support under the program "Investissements d'Avenir" launched by the French Government and implemented by ANR (ANR-10-LABX-0038 and ANR-10-IDEX-0001-02 PSL). D.S.E. was funded by the European Union's Horizon 2020 research and innovation programme under the Marie Skłodowska-Curie grant agreement No 666003. M.D. received financial support from the CNRS, from the ANR (ANR-19-CE02-0012) and from CEFIPRA (62T5-1).

Declaration of Interests
The authors declare that they have no conflicts of interest with the contents of this article.

FIGURE LEGENDS

Figure 1: Nuclear positioning during the first cell division of *D. pachys* embryos. A. DIC still images of asymmetric cell division, showing cortical ruffling followed by smoothening and cleavage. The different phases are labeled with the average times recorded (N = 43), and the exact times for this embryo are given below the images. Nuclear membrane breakdown (NEBD) average time is also indicated. **B.** Cartoon depicting how the position of the nucleus (dark grey sphere) is measured as a percentage of the AP axis from the future posterior pole (0% on x-axis). Left graph: scatter plot of quantification of nuclear position over time, expressed as % from the posterior pole with time normalized to time of start of cleavage. Right plot: outlier embryos that have nuclei located at either ≥ 50% (open circles) or <30% (closed circles) replotted separately to see how they reposition over the course of cell division. All embryos end with cleavage at about 46% from the posterior pole. (N = 43). **C and D.** Centrifugation experiment. Cartoon shows how embryos stuck to a microscope slide are centrifuged in a Falcon tube in a swinging bucket. Centrifugation force is indicated with an arrow labeled CF, and is directed toward the right in all images. Only embryos with their long axis parallel to the centrifugation force (dark grey embryos in the cartoon) are analyzed. Dividing *D. pachys* embryos are centrifuged and observed immediately, and then again during/after the first division. Nuclei are found predominantly on the opposite side as compared to the centrifugal force in the initial observations. **C.** Embryos where the nucleus did not reposition, and where eventually the posterior cell formed as shown by size (top panels) and P1 cell division (bottom panels). **D.** Embryos where the nuclei migrated to the opposite side of the embryo before division, and the posterior cell formed as shown by size (top panels) and the beginning of P1 cell division (bottom panels). Bars 10 μm.

Figure 2: Cortical ruffling and actin cytoskeleton in post-meiotic *D. pachys* embryos. **A.** DIC images of different stages (top) and the corresponding masks that are used to calculate cortical deformations (bottom). **B.** Movies were divided into early and late ruffling and smoothening stages, and embryo contours obtained from the masks were analyzed with an either/or function. In this analysis the white margins indicate unshared pixels between frames, and are a reflection of contour deformation. The graph plots the width of the anterior versus the posterior deformation as measured along the AP axis up to the smoothening phase. The data is roughly linear with a slope of 1 meaning that the activity of the poles is not significantly different (N = 25). **C.** Spinning disc images of fixed staining of F-actin (phalloidin Alexa-488) and DNA (Hoechst) of the *D. pachys* embryo at different stages of cell division: earlier stages at the top (starting with early prometaphase) to late stages at the bottom (ending with two-cell embryo). DNA images are the maximum intensity projection of the embryo stack so as to see both the nucleus (arrows) and the polar bodies (arrowheads), while F-actin is a sum projection of the stack. On the right are accompanying linescans for each actin image; no actin asymmetry is evident at any stage. **D.** The same as **C.**, but with *C. elegans* embryos for comparison. Clear actin asymmetry is visible at early stages in the images and the linescans as per other published works. Bars 10 μm.

Figure 3: Meiotic spindle, microtubules and actin before completion of meiosis in *D. pachys* embryos. **A.** DIC images of a typical meiotic spindle localization and subsequent cleavage. Meiotic spindles are always lateral and closer to the side of the embryo that

becomes the posterior pole. Meiotic spindle and nucleus are marked with white arrows and P1 is labeled. **B.** Confocal images of immunofluorescence visualization of microtubules on the pre-meiotic DNA and the nascent meiotic spindle. Maximum intensity projections of the embryo stack in microtubule and DNA channels and overlays. Zooms of the overlays are shown on the right. As an aside, in this zoom of DNA staining, the fact that the homologous chromosomes of the single pair do not synapse and recombine is evident, and two univalents are in fact observed at the onset of meiotic division. **C.** Spinning disc images of F-actin in pre-meiotic embryos. DNA images are the maximum intensity projection of the embryo stack, while F-actin is a sum projection of the stack. A slight asymmetry is evident by eye and is visible in the linescans. The actin-rich pole is often where the DNA is found and where presumably meiosis will take/is taking place. As evident in the images, pre-meiotic embryos were of more variable size and consistently larger than later-stage fixed embryos, perhaps due to the immature eggshell and osmotic swelling before fixation. Bars 10 μm. Bars on zooms 5 μm.

SUPPLEMENTARY FIGURE AND MOVIE LEGENDS:

Supplementary Figure S1: Overview of *D. pachys* embryonic development. Full embryogenesis of a dissected embryo from the first cell division until hatch. Still images from Supplementary Movie 2. The times on the images correspond to the total elapsed time of the acquisition, and the times under the images are in relation to cleavage start taken as zero. Nine hours after the last still image, the embryo hatches at 38 hours after the beginning of the first cell division. DIC microscopy. Scale bars 10 μm.

Supplementary Movie 1: ***D. pachys* embryo undergoing asymmetric cell division.** Still images are shown in Figure 1A. Elapsed time is shown in the upper left corner. The acquisition runs for about one hour, and the movie acceleration is about 200 x. DIC microscopy. Scale bar 10 μm.

Supplementary Movie 2: **Full embryogenesis of *D. pachys* worm from single cell until hatching**. Still images are shown in Supplementary Figure S1. Elapsed time is shown in the upper left corner. Acceleration varies throughout the film as the time interval is 10 sec for capturing first cell division, 30 sec from 2-cell stage until five hours after cleavage and 3 min for the rest of the acquisition. Scale bar 10 μm.

Supplementary Movie 3: ***D. pachys* embryo undergoing asymmetric cell division after centrifugation: the nucleus does not readjust.** Centrifugation force towards the right. Nucleus begins at left pole of embryo, and the posterior pole is produced at the same side. 13/24 embryos undergo such division. Elapsed time is shown in the upper left corner. The acquisition runs for about one hour, and the movie acceleration is about 200 x. DIC microscopy. Scale bar 1 0μm.

Supplementary Movie 4: ***D. pachys* embryo undergoing asymmetric cell division after centrifugation treatment: the nucleus migrates to the opposite pole.** Centrifugation force towards the right. Nucleus begins at left pole of embryo, but the posterior cell is produced at the opposite side. 11/24 embryos undergo such division. Elapsed time is shown in the upper left corner. The acquisition runs for 1h20min, and the movie acceleration about 200 x. DIC microscopy. Scale bar 10 μm.

Supplementary Movie 5: ***D. pachys* embryo undergoing asymmetric cell division, an example of mask analysis.** Still images are shown in Figure 2A. This is the same embryo that is transformed into a mask in Figure 2B and Supplementary Movie 6. Elapsed time is shown in the upper left corner. The acquisition runs for about one hour, and the movie acceleration is about 200 x. DIC microscopy. Scale bar 10 μm.

Supplementary Movie 6: **Movie of segmentation masks of embryo in Movie 5.** Masks produced using segmentation code and machine learning for automation of segmentation. Scale bar 10 μm.

REFERENCES:

Basham, S. E. and Rose, L. S. (1999). Mutations in ooc-5 and ooc-3 disrupt oocyte formation and the reestablishment of asymmetric PAR protein localization in two-cell *Caenorhabditis elegans* embryos. *Dev. Biol.* **215**: 253-263.

Bienkowska, D. and Cowan, C. R. (2012). Centrosomes can initiate a polarity axis from any position within one-cell *C. elegans* embryos. *Curr. Biol.* **22**: 583-589.

Brauchle, M., Kiontke, K., MacMenamin, P., Fitch, D. H. A. and Piano, F. (2009). Evolution of early embryogenesis in rhabditid nematodes. *Dev. Biol.* **335**: 253-262.

Carvalho, K., Lemière, J., Faqir, F., Manzi, J., Blanchoin, L., Plastino, J., Betz, T. and Sykes, C. (2013). Actin polymerization or myosin contraction: two ways to build up cortical tension for symmetry breaking. *Phil. Trans. R. Soc. B* **368**: 20130005.

Delattre, M. and Goehring, N. W. (2021). The first steps in the life of a worm: themes and variations in asymmetric division in *C. elegans* and other nematodes. *Curr. Top. Dev. Biol.* **144**: 269-308.

Flavel, M. R., Mechler, A., Shahmiri, M., Mathews, E. R., Francks, A. E., Chen, W., Zanker, D., Xian, B., Gao, S., Luo, J. et al. (2018). Growth of *Caenorhabditis elegans* in defined media is dependent on presence of particulate matter. *G3* **8**: 567-575.

Folkmann, A. W. and Seydoux, G. (2019). Spatial regulation of the polarity kinase PAR-1 by parallel inhibitory mechanisms. *Development* **146**: dev171116.

Fradin, H., Kiontke, K., Zegar, C., Gutwein, M., Lucas, J., Kovtun, M., Corcoran, D. L., Baugh, L. R., Fitch, D. H. A., Piano, F. et al. (2017). Genome architecture and evolution of a unichromosomal asexual nematode. *Curr. Biol.* **27**: 2928–2939.

Gan, W. J. and Motegi, F. (2021). Mechanochemical control of symmetry breaking in the *Caenorhabditis elegans* zygote. *Front. Cell Dev. Biol.* **8**: 619869.

Gessele, R., Halatek, J., Würthner, L. and Frey, E. (2020). Geometric cues stabilise long-axis polarisation of PAR protein patterns in *C. elegans*. *Nat. Commun.* **11**: 539.

Goldstein, B. (2001). On the evolution of early development in the Nematoda. *Philos. Trans. R. Soc. Lond. B* **356**: 1521-1531.

Goldstein, B., Frisse, L. M. and Thomas, W. K. (1998). Embryonic axis specification in nematodes: evolution of the first step in development. *Curr. Biol.* **8**: 157-160.

Goldstein, B. and Hird, S. N. (1996). Specification of the anteroposterior axis in *Caenorhabditis elegans*. *Development* **122**: 1467-1474.

Gönczy, P. (2008). Mechanisms of asymmetric cell division: flies and worms pave the way. *Nat. Rev. Mol. Cell Biol.* **9**: 355-366.

Hird, S. N. and White, J. G. (1993). Cortical and cytoplasmic flow polarity in early embryonic cells of *Caenorhabditis elegans*. *J. Cell Biol.* **121**: 1343-1355.

Kapoor, S. and Kotak, S. (2019). Centrosome Aurora A regulates RhoGEF ECT-2 localisation and ensures a single PAR-2 polarity axis in C. elegans embryos. *Development* **146**: dev174565.

Kimura, K. and Kimura, A. (2020). Cytoplasmic streaming drifts the polarity cue and enables posteriorization of the *Caenorhabditis elegans* zygote at the side opposite of sperm entry. *Mol. Biol. Cell* **31**: 1765-1773.

Klinkert, K., Levernier, N., Gross, P., Gentili, C., von Tobel, L., Pierron, M., Busso, C., Herrman, S., Grill, S. W., Kruse, K. et al. (2019). Aurora A depletion reveals centrosome-independent polarization mechanism in *Caenorhabditis elegans eLife* **8**: e44552.

Knoblich, J. A. (2010). Asymmetric cell division: recent developments and their implications for tumour biology. *Nat. Rev. Mol. Cell Biol.* **11**: 849-860.

Lahl, V., Sadler, B. and Schierenberg, E. (2006). Egg development in parthenogenetic nematodes: variations in meiosis and axis formation. *Int. J. Dev. Biol.* **50**: 393-398.

Lahl, V., Schulze, J. and Schierenberg, E. (2009). Differences in embryonic pattern formation between *Caenorhabditis elegans* and its close parthenogenetic relative *Diploscapter coronatus*. *Int. J. Dev. Biol.* **53**: 507-515.

Morton, D. G., Hoose, W. A. and Kemphues, K. J. (2012). A genome-wide RNAi screen for enhancers of *par* mutants reveals new contributors to early embryonic polarity in *Caenorhabditis elegans*. *Genetics* **192**: 929-942.
Munro, E., Nance, J. and Priess, J. R. (2004). Cortical flows powered by asymmetrical contraction transport PAR proteins to establish and maintain anterior-posterior polarity in the early *C. elegans* embryo. *Dev. Cell* **7**: 413-24.
Reich, J. D., Hubatsch, L., Illukkumbura, R., Peglion, F., Bland, T., Hirani, N. and Goehring, N. W. (2019). Regulated activation of the PAR polarity network ensures a timely and specific response to spatial cues. *Curr. Biol.* **29**: 1911-1923.
Reymann, A.-C., Staniscia, F., Erzberger, A., Salbreaux, G. and Grill, S. W. (2016). Cortical flow aligns actin filaments to form a furrow. *eLife* **5**: e17807.
Riche, S., Zouak, M., Argoul, F., Arneodo, A., Pecreaux, J. and Delattre, M. (2013). Evolutionary comparisons reveal a positional switch for spindle pole oscillations in *Caenorhabditis embryos*. *J. Cell Biol.* **201**: 653-662.
Ronneberger, O., Fischer, P. and Brox, T. (2015). U-Net: convolutional networks for biomedicalImage segmentation. *MICCAI* **9351**: 234–241.
Rose, L. and Gönczy, P. (2014). Polarity establishment, asymmetric division and segregation of fate determinants in early *C. elegans* embryos. *Wormbook*: doi/10.1895/wormbook.1.30.2.
Schenk, C., Bringmann, H., Hyman, A. A. and Cowan, C. R. (2010). Cortical domain correction repositions the polarity boundary to match the cytokinesis furrow in *C. elegans* embryos. *Development* **137**: 1743-1753.
Schulze, J. and Schierenberg, E. (2011). Evolution of embryonic development in nematodes. *EvoDevo* **2**: 18.
Sonneville, R. and Gönczy, P. (2004). zyg-11 and cul-2 regulate progression through meiosis II and polarity establishment in *C. elegans*. *Development* **131**: 3527-3542.
Strome, S. (1986). Fluorescence visualization of the distribution of microfilaments in gonads and early embryos of the nematode *Caenorhabditis elegans*. *J. Cell Biol.* **103**: 2241-2252.
Valfort, A.-C., Launay, C., Sémon, M. and Delattre, M. (2018). Evolution of mitotic spindle behavior during the first asymmetric embryonic division of nematodes. *PLOS Biol.* **16**: e2005099.
Wallenfang, M. R. and Seydoux, G. (2000). Polarization of the anterior–posterior axis of *C. elegans* is a microtubule-directed process. *Nature* **408**: 89-92.
Zhao, P., Teng, X., Tantirimudalige, S. N., Nishikawa, M., Wohland, T., Toyama, Y. and Motegi, F. (2019). Aurora-A breaks symmetry in contractile actomyosin networks independently of its role in centrosome maturation. *Dev. Cell* **48**: 631-645.

Figure 1

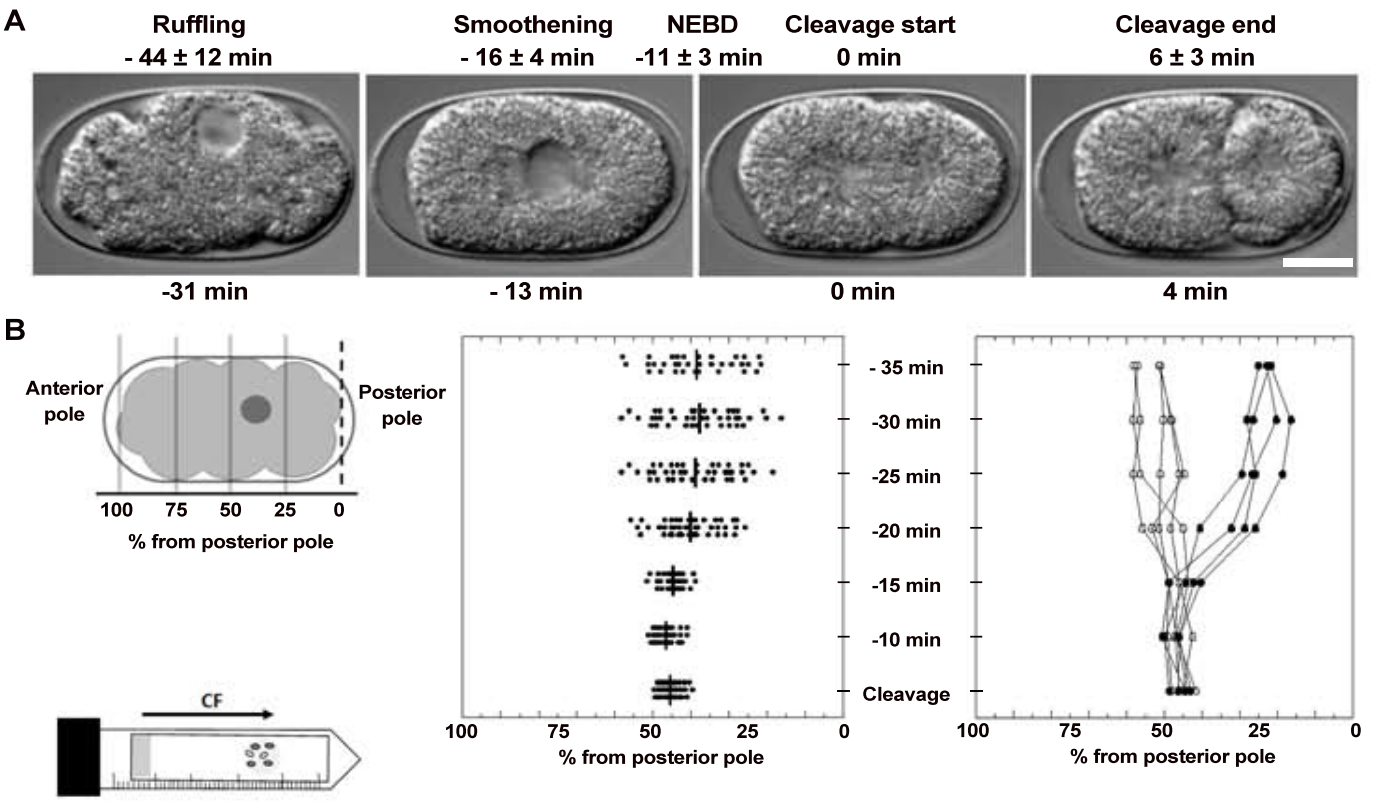
A
Ruffling
- 44 ± 12 min
Smoothening
- 16 ± 4 min
NEBD
-11 ± 3 min
Cleavage start
0 min
Cleavage end
6 ± 3 min
-31 min
- 13 min
0 min
4 min
B
Anterior pole
Posterior pole
100 75 50 25 0
% from posterior pole
CF
- 35 min
-30 min
-25 min
-20 min
-15 min
-10 min
Cleavage
100 75 50 25 0
% from posterior pole
100 75 50 25 0
% from posterior pole
C
Just after centrifugation:
nucleus on the left
(24/27 embryos)
Subsequent division:
P1 on the left
(13/24 embryos)
D
Just after centrifugation:
nucleus on the left
(24/27 embryos)
Subsequent division:
P1 on the right
(11/24 embryos)
CF
CF
CF
CF

Figure 2

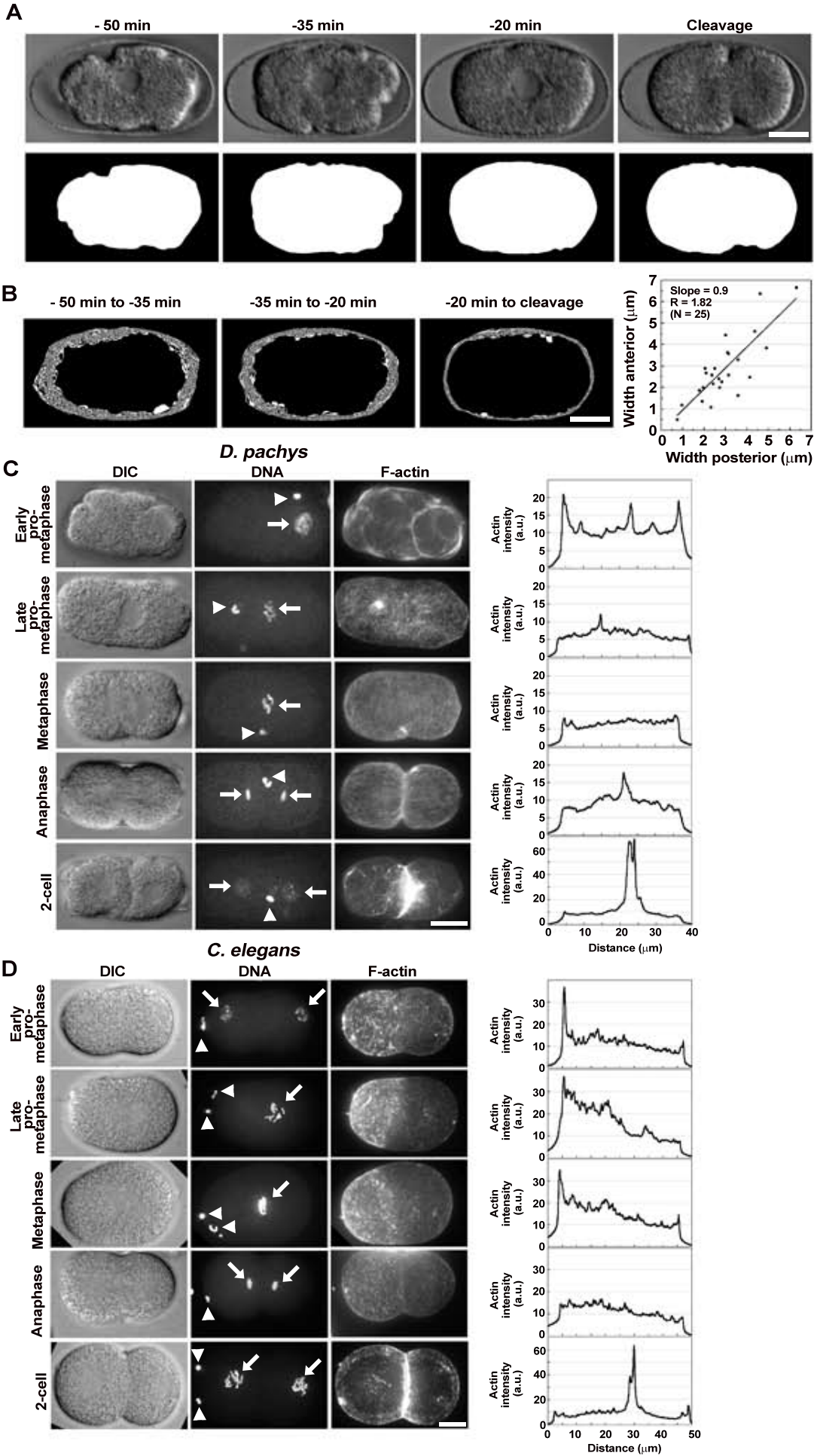
A
- 50 min
-35 min
-20 min
Cleavage
B
- 50 min to -35 min
-35 min to -20 min
-20 min to cleavage
Slope = 0.9
R = 1.82
(N = 25)
Width anterior (μm)
Width posterior (μm)
C
D. pachys
DIC
DNA
F-actin
Early pro-metaphase
Late pro-metaphase
Metaphase
Anaphase
2-cell
Actin intensity (a.u.)
Distance (μm)
D
C. elegans
DIC
DNA
F-actin
Early pro-metaphase
Late pro-metaphase
Metaphase
Anaphase
2-cell
Actin intensity (a.u.)
Distance (μm)

Figure 3

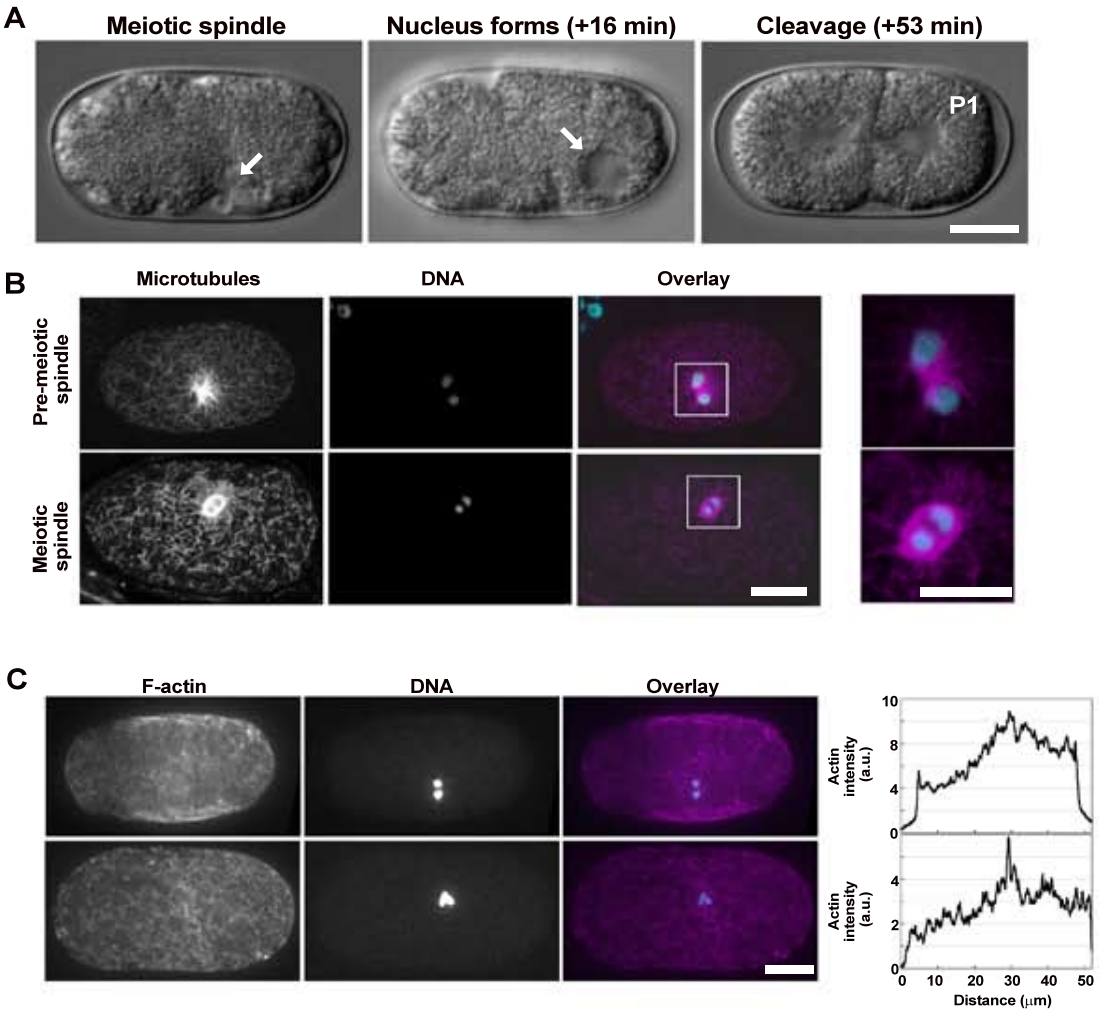
A
Meiotic spindle
Nucleus forms (+16 min)
Cleavage (+53 min)
P1
B
Microtubules
DNA
Overlay
Pre-meiotic spindle
Meiotic spindle
C
F-actin
DNA
Overlay
Actin intensity (a.u.)
Actin intensity (a.u.)
Distance (μm)

Supplemenatary Figure S1

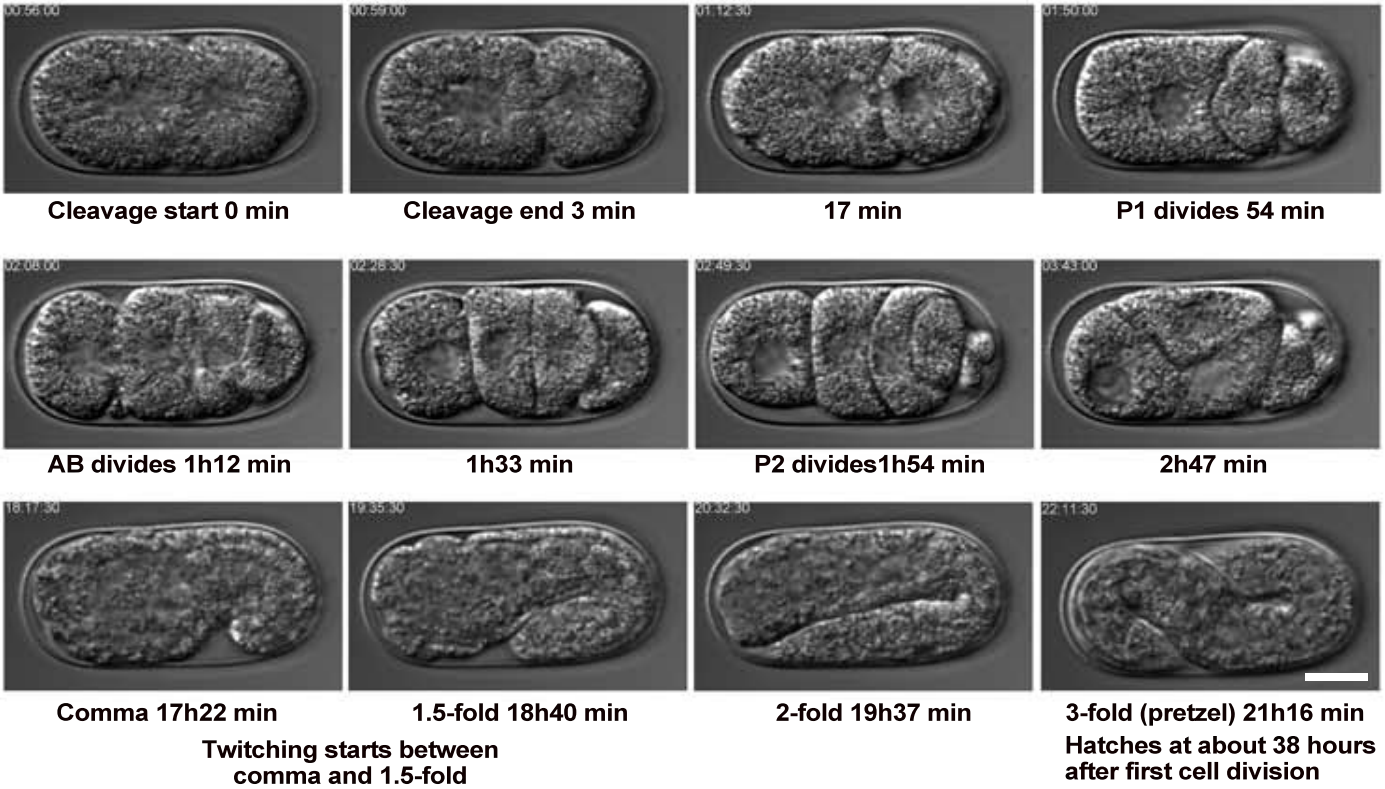

RÉSUMÉ

La division cellulaire asymétrique est un processus essentiel du développement. Ce processus ainsi que sa régulation ont fait l'objet de nombreuses études chez l'embryon de *Caenorhabditis elegans*. La division asymétrique de l'embryon unicellulaire est un processus conservé à travers les espèces de nématodes, cependant les caractéristiques cellulaires menant à la division sont étonnamment variables. Au cours de mon doctorat, j'ai voulu étudier ces différences en utilisant deux embryons non-*C. elegans* : *Diploscapter pachys et Pristionchus pacificus. D. pachys* est le parent parthénogénétique le plus proche de *C. elegans*. La polarité étant induite par le sperme chez *C. elegans*, on ne peut expliquer ce qui brise la symétrie chez *D. pachys*. Mes résultats montrent que le noyau occupe le plus souvent l'hémisphère de *D. pachys* qui deviendra le pole postérieur. Dans les embryons où il est astreint à un pôle par centrifugation, le noyau fini par revenir à son pôle préférentiel. Même si l'embryon est polarisé, l'agitation corticale et le cytosquelette d'actine semblent identiques aux deux pôles. D'autre part, la position du fuseau méiotique est corrélée avec la future cellule postérieure. Dans certains ovocytes, on observe des structures de microtubules émanant du fuseau méiotique combiné à un faible enrichissement en actine au future pôle postérieur. Finalement, mon principal projet de thèse montre que la polarité de *D. pachys* est atteinte durant la méiose, au cours de laquelle le fuseau méiotique pourrait jouer un rôle par un mécanisme présent mais inhibé chez *C. elegans*. Chez *P. pacificus*, la transgénèse biolistique a été récemment utilisée avec succès. Toutefois, par manque d'un marqueur de sélection fiable, il était illusoire de poursuivre cette approche. En conclusion, les résultats de ma thèse contribuent à une meilleure compréhension de l'embryogénèse hors *C. elegans*. Ils soulignent l'importance de ces espèces dans l'optique d'études comparatives.

MOTS CLÉS

division cellulaire asymétrique, embryons non-*C. elegans*, études comparatives, bris de symétrie, actine, polarité, parthénogenèse, aster de microtubules

ABSTRACT

Asymmetric cell division is an essential process of development. The process and its regulation have been studied extensively in the *Caenorhabditis elegans* embryo. Asymmetric division of the single-cell embryo is a conserved process in nematode species, however, the cellular features leading up to division are surprisingly variable. During my PhD, I aimed to study these differences by using two non-*C. elegans* embryos: *Diploscapter pachys* and *Pristionchus pacificus*. *D. pachys* is the closest parthenogenetic relative to *C. elegans*. Since the polarity cue in *C. elegans* is brought by the sperm, how polarity is triggered in *D. pachys* remains unknown. My results show that the nucleus inhabits principally the hemisphere of the *D. pachys* embryo that will become the posterior pole. In embryos where the nucleus is forced to one pole by centrifugation, it returns to its preferred pole. Although the embryo is polarized, cortical ruffling and actin cytoskeleton at both poles appear identical. Interestingly, the location of the meiotic spindle also correlates with the future posterior cell. In some oocytes, a slight actin enrichment along with unusual microtubule structures emanating from the meiotic spindle are observed at the future posterior pole. Overall, my main PhD project shows that polarity of the *D. pachys* embryo is attained during meiosis wherein the meiotic spindle could potentially be playing a role by a mechanism that may be present but suppressed in *C. elegans*. For *P. pacificus*, biolistic transgenesis has been shown recently successful. However, due to a lack of a stringent selection marker, the continuation of this project was unfeasible during my PhD. Altogether, the results of my PhD add to the understanding of non-*C. elegans* early embryogenesis and emphasizes on the importance of using these species for comparative studies.

KEYWORDS

asymmetric cell division, non-*C. elegans* embryos, comparative studies, symmetry breaking, actin, polarity, parthenogenesis, microtubule aster